

Dissertation zur Erlangung des Doktorgrades  
der Fakultät für Chemie und Pharmazie  
der Ludwig-Maximilians-Universität München

**Deciphering the role of HAX1 in neutrophil differentiation**

von Yanxin Fan

aus

Beijing, China

2021

## Erklärung

Diese Dissertation wurde im Sinne von § 7 der Promotionsordnung vom 28. November 2011 von Herrn Prof. Dr. Christoph Klein betreut und von Herrn Prof. Dr. Klaus Förstemann von der Fakultät für Chemie und Pharmazie vertreten.

## Eidesstattliche Versicherung

Diese Dissertation wurde eigenständig und ohne unerlaubte Hilfe erarbeitet.

München, 08.10.2021

Yanxin Fan

Dissertation eingereicht am 18.10.2021

1. Gutachterin / 1. Gutachter: Prof. Dr. Klaus Förstemann

2. Gutachterin / 2. Gutachter: Prof. Dr. Christoph Klein

Mündliche Prüfung am 21.03.2022

For my family

---

**CONTENT**

<b>ABSTRACT .....</b>	<b>1</b>
<b>I INTRODUCTION.....</b>	<b>2</b>
1 Severe congenital neutropenia and HAX1 .....	2
1.1 Severe congenital neutropenia (SCN).....	2
1.2 Kostmann syndrome .....	4
1.3 HAX1 .....	4
2 Cellular proteostasis.....	6
2.1 Protein synthesis control.....	7
2.2 Chaperones.....	8
2.3 UPS and autophagy .....	9
2.4 Protein responses to perturbed proteostasis .....	10
2.5 Proteostasis and disease.....	12
3 Mitochondria and mitoproteostasis .....	13
3.1 General introduction of mitochondria .....	13
3.2 The oxidative phosphorylation system and mitochondrial superoxide (O <sub>2</sub> <sup>-</sup> ) production.....	14
3.3 Mitochondrial supercomplexes .....	16
3.4 Regulation of mitochondrial proteostasis .....	17
<b>II MATERIALS AND METHODS.....</b>	<b>24</b>
1 Materials .....	24
1.1 Reagent.....	24
1.2 Kits and disposals .....	26
1.3 Buffers and solutions.....	27
1.4 Antibodies.....	30
1.5 Plasmids and Oligonucleotides .....	31
1.6 Cell lines.....	36
1.7 Animals.....	36
1.8 Equipment and software .....	37
2 Methods .....	38
2.1 Mice analysis.....	38
2.2 Cultivation of human cells.....	40
2.3 iPSCs associated cell culture and experiments.....	40
2.4 Generation of gene knockout cell lines using the CRISPR-Cas9 system 41	
2.5 Generation of stable cell lines with overexpressed genes.....	42
2.6 Inhibitor studies .....	42
2.7 Mitochondrial isolation .....	43
2.8 Mitochondrial swelling experiment.....	43
2.9 Mitochondrial carbonate extraction .....	43

2.10	Immunoprecipitation of proteins .....	43
2.11	Immunofluorescent studies.....	44
2.12	In-gel-mass spectrometry .....	44
2.13	SILAC analysis.....	45
2.14	Interactome analysis of HSP27 .....	46
2.15	Quantification and statistical analysis.....	46
2.16	Molecular biology techniques .....	47
2.17	Protein extraction and protein concentration .....	48
2.18	Measurement of mitochondrial complex I and IV activity .....	48
2.19	Measurement of mitochondrial ROS .....	48
<b>III</b>	<b>RESULTS.....</b>	<b>49</b>
1	The functional study of Hax1 in a mouse model .....	49
1.1	Hax1 <sup>-/-</sup> mice .....	49
1.2	Competitive bone marrow chimeras.....	50
1.3	Hax1 <sup>ff</sup> LysM <sup>cre/+</sup> mice .....	52
2	HAX1 functional study in human cells .....	54
2.1	HAX1 localizes to the mitochondrial intermembrane space.....	54
2.2	CLPB controls HAX1 disaggregation .....	58
2.3	Mitochondrial protein quality control in HAX1- and CLPB-deficiency ..	69
2.4	HAX1 maintains solubility of HSP27 in mitochondria.....	74
2.5	HSP27 restores perturbed mitochondrial proteostasis in HAX1 deficient cells. 80	
2.6	HSP27 is associated with mitochondrial complexes and translation, whose reconstitution recovers mitochondrial oxidative stress in HAX1 deficiency.....	83
2.7	HSP27 reconstitutes HAX1 deficiency in iPSCs model.....	86
<b>IV</b>	<b>DISCUSSION .....</b>	<b>90</b>
1	HAX1 is a mitochondrial IMS protein.....	90
1.1	HAX1 is the binding partner of CLPB.....	91
1.2	Roles of CLPB in mitochondrial biology .....	92
1.3	Perturbed proteostasis in HAX1 and CLPB deficiency.....	93
2	HSP27 and perturbed mitochondrial proteostasis.....	94
2.1	The cellular localization of HSP27.....	94
2.2	HSP27 and mitochondrial proteostasis .....	95
2.3	The phosphorylation of HSP27.....	97
2.4	The reconstitution of HSP27 in PLB-985 cells and iPS cells.....	98
<b>V</b>	<b>SUMMARY.....</b>	<b>99</b>
<b>VI</b>	<b>BIBLIOGRAPHY.....</b>	<b>100</b>
<b>VII</b>	<b>ACKNOWLEDGEMENT.....</b>	<b>117</b>
<b>VIII</b>	<b>CURRICULUM VITAE .....</b>	<b>119</b>

## Figures and Tables

Figure 1. Myeloid maturation arrest in severe congenital neutropenia. ....	3
Figure 2. An overview of potential cellular localizations of HAX1.....	6
Figure 3. Scheme illustrating main modules of the proteostasis network.....	7
Figure 4. Protein fates in the proteostasis network.....	9
Figure 5. Stress responses for the maintenance of cellular proteostasis. ....	10
Figure 6. General architecture of mitochondria.....	13
Figure 7. The Oxidative phosphorylation system (OXPHOS). ....	15
Figure 8. Different forms of mitochondrial supercomplexes located in cristae. .....	17
Figure 9. Proteolytic systems in mitochondrial proteostasis.....	20
Figure 10. The main axes of mammalian UPR <sup>mt</sup> . ....	22
Figure 11. Altered erythropoiesis in Hax1-deficient mice.....	49
Figure 12. Generation of bone marrow chimeras using X-ray irradiation. ....	50
Figure 13. FACS analysis of developmental potential of WT and Hax1-KO cells in bone marrow. ....	51
Figure 14. FACS analysis of developmental potential of WT and Hax1-KO cells in spleen and thymus. ....	52
Figure 15. The detection of Hax1 expression in neutrophils from WT and LysM <sup>cre/+</sup> Hax1 <sup>ff</sup> mice. ....	53
Figure 16. Analysis of neutrophils and bone marrow progenitors in WT and LysM <sup>cre/+</sup> Hax1 <sup>ff</sup> mice. ....	53
Figure 17. The scheme of mitochondrial swelling experiment. ....	54
Figure 18. Submitochondrial localization of HAX1 analyzed by protease protection. ....	55
Figure 19. The scheme of mitochondrial carbonate extraction. ....	56
Figure 20. HAX1 is a membrane-bound protein. ....	57
Figure 21. Co-staining of HAX1 and OPA1 in HeLa cells.....	57
Figure 22. The specificity of HAX1 staining. ....	58
Figure 23. Analysis of the HAX1FLAG immunoprecipitation experiment by Coomassie-blue staining. ....	59
Figure 24. HAX1 interacts with CLPB. ....	61
Figure 25. CLPB is located in mitochondrial intermembrane space. ....	61

Figure 26. Costaining of HAX1, CLPB and OPA1 in HeLa cells. ....	62
Figure 27. The expression of HAX1 is reduced in the soluble fraction of cells lacking CLPB.....	63
Figure 28. In the absence of CLPB, HAX1 was characterized in punctiform..	64
Figure 29. HAX1 became insoluble in the absence of CLPB. ....	65
Figure 31. Identification the predominant isoform of CLPB.....	67
Figure 33. Scheme of SILAC-based workflow. ....	69
Figure 34. Increased mitochondrial protein synthesis in HAX1 <sup>-/-</sup> and CLPB <sup>-/-</sup> cells. ....	70
Figure 36. The protein synthesis and persistence within glycolysis pathway and Golgi pathway. ....	72
Figure 38. HAX1 deficiency induced elevated mtROS production.....	74
Figure 39. The existence of HSP27 was reduced in the absence of HAX1 or CLPB.....	75
Figure 40. HSP27 was more detectable in whole cell lysates in comparison to hypertonic lysis. ....	75
Figure 41. A dephosphorylated form of HSP27 remained in the pellet after solubilization by hypertonic solution.....	76
Figure 42. HSP27 remained in punctiform in the absence of HAX1 after pre- extraction treatment. ....	77
Figure 44. HSP27 formed in punctiform in HAX1-deficient mitochondria after pre-extraction treatment. ....	79
Figure 45. The faster migrating form of HSP27 is more resistant to carbonate extraction or detergent lysis than the upper band of HSP27, in the absence of HAX1 or CLPB.....	80
Figure 46. PRKD2 was reduced in the absence of HAX1. ....	81
Figure 47. PRKD2 was down-regulated in the absence of HAX1.....	82
Figure 48. PRKD2 and HSP27 were located in mitochondrial IMS and matrix. .....	83
Figure 49. Inhibition of the activity or reduced expression of PRKD2 impairs HSP27's phosphorylation. ....	83
Figure 50. The interactome of HSP27 in mitochondria.....	84
Figure 51. HAX1 deficient cells displayed mitochondrial unfolded protein response by activating Sirt3-FOXO3a-LC3 pathway and the	

induction of autophagy was enhanced upon MG132 treatment in the absence of HAX1.....	85
Figure 52. The reconstitution of either HAX1 or HSP27 reversed the elevated mitochondrial ROS production in the absence of HAX1.....	86
Figure 53. The overexpression of HAX1 and HSP27 in iPSCs. ....	87
Figure 54. The analysis of live floating cell counts.....	88
Figure 55. FACS assay of iPSCs with mcherry+CD11b/CD33low. ....	88
Figure 56. Cytospin of differentiated iPSCs. ....	89
Table 1. The summary of reagent included in this study. ....	24
Table 2. The summary of kits and disposals included in this study .....	26
Table 3. The summary of solutions included in this study .....	27
Table 4. List of antibodies in immunofluorescence analysis and Western blotting.....	30
Table 5. The summary of plasmids included in this work .....	31
Table 6. The summary of oligonucleotides of this work .....	33
Table 7. The summary of cell lines applied for this work .....	36
Table 8. The summary of equipment applied for this work .....	37
Table 9. The summary of softwares applied in this work .....	38
Table 10. List of identified HAX1-binding proteins upon immunoprecipitation	60



## Abbreviations

%	Percent
°C	Grad Celsius
ANC	Absolute neutrophil count
ANK	Ankyrin repeats domain
ALP	Autophagy- lysosomal pathway
ATP	Adenosine-5'-triphosphate
BH	Bcl-2 homology
CD	Cluster of differentiation
CTD	Carboxy terminal nucleotide binding domain
DAPI	4',6-Diamidin-2-phenylindol
DNA	Deoxyribonucleic acid
EM	EDTA, MOPS
ER	Endoplasmic Reticulum
FACS	Fluorescence activated cell sorting
HEPES	4-(2-hydroxyethyl)-1-piperazineethanesulfonic acid
HET	Heterozygosity
HSPs	Heat shock proteins
IgG	Immunoglobulin G
IM	Mitochondrial inner membrane
IMS	Mitochondrial intermembrane space
IP	Immunoprecipitation
IV	Intravenous(ly)
kDa	kilo Dalton
KO	Knock-out
LFQ	Label-free quantitation
min	Minute
mL	Microliter
MMP	Mitochondrial membrane potential
MS	Mass spectrometry
mt	Mitochondrial
MTS	Mitochondrial target sequence

## Abbreviations

---

MW	Molecular weight
NTD	Amino-terminal domain
OD	Optical density
OM	Mitochondrial outer membrane
OXPPOS	Oxidative phosphorylation
PCR	Polymerase chain reaction
PEST	Proline, glutamic acid, serine, threonine
pH	Potential of hydrogen
PK	Proteinase K
PN	Proteostasis network
PRRL	Lentivirus transfer vector construct containing chimeric Rous sarcoma virus HIV 5' LTRs
RBC	Red blood cells
RNA	Ribonucleic acid
ROS	Reactive oxygen species
rpm	Rotations per minute
SCN	Severe congenital neutropenia
SDS-PAGE	Sodium dodecyl sulfate-polyacrylamide gel
SEM	Sucrose, EDTA, MOPS
shRNA	Short hairpin RNA
SILAC	Stable isotope labelling by amino acids in cell culture
TCA	Tricarboxylic acid
TH	Trehalose, HEPES
TMD	Transmembrane domain
UPR	Unfolded protein response
UPS	Ubiquitin- proteasome system
WT	Wild type
µg	Microgram
µm	Micrometer
µL	Microliter

## ABSTRACT

Loss-of-function mutations in HAX1 (HS1-associated protein X1) in humans result in autosomal recessive severe congenital neutropenia (SCN), yet the exact molecular function of HAX1 remains unclear. Here, we aimed to determine its specific cellular function and elucidate potential pathophysiology related to HAX1 deficiency. Using mitochondrial swelling and carbonate extraction methods, we demonstrate that HAX1 is located in the mitochondrial intermembrane space. We performed mass-spectrometry (MS) studies and identified Caseinolytic peptidase B protein homolog (CLPB) as a novel interacting protein of HAX1 in HEK293T cells. CLPB is a member of the ATPase superfamily associated with diverse cellular activities (AAA+), which was previously shown to serve as a mitochondrial disaggregase in mammalian cells. Biallelic mutations in CLPB cause a rare neurological disorder associated with impaired cognitive development, 3-methylglutaconic aciduria, and congenital neutropenia. We show that human mutations leading to SCN in either HAX1 or CLPB disrupt the mutual interactions between both proteins of the corresponding proteins. Using an approach combining SILAC and MS, we reveal that both HAX1 and CLPB deficiencies in myeloid leukemia cell lines cause perturbed mitochondrial protein turnover, mainly in the respiratory complex I, respiratory complex III and tricarboxylic acid cycle (TCA cycle). As a result, mtROS production is enhanced in the absence of HAX1. In comparative studies of the proteome (WT vs HAX1 deficient PLB-985 cells), HSP27 is found to be mostly dysregulated in HAX1<sup>-/-</sup> PLB-985 cells. Intriguingly, through a series of biochemical methods, such as Western blotting of cellular extracts upon fractionation, as well as by confocal microscopy experiments, we found a reduced phosphorylation state and reduced solubility of HSP27 in HAX1<sup>-/-</sup> cells. Further interactome assay of HSP27 demonstrate that HSP27 is associated with respiratory complexes and ribosomal subunits in mitochondria. Thus, these data indicate a critical involvement of the CLPB/HAX1 axis in maintaining mitochondrial complex stability and mitochondrial protein synthesis. Importantly, HSP27's reconstitution reverses the elevated ROS production in HAX1<sup>-/-</sup> PLB-985 cells and the perturbed neutrophil differentiation in HAX1<sup>-/-</sup> iPSCs model. Our study discovers a new and essential role of HAX1 in maintenance of mitochondrial proteostasis.

# I INTRODUCTION

## 1 Severe congenital neutropenia and HAX1

### 1.1 Severe congenital neutropenia (SCN)

Severe congenital neutropenia (SCN) is characterized by a reduced number of peripheral blood neutrophil granulocytes, often associated with promyeloid or myeloid maturation arrest in the bone marrow. Patients with SCN are characterized by an absolute neutrophil count (ANC) less than 500 per microliter. As a result, SCN patients already suffered from severe bacterial infections during first few months after birth. For example, they commonly present omphalitis, bronchitis, otitis, skin abscesses or pneumonia (Klein, 2011).

SCN patients may as well appear to be more vulnerable to invasive fungal infections and the pus formation is evidently reduced upon infections. Moreover, many of them suffer from osteopenia or osteoporosis due to decreased bone mineral density (Borzutzky et al., 2006; Yakisan et al., 1997). SCN is not a single nosological entity but rather comprises a wide array of diseases. SCN is found in association with syndromic diseases, such as metabolic diseases, bone marrow failure syndromes and oculocutaneous albinism (Spoor et al., 2019). SCN may furthermore be associated with autoinflammatory and autoimmune disorders, hematological malignancy and neuropsychiatric symptoms (Spoor et al., 2019).

Most SCN patients show not only quantitative but also qualitative neutrophil aberrations. As indicated in Figure 1, neutrophil maturation is arrested between promyelocyte stage and myelocyte stage. In addition, defected neutrophils morphologically aberrant in aspects of remarkable vacuolization and defective azurophilic granules (Klein, 2011). Due to dysfunctional granule proteins, aberrant neutrophils may functionally deficient in capacity of migration and activity of bacterial killing (Putsep et al., 2002). In myeloid progenitor cells increased apoptosis has been shown to be one important mechanism responsible for neutropenia in certain SCN patients with defined mutations.

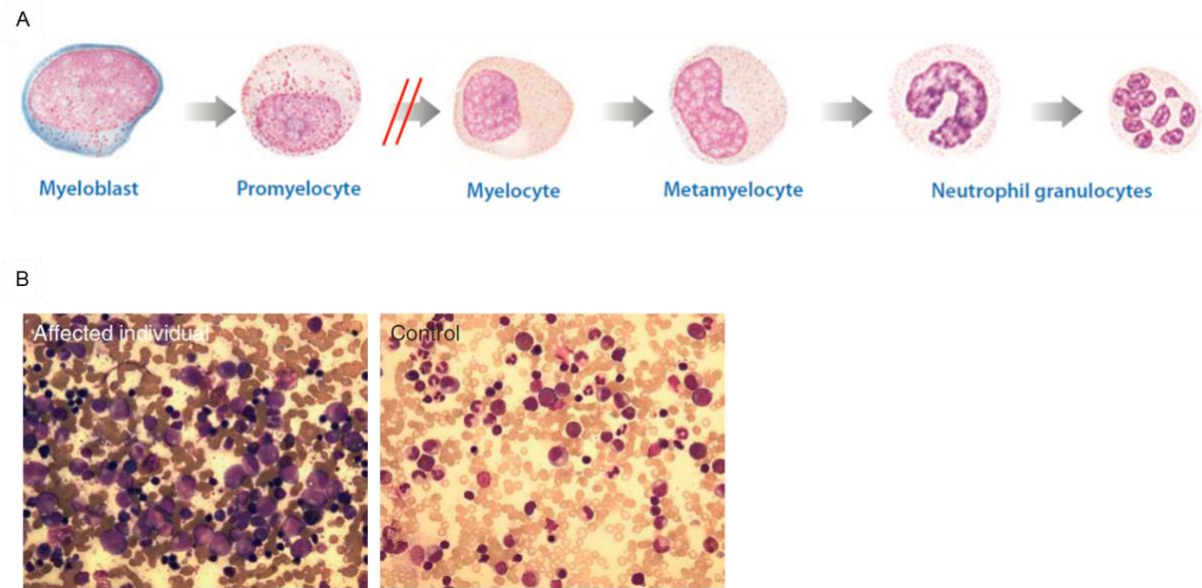


**Figure 1. Myeloid maturation arrest in severe congenital neutropenia.** Taken from (Klein, 2011; Klein et al., 2007). (A) Maturation arrest between promyelocyte and myelocyte; (B) illustration of Giemsa-stained bone marrow aspirate smear in affected individual with SCN. Bone marrow from the healthy serves as a control.

SCN constitutes a heterogeneous group of diseases. Over the last decades, a few genes have been discovered accounting for the syndrome. The largest subgroup (about 60% in central European patients) of SCN is identified with mutations in *ELANE*, which is in charge of encoding neutrophil elastase. SCN patients with *ELANE* deficiency demonstrate upregulated ER stress, indicating by the elevation of BiP and the cleavage of XBP-1 (Grenda et al., 2007; Kollner et al., 2006). In 20%-25% SCN patients, in particular those of Turkish origin, mutations in *HAX1* are found. *HAX1*-deficiency causes decreased mitochondrial membrane potential in patients' neutrophils (Klein et al., 2007).

To date, more than 20 genes involved in various biological functions have been identified as being causative for SCN (Donadieu et al., 2017). Of note, one gene could contribute to a 'constitutional defect' associated with a germline mutation. On the other hand, it could be related to leukemogenesis by a somatic genetic event (Donadieu et al., 2017). An increasing number of genetic deficiencies continue to be identified, which further underlines the growing diversity of SCN. Recent examples are defects in *G6PC3* (Boztug et al., 2009), *STK4* (Abdollahpour et al., 2012), *CSF3R* (Triot et al., 2014), *JAGN1* (Boztug et al., 2014), *SMARCD2* (Witzel et al.,

2017), SRP54 (Bellanne-Chantelot et al., 2018) and p14/LAMTOR2 (Lyszkiewicz et al., 2019). Despite the genetic etiologies of SCN is increasingly discovered, the molecular pathophysiology based on these disorders remains elusive.

Therapy of congenital neutropenia aims first and foremost at preventing life-threatening microbial infections. The standard therapy is daily subcutaneous G-CSF administration. This promotes a substantial increase in neutrophils count of peripheral blood. Thus, G-CSF therapy is able to evidently reduce infections and significantly improve patients' life expectancy and quality. However, some patients can hardly respond to G-CSF treatment and some patients develop clonal hematopoietic hematopoiesis, such as acute myeloid leukemia (AML) and myelodysplastic syndromes (MDS). In this case, allogeneic hematopoietic stem cell transplantation (AHSCT) appears to be the only curative treatment for those patients.

## **1.2 Kostmann syndrome**

The first child with agranulocytosis were recognized by the pediatrician Rolf Kostmann in a consanguineous family from Sweden (Kostmann, 1950). In 1956, Kostmann reported the analysis of 6 children with "infantile genetic agranulocytosis", which is referred as "Severe congenital neutropenia" today (Kostmann, 1956). Typical clinical manifestations of those patients included various bacterial infections, such as otitis, abscesses, skin infections, tonsillitis or sepsis (Klein, 2017). Kostmann recognized that the pattern of inheritance is autosomal recessive and already defined that there is a maturation arrest during the neutrophil differentiation by the proof of Giemsa-stained bone marrow smears (Klein, 2017).

The genetic etiology and pathomechanisms of Kostmann syndrome remained elusive for the following 50 years. Our group proved that HAX1 was the SCN-causative gene variant in both Turkish patients and the original pedigree patients recognized by Kostmann. In the absence of HAX1, the inner mitochondrial membrane potential in patient neutrophils is reduced and therefore cells are prone to premature apoptosis (Klein et al., 2007).

## **1.3 HAX1**

HAX1 was originally identified by the Suzuki group in a yeast-two-hybrid screening study (Suzuki et al., 1997). Using protein HS1 (HCLS1) as a bait protein, Suzuki et

al. were able to isolate the cDNA of a newly found protein, namely HAX1 (HS1-associated protein X1) (Suzuki et al., 1997). HAX1 primarily locates in mitochondria (Suzuki et al., 1997). A series of following studies demonstrated that HAX1 could as well be related to the nuclear membrane and the endoplasmic reticulum (ER) (Cilenti et al., 2004; Ortiz et al., 2004).

In Hax1-deficient mice, researchers found that Hax1 facilitated the processing of Htra2 by Parl, so that processed Htra2 functioned as an anti-apoptotic protein in mitochondrial intermembrane space (Chao et al., 2008). Therefore, these authors assumed that defective processing of anti-apoptotic Htra2 enhanced cellular apoptosis, contributing to an early cell death observed in the neuronal and lymphocytic system of Hax1-deficient mice. HAX1 can be cleaved into two fragments by Granzyme B (Han et al., 2010). The N-terminal fragment mediates mitochondrial depolarization after cleavage in mitochondria, while the C-terminal fragment is released to the cytosol (Han et al., 2010). Moreover, HAX1 is shown to interact with anti-apoptotic protein XIAP1 to prevent degradation of XIAP1 by the proteasome, which eventually results in cell survival (Kang et al., 2010). Furthermore, HAX1 has been identified as an interactor of SERCA2. It reported that HAX1 regulates the protein expression of SERCA2 so as to facilitate cell survival (Vafiadaki et al., 2009).

Several studies link HAX1 to the cytoskeleton. For example, HAX1 is reported to interact with PKD2 and cortactin, which may play a role in formation of cell-matrix contacts (Gallagher et al., 2000). Moreover, HAX1 is shown to negatively control integrin-mediated adhesion through an interaction with RhoA (Cavnar et al., 2011). At the actin cytoskeleton, HAX1 appears to interact with Pelota (Pelo) for degrading aberrant RNAs (Burnicka-Turek et al., 2010). In addition, HAX1 has acted as a transcriptional regulatory element by specifically binding to the 3' UTR of vimentin encoding mRNAs (Al-Maghrebi et al., 2002) and DNA polymerase beta (Sarnowska et al., 2007). In neuronal cells, Zhang et al. discovered that HAX1 mediates interaction of KCNC3 with ARP2/3, leading to an inactivated Kv3.3 potassium channel (Zhang et al., 2016). To further complicate a multifaceted mystery, HAX1 was reported to shuttle between nucleus and cytosol, which relate functions of HAX1 to mRNA processing (Grzybowska et al., 2013). Thus, HAX1 may be involved in a

wide array of putative functions (Figure 2), yet no unifying hypothesis has yet elucidated the multifunction of HAX1.

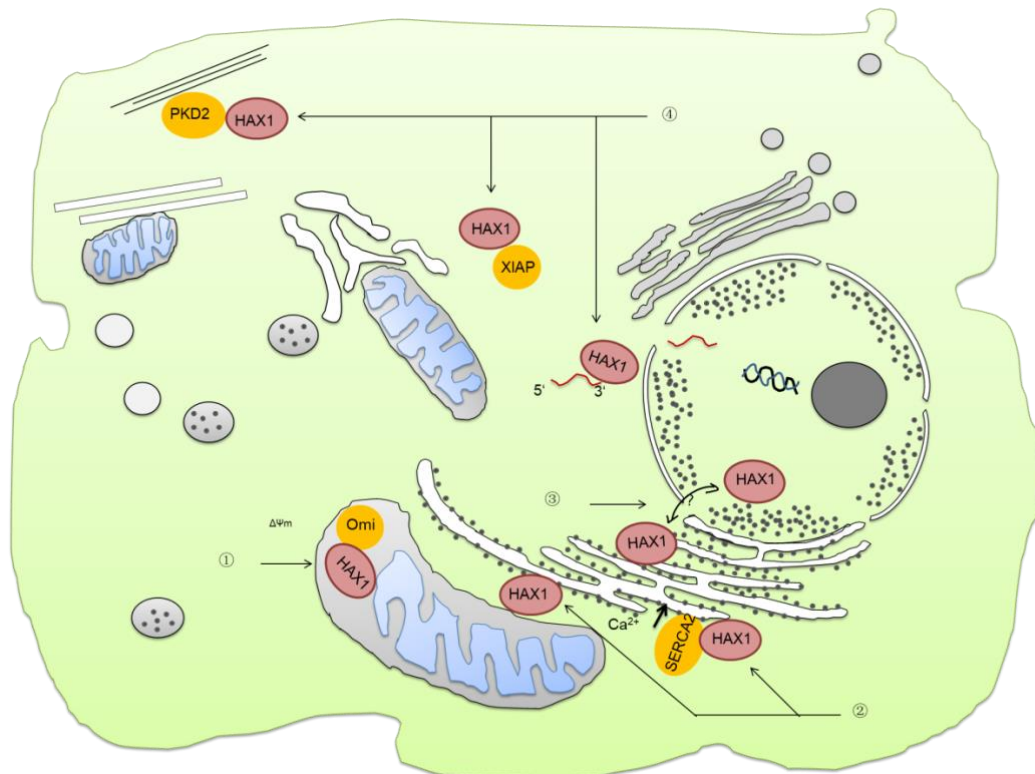


**Figure 2. An overview of potential cellular localizations of HAX1.** Taken from (Klein, 2017). 1) mitochondria, 2) endoplasmic reticulum, 3) perinuclear membrane, and 4) cytosol.

## 2 Cellular proteostasis

At any given time, human cells express ca. 10.000 proteins, most of which require correct and efficient folding to accomplish their biological function (Balchin et al., 2016; Kulak et al., 2017). In the crowded intracellular space, production, folding, conformational maintenance, spatio-temporal trafficking, control of protein abundance and disposal by degradation must be tightly controlled so that an intact proteome can be maintained. The balance of protein production, maintenance and decay is referred to as “proteostasis”. A proteostasis network (PN) is mainly composed of three modules, namely protein synthesis, protein folding and conformational maintenance, and protein degradation (Jayaraj et al., 2020).



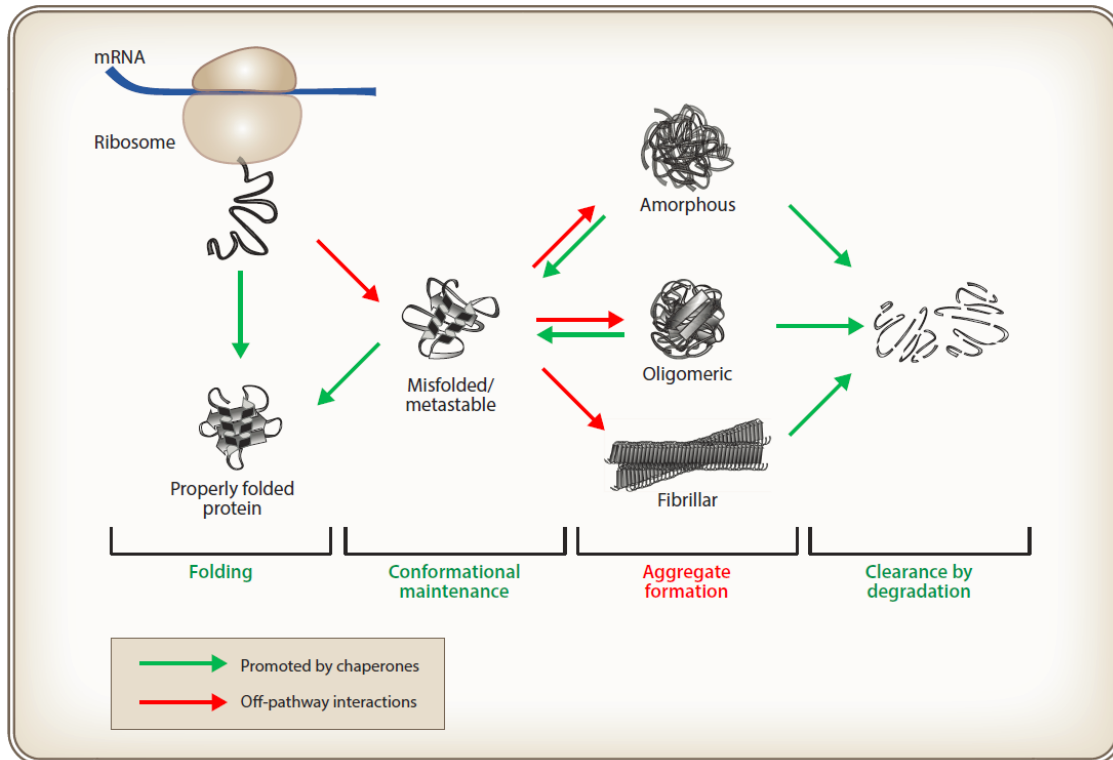


**Figure 3. Scheme illustrating main modules of the proteostasis network.** Taken from (Hartl, 2017).

## 2.1 Protein synthesis control

For proper nascent polypeptide chain synthesis, around 300 protein components are directly involved in the constituents of the translational machinery (Rouillard et al., 2016; Wolff et al., 2014). During protein translation, specific chaperones associate with the nascent chain emerging from ribosome. This interaction protect the proper folding of nascent polypeptides by preventing misfolding of the nascent chain and assisting in the process of cotranslational folding on the ribosome (Klaips et al., 2018). Concomitantly, UPS (ubiquitin–proteasome system) plays a role in the process of ribosomal quality-control by removing stalled nascent polypeptides during protein synthesis (Amm et al., 2014). Some newly synthesized proteins may fold cotranslationally within the polypeptide exit tunnel or at the surface of the ribosome. Some might completely folded when they are released from ribosomes (Kaiser and Liu, 2018; Liutkute et al., 2020). For some proteins, the folding and assembly into oligomeric complexes is mediated by various sorts of chaperone (Balchin et al., 2016; Langer et al., 1992). In addition, many chaperones also

participate in processes after protein synthesis. For example, they may also take a part in protein refolding, protein disaggregation and protein degradation (Cristofani et al., 2017).

## 2.2 Chaperones

The human genome encodes approximately 332 chaperones and co-chaperones (Brehme et al., 2014). In general, they are grouped via their molecular weight (MW). Many chaperones are identified as heat shock proteins (Hsps) because they respond to a wide variety of physical and metabolic stress, in particular to thermal stress challenging the folding of proteins. The main classes of chaperones are composed of ATP-dependent and ATP-independent heat shock proteins. ATP-dependent HSPs are including Hsp60s, Hsp70s, Hsp90s and Hsp100s. Yet, only some small HSPs are ATP-independent. Small heat shock proteins cooperate with regulating co-chaperones for specifying and selecting client substrates (Brehme and Voisine, 2016; Jayaraj et al., 2020)

The Hsp70 chaperone family (DnaK in prokaryotes), in cooperation with the Hsp40 class, participates in the initial folding of nascent chains, protein conformational maintenance, disaggregation and degradation of misfolded proteins (Hartl and Hayer-Hartl, 2002; Meimaridou et al., 2009; Tessarz et al., 2008). Additionally, Hsp60s adopt client proteins that fail to be processed by Hsp70/Hsp40 system. At the downstream of Hsp70, Hsp90 chaperone system functions as signaling players. They involve in the conformational regulation of particular proteins engaged in cell signaling (Balchin et al., 2016; Pratt et al., 2015; Sharma et al., 2012; Taipale et al., 2012).

Together with the Hsp70 system, sHsps mechanistically bind misfolded or unfolded proteins and prevent them from the accumulation of toxic aggregate species in an ATP-independent fashion, which is critical for preserving the proteome stability (Haslbeck et al., 2019). However, when the system is overloaded, partially misfolded or misfolded species will form aggregates (Klaips et al., 2018). On the other hand, aggregates associated with sHsps and chaperone cofactors are able to be further processed (Bakthisaran et al., 2015; Haslbeck et al., 2005; Mogk et al., 2003; Zwirowski et al., 2017) and eventually disaggregated by Hsp70/Hsp40/Hsp110 machineries (Rampelt et al., 2012; Shorter, 2011). The cellular disaggregation

capacity can be further promoted by a group of AAA+ ATPase family proteins (ClpB in *Escherichia*, Hsp104 in yeast and CLPB in metazoans) and has been shown to cooperate with Hsp70/Hsp40 cofactors for aggregate extraction (Cupo and Shorter, 2020; Doyle and Wickner, 2009; Wegrzyn et al., 2001).

### 2.3 UPS and autophagy

Whenever intervention of chaperones is unable to prevent protein misfolding, terminally misfolded proteins have to be cleared via the cellular degradation machinery. Proteolytic degradation mainly acts by the ubiquitin-proteasome system (UPS) and chaperone-mediated lysosomal degradation (Forster et al., 2013; Varshavsky, 2017). During UPS-mediated degradation, substrates covalently modified with ubiquitin are recognized by the 26S proteasome and are further unfolded by the 19S regulatory particle before eventual degradation via the 20S catalytic unit (Zheng and Shabek, 2017). While the insoluble aggregates and larger inclusions can be further removed by the selective autophagy together with lysosomal degradation (Galluzzi et al., 2017; Kaushik and Cuervo, 2018).

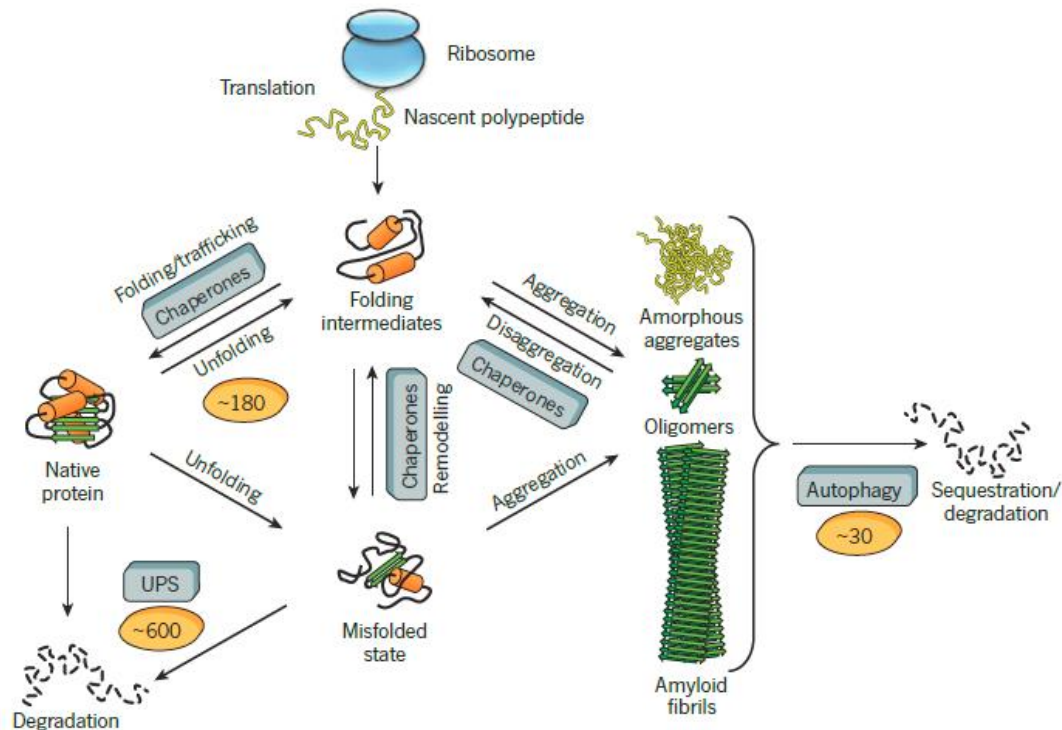


**Figure 4. Protein fates in the proteostasis network.** Taken from (Hartl, 2011). The proteostasis network is composed of various chaperone pathways (180 different chaperone components), for newly synthesized proteins' folding and protein native conformation maintenance, for misfolded proteins' remodeling and for protein degradation. The latter can be mediated by ubiquitin-

proteasome system (UPS) (~600 components) and the autophagy- lysosomal pathway (ALP) (~30 components).

## 2.4 Protein responses to perturbed proteostasis

A variety of signaling pathways react to perturbed proteostasis to allow the coordination of a functionally competent proteome. Different stress-response pathways are activated so that cells can accordingly adjust to cellular stress. As a result, client substrates are less loaded and aggregated proteins are dissolved. Meantime, components of PN (proteostasis network) are upregulated (Figure 5). Therefore, cells manage to be responsive to changes inside or outside cells through monitoring and adjusting proteome status in a real-time manner (Klaips et al., 2018).

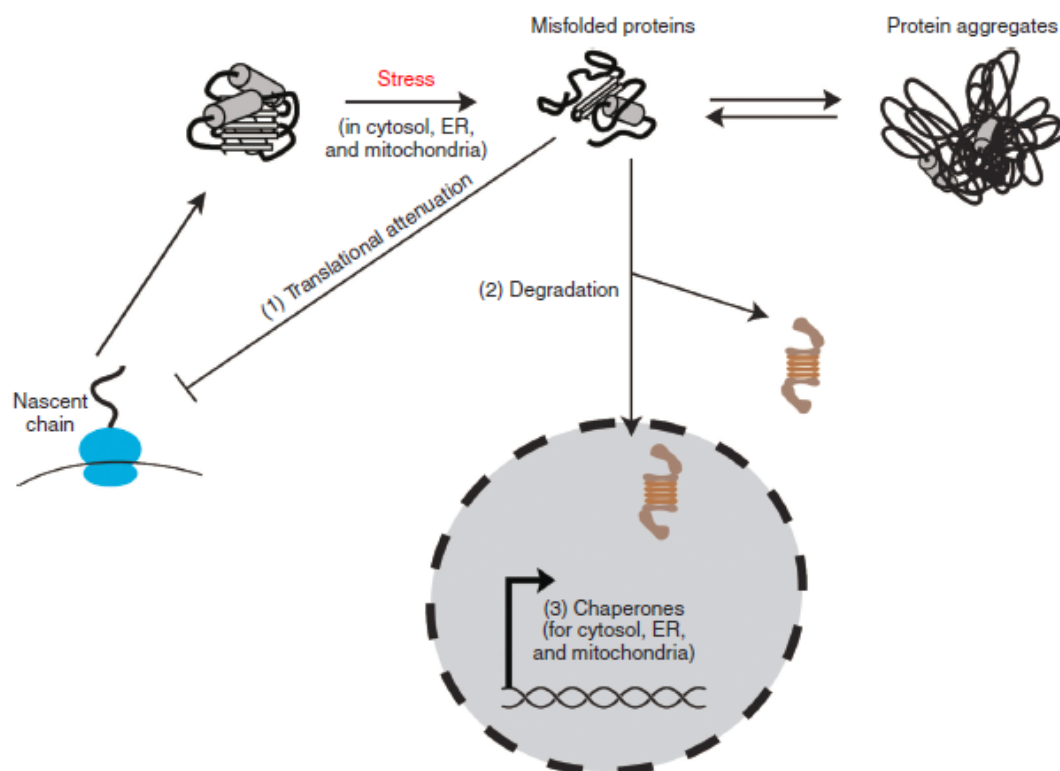


**Figure 5. Stress responses for the maintenance of cellular proteostasis.** Taken from (Gopal G. Jayaraj et al., 2020). In response to protein damage in a variety of cellular localizations, the competence of proteostasis is regulated and with adjustment to meet specific cellular requests. This includes translational decay to reduce the load on the folding machineries (1) releasing chaperone involved in removing misfolded and aggregated proteins (Mu et al.) (2), and activation of transcriptional stress response pathways, expanding chaperone pools that can be used for protein folding and degradation (3).

To deal with cytosolic stress, cells have evolved the cytosolic heat stress response, which is mediated by heat shock factor 1 (HSF1) in eukaryotes (Anckar and Sistonen, 2011; Vabulas et al., 2010). Upon cellular stress, HSF1 is activated to transcriptionally activate a variety of molecular chaperones (Hsps) and other quality-control components. These chaperones further protect protein from aggregation and participate in the process of protein refolding or degradation by the UPS (Jayaraj et al., 2020; Richter et al., 2010). In addition, HSF1 acts to transiently attenuate protein translation (Li et al., 2013a; Shalgi et al., 2013). Once the stressor is removed, HSF1 is supposed to be deactivated by a negative-feedback loop so that cellular proteostasis can be again guaranteed (Krakowiak et al., 2018).

In each organelle, specific response pathway in response to transcriptional stress are applied, such as the unfolded protein response pathways of endoplasmic reticulum (UPR<sup>ER</sup>) and mitochondria (UPR<sup>mt</sup>), to prevent accumulation of misfolded proteins in specific organelles (Karagoz et al., 2019; Walter and Ron, 2011). The UPR is sensed by three transmembrane signaling proteins. They are inositol requiring element 1 (IRE1), PKR-like endoplasmic reticulum kinase (PERK) and activating transcription factor 6 (ATF6). These signaling proteins are activated and induce a variety of downstream transcription factors, in an effort to generate a number of proteostasis items (Klaips et al., 2018; Okada et al., 2002; Walter and Ron, 2011).

PERK phosphorylates and deactivates the eukaryotic translation initiation factor 2 $\alpha$  (eIF2 $\alpha$ ), resulting in translational decay (Frakes and Dillin, 2017; Walter and Ron, 2011). ATF6 is proteolytically cleaved and translocated to the nucleus to transcriptionally promote the activation of chaperones in endoplasmic reticulum. Similarly, ATF5 is responsible for transcriptional induction of chaperones to mitochondrial unfolded protein response. IRE1 splices the mRNA of XBP1, leading to a transcriptional activation of genes associated with misfolded protein export and degradation (Jovaisaite et al., 2014).

An increasing number of studies demonstrate that a crosstalk among different stress-induced responsive pathways is of importance for cell fitness. For example, UPR<sup>ER</sup> leads to the cellular aggregation of metastable proteins (Hamdan et al.,

2017). Moreover, UPR<sup>mt</sup> increases the levels and activity of chaperones and the proteasome system in the cytosol to reduce the impact of toxic aggregates (Boos et al., 2020). Whereas the detailed mechanisms for UPR induction is different from that of the heat shock reaction in cytosol, both share a final determination: an increase in quality-control elements and a decrease in transient attenuation of translation of potentially misfolded substrates (Klaips et al., 2018).

## 2.5 Proteostasis and disease

Safeguarding and maintaining an intact cellular proteome (“proteostasis”) relies on complex control mechanisms, such as chaperones and quality-control items that are functionally associated with machineries regulating protein degradation (Klaips et al., 2018). Several common and age-related human diseases (e.g., Alzheimer and Parkinson disease, type II diabetes) have been linked to aberrant proteostasis leading to intractable amyloid aggregates (Chiti and Dobson, 2017). In particular, neurological diseases have served as a prime paradigm for understanding the pathological role of aberrant protein aggregation in cells (Dubnikov and Cohen, 2017; Hartl, 2017). With few exceptions (e.g. alpha-1-antitrypsin deficiency, Heinz body anemia, inherited amyloidosis), proteostasis in rare monogenic diseases affecting non-neurological cells has not systematically been addressed (Mannini and Chiti, 2017).

Understanding the mechanisms controlling proteostatic networks is highly relevant for the development of novel therapies. In neuronal diseases, several strategies to modulate proteostatic networks using expression of co-chaperones (Klaips et al., 2018), small molecules disrupting the stress-induced dephosphorylation of the  $\alpha$  subunit of translation initiation factor 2 (eIF2 $\alpha$ ) (Tsaytler et al., 2011) or inhibiting the deubiquitinating activity of human USP14 (Lee et al., 2011) have been proposed. Enhancing stress-response pathways (e.g. by small molecules or the transcription factor HSF-1) has been shown to be associated with life-span extension and “proteostatic health” (Kasuske and Hansen, 2018; Mu et al., 2008). Recently, mitochondrial translation and mitophagy pathways have been targeted to increase the fitness and lifespan of worms and transgenic mouse models of Alzheimer's disease (Sorrentino et al., 2017). Even though novel therapeutic strategies aiming at reconstitution of proteostatic networks in neurodegenerative disorders have not

yet resulted in clinical breakthroughs, current data indicate that promising new principles emerge in cell and animal models.

### 3 Mitochondria and mitoproteostasis

#### 3.1 General introduction of mitochondria

Mitochondria are often seen as the “powerhouses” for the cell. Their ATP generation via oxidative phosphorylation (OXPHOS) is highly relevant for cellular function. While the origin of mitochondria remains a matter of debate, the most widely accepted explanation is the endosymbiotic hypothesis. According to this hypothesis, mitochondria arise from a proteobacterium, engulfed and thereby annexed by some ancestral type of eukaryotic host cell (Gray, 2014; Imachi et al., 2020; Martin, 2017; Martin et al., 2015). Since that time, and strikingly different from other eukaryotic organelles, mitochondria have retained two phospholipid bilayers: the outer membrane (OM), which separates mitochondria from the cytosol; the inner membrane (IM), which encompasses an aqueous compartment, namely mitochondrial matrix. The intermembrane space (IMS), another fluid compartment, exists between the two mitochondrial membranes (Palade, 1953). In addition, there are lamellae of the IM, folding inwards and thus generating sequestered zone, namely “cristae” (Figure 6). These foldings allow more membrane to be packed into the mitochondrion. Cristae are the sites, where the oxidative phosphorylation system (OXPHOS) exists and functions for mitochondrial ATP production (Cogliati et al., 2016; Stoldt et al., 2018).

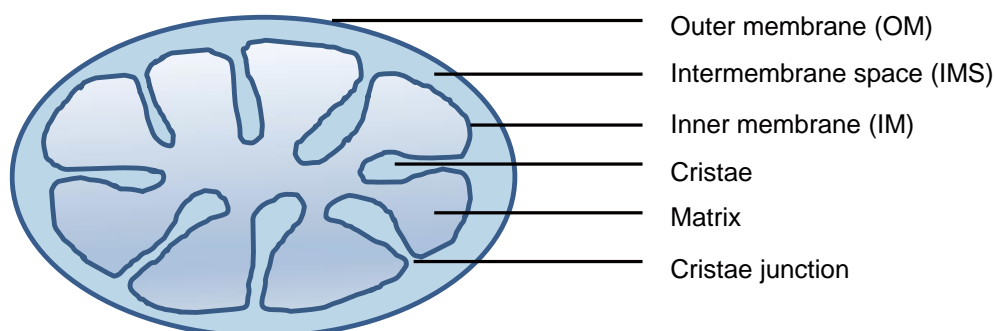


**Figure 6. General architecture of mitochondria.**

In addition to cellular ATP production, mitochondria are fully or partially involved in many metabolic pathways and cycles, such as the TCA cycle, fatty acid oxidation,

one-carbon cycle, urea cycle, heme biosynthesis, cardiolipin synthesis, quinone and steroid biosynthesis (Eaton et al., 1996; Lill, 2009). Moreover, mitochondria are supposed to participate in the process of synthesizing heme and iron sulfur clusters, as well as various signalling pathways, such as calcium signalling and apoptosis (Stehling and Lill, 2013; Vandecasteele et al., 2001; Wang and Youle, 2009). Additionally, mitochondria are involved in controlling innate immunity, developmental processes as well as aging (Green, 2005; Weinberg et al., 2015).

### **3.2 The oxidative phosphorylation system and mitochondrial superoxide ( $O_2^{\cdot-}$ ) production**

The oxidative phosphorylation system (OXPHOS) consists of four multimeric complexes: complex I, II, III and IV. These four complexes incorporate with complex V (ATP synthase) in biosynthesis of ATP (adenosine-5'-triphosphate). Except for mitochondrial complex II whose proteins are all encoded by the nuclear genome, all other complexes are encoded by both the nuclear and mitochondrial genome. In an 'orthodox' state, through chemical reactions of OXPHOS, electrons provided by the citric cycle are transferred through four complexes and utilized to reduce oxygen to water. During the electrons transfer, a proton gradient is thus generated on both sides of mitochondrial inner membrane. The proton gradient is further employed to generate ATP via mitochondrial complex V (Figure 7).

Not surprisingly, the process of electron transport is highly complex. First, electrons are transferred from the TCA cycle (tricarboxylic acid cycle) or  $\beta$ -oxidation, via the reducing equivalents NADH or FADH<sub>2</sub> to the complex I (NADH:ubiquinone oxidoreductase) or to complex II (succinate dehydrogenase) (Zhu et al., 2016). During the oxidative reaction of NADH within complex I (NADH:ubiquinone oxidoreductase), four protons are pumped from matrix into IMS. Of note, complex II (succinate dehydrogenase) transports electrons but does not pump protons as a result of insufficient energy production. Both complexes transfer electrons to ubiquinone (Q), which transfers its electrons through the membrane to complex III (ubiquinol cytochrome c reductase). Complex III transfers cytochrome c electrons and two more protons are pumped out to the mitochondrial intermembrane space with energy yield (Guzy et al., 2005). Cytochrome c, bound to the outer face of the



inner membrane, brings electrons to cytochrome c oxidase (complex IV), from which four electrons are ultimately passed to oxygen (forming water), while protons are being transferred across the IM to the IMS (Castresana et al., 1994). Thus, electrons pass through the electron transport chain (ETC) and release energy to pump protons out of the mitochondrial matrix, which generates an electrochemical gradient. When protons flow back, they pass through F1F0ATP synthase (complex V) and drive ATP synthesis.

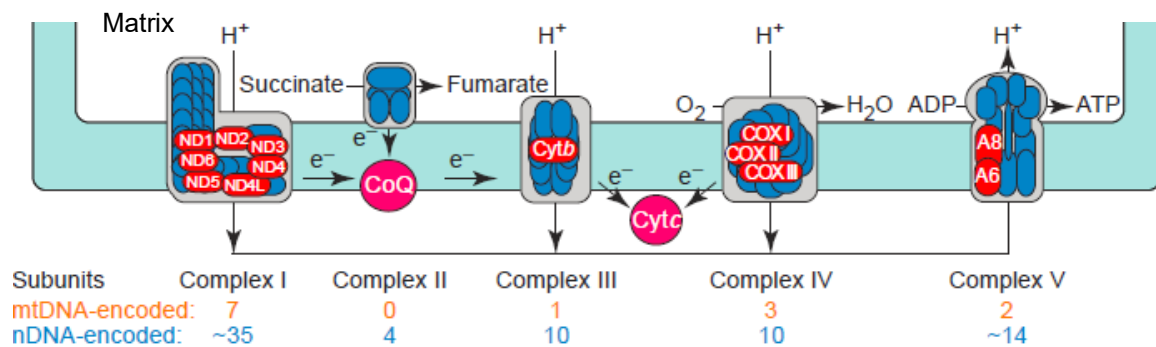


**Figure 7. The Oxidative phosphorylation system (OXPHOS).** Taken from (Schon, 2000). OXPHOS complexes are composed of nuclear DNA-encoded (blue) and mitochondrial DNA-encoded components (red). Electrons are transferred to the first two complexes (complex I and II) from the mitochondrial matrix and passed to complex IV for reducing oxygen into water. A proton gradient is generated along with electron transport via the complexes I, III and IV, which fuels complex V for ATP synthesis.

Along the cascade of ATP synthesis, electrons may leak from the ETC (reverse electron transfer) and react improperly with  $O_2$  to generate superoxide ( $O_2^{\cdot-}$ ). The superoxide anion can be further converted into hydrogen peroxide ( $H_2O_2$ ) and hydroxyl radical ( $\cdot OH$ ). The combination of these three species is the so-called reactive oxygen species (ROS). Complex I and complex III are thought to be the main sites in the ETC for producing superoxide. Under normal conditions (forward electron transfer mode), little superoxide is produced in mitochondrial complexes. However, when complex I inhibitors such as rotenone are added, electrons are reversely transferred to react with oxygen. This leads to a release of superoxide from complex I to the matrix (Ramsay and Singer, 1992). Similar to the consequences of complex I dysfunction, an extensive amount of superoxide is

produced in the IMS when the activity of complex III is impaired (e.g. by its inhibitor antimycin (Quinlan et al., 2011). As a multi-subunit complex (14 core and 31 accessory proteins), complex I is specifically characterized by a slow transition of active to deactive state, suggesting gross conformational rearrangements of complex I, which may in part be involved in its superoxide production (Gavrikova and Vinogradov, 1999).

Once complex II was considered to produce superoxide only upon impairments or mutations arising in the complex (Yankovskaya et al., 2003). The thought has been questioned when complex II is shown to be able to generate superoxide in the forward reaction via its prosthetic flavin adenine nucleotide moiety (Quinlan et al., 2012). Since the experimental ambient (5-10mM) concentrations of succinate exceed the physiological succinate levels in the tissue (in a range of hundreds of micromoles), the involvement of complex II in ROS formation still remains undetermined (Zorov et al., 2014). Besides, superoxide could be generated by other mitochondrial components, such as  $\alpha$ -ketoglutarate dehydrogenase,  $\alpha$ -glycerophosphate dehydrogenase and dihydroorotate dehydrogenase (Venditti et al., 2013).

### **3.3 Mitochondrial supercomplexes**

The functional organization of OXPHOS complexes has been largely discussed. Based on the 'plasticity model', OXPHOS complexes are thought to be existed in single complexes and supercomplexes (SCs) of distinct constitution and stoichiometry (Cogliati et al., 2016). The identification of supercomplexes was reported by Schaeffer et al in 2000, who resolved OXPHOS complexes and supercomplexes via BN-PAGE (Milenkovic et al., 2017; Schagger and Pfeiffer, 2000). Recent studies indicate that the major recognized supercomplexes incorporate heterogenic OXPHOS complexes, which can be mainly categorized into three species: complex I+III, I+III+IV, and III+IV (Acin-Perez et al., 2008; Dudkina et al., 2005; Lobo-Jarne and Ugalde, 2018; Schagger, 2001; Stroh et al., 2004) (Figure 8). This existing assembly group allows a more efficient electron transfer and reduces the production of mitochondrial ROS (Bianchi et al., 2004; Lopez-Fabuel et al., 2016). Complex I is mostly identified to be related with SCs as for its enhanced stability (Cogliati et al., 2016). Additionally, complex III and IV are capable of forming

homodimers (Letts and Sazanov, 2017). Yet, complex V can be found as a monomer or as a homodimer, not associating with any other complexes, which is thought to be crucial for cristae formation (Hahn et al., 2016).

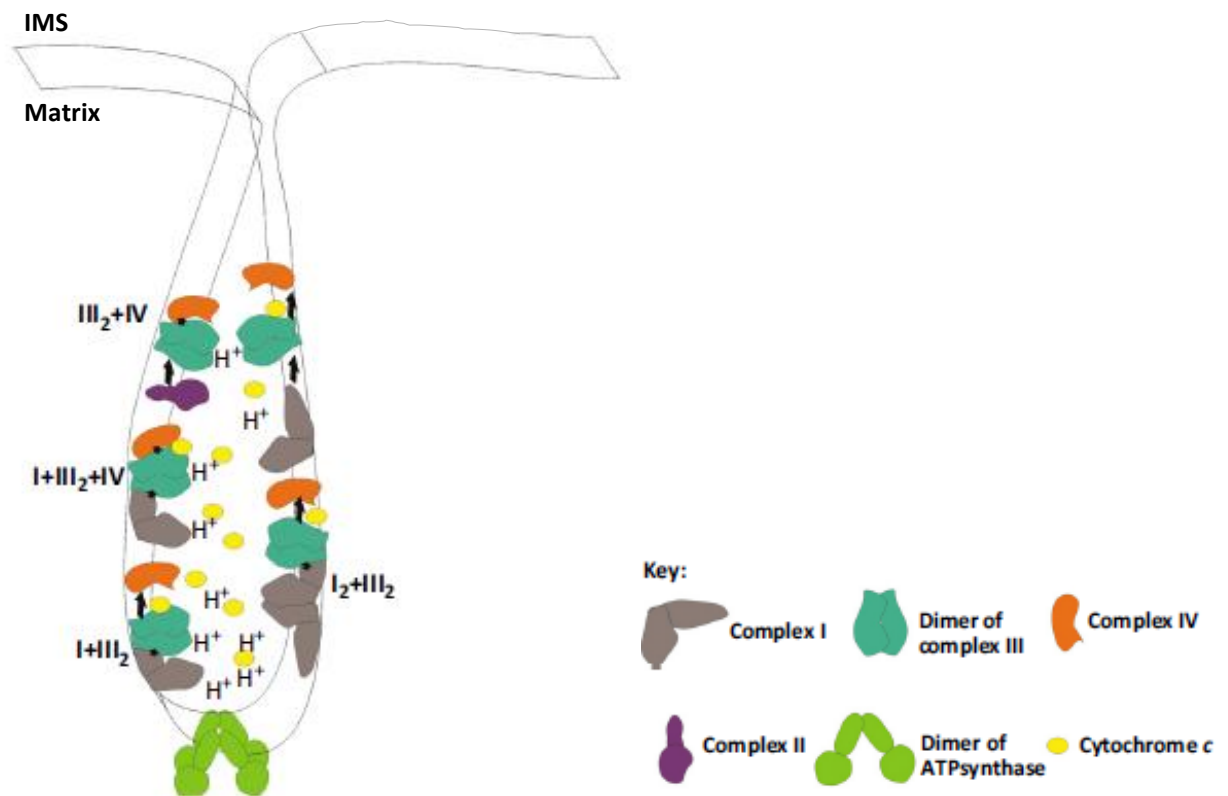


**Figure 8. Different forms of mitochondrial supercomplexes located in cristae.** Taken from (Cogliati et al., 2016).

### 3.4 Regulation of mitochondrial proteostasis

The mitochondrial proteome consists of more than 1000 proteins, but only 13 proteins are encoded by the mitochondrial DNA. They are all components of OXPHOS (Anderson, 1981). The vast majority of mitochondrial proteins is synthesized in the cytosol and subsequently imported into the organelle via the TIM/TOM (translocase of inner and outer membrane) complexes (Chacinska et al., 2009; Neupert and Herrmann, 2007). In view of the high protein concentration within mitochondria maintenance of mitochondrial protein homeostasis is a unique challenge (Naresh and Haynes, 2019).

### 3.4.1 Mitochondrial protein synthesis

To maintain organelle homeostasis, mitochondria have developed several regulatory mechanisms. Alterations of cytosolic translation contributes to mitochondria-encoded protein synthesis, via control of translational activators (Couvillion et al., 2016). Furthermore, mitochondrial ribosomes exhibit translational plasticity to adjust mitochondrial translation to the availability of nuclear-encoded subunits and thereby adapt mitochondrial protein production to the cellular demands (Richter-Dennerlein et al., 2016). Thus, though mitochondrial double membranes separate cytoribosomes from mitoribosomes and a lack of shared components between nuclear and mitochondrial translation systems, translation regulation of OXPHOS subunits from two genomes can still be synchronized across cellular compartments (Couvillion et al., 2016).

### 3.4.2 Protection during protein import

Nuclear-encoded proteins have to translocate across mitochondrial membranes. This process is mediated by the outer mitochondrial membrane (TOM) complex and the inner membrane TIM23 complex. The TOM complex (consisting of Tom70, Tom40, Tom22, Tom20, Tom7, Tom6 and Tom5) functions as general entry gate for preproteins into mitochondria, mediating proteins transfer across the outer membrane (Asai et al., 2004; Bolliger et al., 1995; Komiya et al., 1998; Mayer et al., 1995). The inner membrane TIM23 complex (consisting of Tim50, Tim44, Tim23, Tim21, Tim17, Tim16/Pam16, Tim14/Pam18, mtHsp70 and Mge1) mediates translocation of preproteins across and into the inner membrane, resulting from a protein-conducting channel and the import motor in Tim23 complex (Chacinska et al., 2005; Donzeau et al., 2000; Matouschek et al., 2000; Mayer et al., 1995; Moro et al., 1999; Ungermann et al., 1994).

Mitochondrial precursor proteins can smoothly be transported through pore structures consisting of translocons on the basis of being kept unfolded (Mokranjac et al., 2003). As a result, hydrophobic regions of premature proteins are at high risk to unwanted protein–protein interaction and consequently possible aggregation. However, these undesired consequences are routinely controlled by a group of chaperones (Baker et al., 2011). For example, Hsp70 and Hsp90 guide newly synthesized proteins to the mitochondrial surface and then mtHsp70 mediates the

process of importing newly synthesized precursors into mitochondria. Along with the import, mtHsp70 involves as well in removing the mitochondrial targeting peptides from N-terminal of individual protein in an ATP-dependent manner (Kang et al., 1990). Concomitantly, mtHsp70 can also maintain proteins in an unfolded conformation for a correct tertiary structure after entering mitochondria. In addition, Hsp60, in conjunction with Hsp10, encapsulates and allows proteins to fold in the crowded milieu of the mitochondrial matrix (Horwich et al., 1999).

### **3.4.3 Mitochondrial proteases**

In addition to chaperones, proteases also play critical roles in mitochondrial proteostasis. Proteases are responsible to alleviate mitochondrial stress caused by degrading unfolded proteins (e.g., proteins unable to be refolded, redundantly unassembled subunits or unwanted by-products of OXPHOS). HtrA2 allows unfolded respiratory chain subunits to be cleared in the IMS (Baker et al., 2011). There inserted two species of AAA<sup>+</sup> metalloprotease securing appropriate proteolysis in mitochondrial innermembrane (Koppen and Langer, 2007): i-AAA protease acting in IMS and m-AAA protease functioning in mitochondrial matrix. Both proteases act to degrade various misfolded or unassembled IM proteins, peripherally connected or incorporated into the IM (Arlt et al., 1996; Korbel et al., 2004; Leonhard et al., 1996). Furthermore, the proteases Lon and ClpP remove impaired proteins from the mitochondrial matrix (Fischer et al., 2012) (Figure 9).

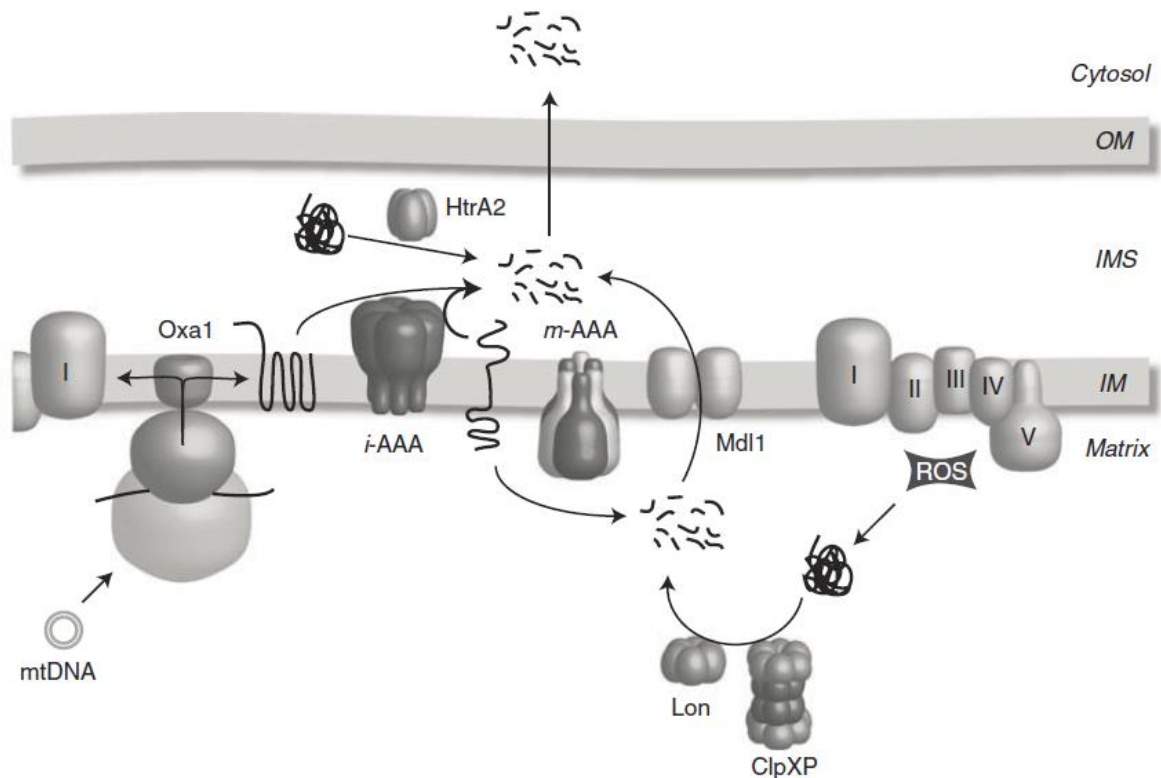


**Figure 9. Proteolytic systems in mitochondrial proteostasis.** Taken from (Baker et al., 2011). mtDNA encoded subunits were synthesized via mitochondrial ribosomes and inserted into the IM by Oxa1 prior to assembly with imported nuclear encoded subunits. Misformed protein components associated with mitochondrial innermembrane are degraded by AAA protease complexes (Michael J. Baker et al., 2011). Misformed protein components in the matrix are degenerated by Lon or ClpXP. Resolved peptides created in the mitochondrial matrix are further released from the matrix via transporter Mdl1 into cytosol. HtrA2 is supposed to function in degradation of misformed protein in the IMS.

Not only the i-AAA protease, but also the inner membrane protease PARL (presenilin associated rhomboid like protease) acts in the IMS to control protein quality. PARL is recognized to process PINK (the PTEN-induced kinase) so that it can further act in the regulation of mitophagy and the activity of respiratory complex I. PARL also cleaves PGAM5 (a mitochondrial phosphatase), which plays a role in mitophagy, mitochondrial fission and cell death (Chen et al., 2014; Jin et al., 2010; Morais et al., 2014; Sekine et al., 2012; Wang et al., 2012). Another substrate of PARL is SMAC. Upon proteolytical processing, SMAC is further released into the cytosol and activates caspase signaling by prohibiting inhibitors of apoptosis (IAPs) (Saita et al., 2017). PARL associates with SLP2 (stomatin-like protein 2) and the i-AAA protease

YME1L as a proteolytic hub in the IM to mediate the processing of PINK1 and PGAM5 in the IMS (Wai et al., 2016).

#### **3.4.4 Mitochondrial dynamics regulated by UPS and autophagy**

The UPS is an important multicomponent system, accounting for removing proteins from various cellular compartments in cytosol (Hershko, 2005). Several lines of evidence show that the UPS is also involved in mitochondrial protein quality control. First, the OM is accessible to the UPS machinery. Certain mitochondrial outer membrane proteins are ubiquitinated prior to be degraded via the UPS system (Livnat-Levanon and Glickman, 2011). Furthermore, mistargeted mitochondrial precursor proteins can be removed via the UPS. Moreover, the turnover of proteins residing in IMS and IM is dependent on the proteasome (Radke et al., 2008). Intriguingly, inactivation of the proteasome prevents protein turnover of mitochondrial matrix proteins, suggesting that proteins in matrix can be transported out of OM for the degradation via proteasome (Azzu and Brand, 2010; Heo and Rutter, 2011; Margineantu et al., 2007).

Mitochondria dynamically proceed with fission and fusion events which also contribute to maintain proteostasis and regular protein function (Chan et al., 2011; Tanaka et al., 2010). Fusion combines mitochondrial pools and thus dilute impaired proteins, in particular in response to moderate mitochondria damage. In contrast, fission contributes to discarding damaged portions from a healthy mitochondrial network. Fission follows severe damage to mitochondria and usually precedes final disposal via mitophagy (Okamoto et al., 2009). Loss of the mitochondrial fusion moderator lead to a decreased activity of mitochondrial complexes (Chen et al., 2007; Tatsuta and Langer, 2008). Impaired mitochondrial fission prohibits the removal of defective mitochondria by autophagy (Tanaka et al., 2010).

#### **3.4.5 Mitochondrial unfolded protein response (UPR<sup>mt</sup>)**

Activation of the UPR<sup>mt</sup> results from a wide range of proteotoxic stresses, such as impairment of mitochondrial translation, interference of mitochondrial chaperones or proteases, excessive reactive oxygen species (ROS) and misfolded protein (Fiorese and Haynes, 2017; Haynes et al., 2007; Houtkooper et al., 2013; Munch and Harper, 2016; Zhao et al., 2002). In line with cytosolic UPR, a mitochondrial-specific UPR has evolved to manage imbalanced mitochondrial proteostasis via mitochondrial-

nuclear signaling to regulate the unfolded protein load (protein import and translation), mitochondrial folding capacity, antioxidant capacity and protein quality control (Munch, 2018). Specifically, UPR<sup>mt</sup> encompasses three pathways, the CHOP axis (canonical axis), the Sirtuin axis, and the Era axis (Figure 10).

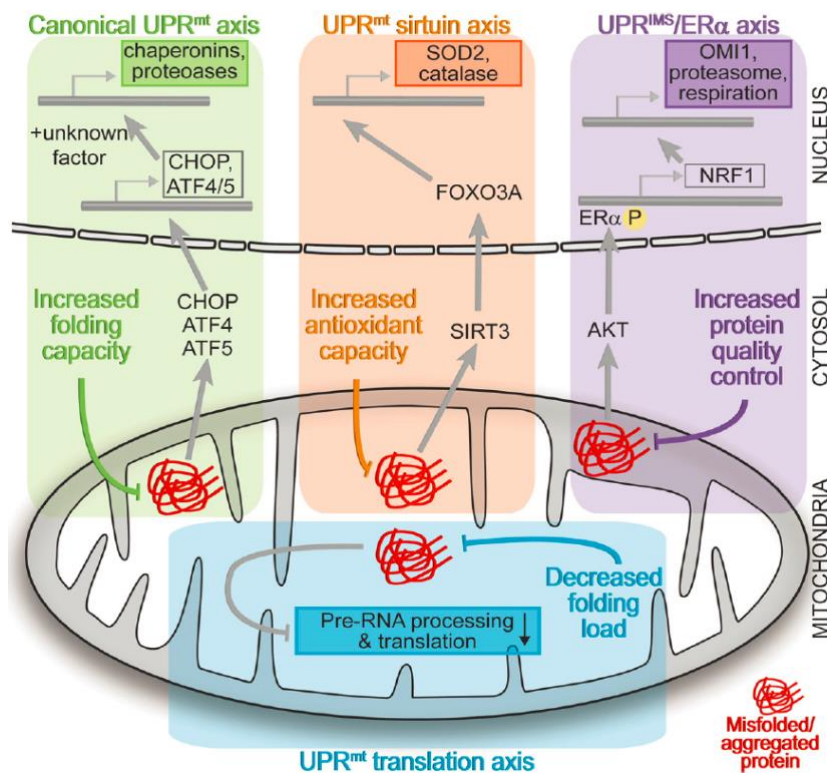


**Figure 10.** The main axes of mammalian UPR<sup>mt</sup>. Taken from (Munch, 2018).

UPR<sup>mt</sup> axes are activated upon mitochondrial proteotoxic stress as a result of protein misfolding or aggregation inside mitochondria. The canonical UPR<sup>mt</sup> axis contributes to translocations and varied expressions of CHOP, ATF4, and ATF5 (Fusakio et al., 2016; Teske et al., 2013; Zhao et al., 2002). Together with other currently unknown transcription factors, this axis induces elevated chaperonins, chaperones, and proteases to expand the folding capacity inside mitochondria (Aldridge et al., 2007; Pakos-Zebrucka et al., 2016). Moreover, UPR<sup>mt</sup> sirtuin axis is activated and results in deacetylation and relocalization of FOXO3A, which upregulates the expression of SOD2 and catalase. This is of importance as an antioxidant response in mitochondria (Brunet et al., 2004; Sundaresan et al., 2009; Tao et al., 2014). In the mitochondrial intermembrane space, misformed proteins trigger the UPR<sup>IMS</sup>-ER $\alpha$  axis, acting via AKT and ROS-dependent phosphorylation



of ER $\alpha$  and NRF1 initiation (Papa and Germain, 2014; Scarpulla, 2006; Zhang et al., 2014). The activation of UPR<sup>IMS</sup>-ER $\alpha$  axis further increases protease activity, adjustment of respiration levels, and escalated proteasome activity – all these factors contribute to increased protein quality control capacity (Kenny and Germain, 2017; Papa and Germain, 2011; Radke et al., 2008). As a local stress response, the UPR<sup>mt</sup> translation axis is activated to decrease the unfolded protein load, due to perturbed proteostasis in the matrix. Specifically, protein translation and protein import are reduced (Bernstein et al., 2012; Kang et al., 2007; Nargund et al., 2015; Nargund et al., 2012). Even though the UPR<sup>mt</sup> axes are based on molecularly distinct pathways, they are thought to be reciprocally beneficial and initiated in parallel (Munch, 2018).

## II MATERIALS AND METHODS

### 1 Materials

#### 1.1 Reagent

Table 1. The summary of reagent included in this study.

Chemical	Supplier
2-mercaptoethanol ( $\beta$ -mercaptoethanol)	Sigma-Aldrich
Acetone	AppliChem
Acrylamide/bisacrylamide (37.5:1) solution	Roth
Agarose Basic	AppliChem
Ampicillin	AppliChem
Anti-FLAG M2 agarose beads	Sigma-Aldrich
Antimycin A	Sigma-Aldrich
BlueRay Prestained Protein Marker	Jenabioscience
Borsaeure	Carl Roth
Bovine serum albumin (BSA)	AppliChem
Bromophenol Blue	Merck
Calcium chloride ( $\text{CaCl}_2$ )	Carl Roth
Digitonin	Sigma
DMEM (Dulbecco's Modified Eagle Medium)	Gibco
DMSO (dimethylsulfoxide)	AppliChem
DNA Ladder Mid Range	JenaBioscience
Doxycyclin	Sigma
DTT (1,4-dithiothreitol)	Carl Roth
EDTA dihydrate	BioChemica
Ethanol	Sigma
Ethidium bromide	AppliChem

Glucose	Carl Roth
Glycerol	Sigma-Aldrich
Glycine	Carl Roth
HEPES	Carl Roth
Hydrochloric acid (HCl) 37%	Carl Roth
L-Glutamine 200 mM	ThermoFisher
Magnesium chloride (MgCl <sub>2</sub> )	Merck
Methanol	Carl Roth
Milk powder	Carl Roth
MOPS (morpholinopropanesulfonic acid)	Sigma-Aldrich
NP-40 Alternative	Sigma-Aldrich
Onetaq DNA Polymerase	NEB
Oligonucleotides	Eurofin genomics
Opti-MEM	Gibco
Penicillin-Streptomycin (10,000 U/mL)	Gibco
Pierce Protein A Agarose	ThermoFisher
Pierce Protein G Agarose	ThermoFisher
PMSF (phenylmethanesulfonyluoride)	Carl Roth
Poly-L-lysine hydrobromide	Sigma
Potassium chloride (KCl)	Roth
Potassium dihydrogen phosphate (KH <sub>2</sub> PO <sub>4</sub> )	Merck
Potassium hydroxide (KOH)	Carl Roth
Protease Inhibitor Cocktail Tablets (EDTA-free)	Roche
Ponceau S	Applichem
Proteinase K	PEQLAB
Puromycin	Invivogen
Restrictive enzymes	ThermoFisher
Roti-Quant® reagent	Carl Roth
RT-PCR related buffer	ThermoFisher

SDS (sodium dodecyl sulfate)	Carl Roth
Sodium acetat	Carl Roth
Sodium chloride (NaCl)	Carl Roth
Sodium hydroxide (NaOH)	Carl Roth
Sodium bicarbonate (Na <sub>2</sub> CO <sub>3</sub> )	Sigma-Aldrich
Sodium hydrogen carbonate (NaHCO <sub>3</sub> )	Merck
di-Sodium hydrogen phosphate (Na <sub>2</sub> HPO <sub>4</sub> )	AppliChem
Sodium pyruvate 100x	Thermofisher
D(+)-Sucrose, RNase Free and DNase Free	Carl Roth
Tetramethylethylenediamine (TEMED)	Carl Roth
Trehalose	Carl Roth
Trichloroacetic acid (TCA)	Sigma-Aldrich
Tris	Carl Roth
Triton X-100	Sigma-Aldrich
Trypsin for cell culture	Gibco
Tween-20	Carl Roth
Urea	Carl Roth

## 1.2 Kits and disposals

Table 2. The summary of kits and disposals included in this study

Product	Supplier
Amersham Hybond P 0.45 PVDF	GE Healthcare
Anti-FLAG M2 Affinity Gel	Sigma
Amersham Protran 0.2 NC	GE Healthcare
Cell culture falcons	Sarstedt
Cell culture flasks	Sarstedt
Cell culture plates	Sarstedt

Complex I Enzyme Activity Microplate Assay Kit	abcam
Complex IV Enzyme Activity Microplate Assay Kit	abcam
Fast Digest restriction enzymes	ThermoFisher
High-Capacity cDNA Reverse Transcription Kit	ThermoFisher
High Range DNA Ladder	JenaBioscience
Human Stem Cell Nucleofactor Kit 2	Lonza
Mid-Range DNA Ladder	JenaBioscience
Microtube/ Eppitubes	Sarstedt
Pfu1 polymerase	Promega
pGEM-T Vector Kit	Promega
Pipette tips	Biozym
Q5 High-Fidelity DNA Polymerase	NEB
Qiagen MaxiPrep Kit	Qiagen
RNA purification mini kit	ThermoFisher
Stemflex Medium Combo Kit	ThermoFisher
Whatman gel blotting paper	Sigma
Zymoclean Gel DNA Recovery Kits	Zymo
Zyppy Plasmid Miniprep Kit	Zymo

### 1.3 Buffers and solutions

Table 3. The summary of solutions included in this study

<b>Solution</b>	<b>Recipe</b>
Agarose gel solution	1-2% agarose, TBE buffer
Antibody dilution solution	5% BSA in TBST buffer or 5% milk in PBS
Blocking solution (Western blotting)	10% milk powder in PBST
Blocking solution (Slides preparation)	3% BSA, 0.05% Tween in slides washing solution
Blotting buffer	25 mM Tris, 192 mM glycine, 10-15% methanol
Carbonate extraction buffer	0.1M Na <sub>2</sub> CO <sub>3</sub> ; 0.1M NaHCO <sub>3</sub>
Cell culture medium	DMEM (Dulbecco's Modified Eagle Medium) or RPMI (Roswell Park Memorial Institute) supplemented with 10% (v/v) fetal bovine serum, 2 mM L-Glutamine, with penicillin streptomycin (filtered)
Digitonin stock solution	5% digitonin in H <sub>2</sub> O
DNA loading dye	10% saccharose, 0.25% OrangeG
EM buffer	1 mM EDTA, 10 mM MOPS/KOH pH 7.2
Fast lysate buffer (genomic DNA extraction)	50 mM KCl, 10 mM Tris-HCl (pH 8.0), 2.5 mM MgCl <sub>2</sub> , 0.45% NP-40, 0.45% Tween 20, 20 mg/mL Proteinase K
Fixation buffer	3.7% PFA (PFA stock diluted with PBS)
Hypotonic buffer (CST cell lysis buffer)	20 mM Tris-HCl (pH 7.5), 150 mM NaCl, 1 mM Na <sub>2</sub> EDTA, 1 mM EGTA, 1% Triton, 2.5 mM sodium pyrophosphate, 1 mM beta-glycerophosphate, 1 mM Na <sub>3</sub> VO <sub>4</sub> , 1 µg/ml leupeptin
iPSCs culture medium	mTeSR Plus basal medium with mTeSR Plus Supplement

iPSCs differentiation medium	StemPro-34 SFM Complete Medium
Laemmli buffer (6X)	300mM Tris (pH 6.8), 9% SDS, 44% Glycerol, 0.06% bromophenol blue
Permeabilization buffer	0.2% Triton in TBS buffer
Quenching solution	50mM NH <sub>4</sub> Cl
RIPA buffer (for immunoprecipitation)	150 mM NaCl, 25 mM Tris-HCl (pH 7.4), 1 mM EDTA, 1% NP40, 5% Glycerol, 2.5 mM Sodium pyrophosphate, 50 mM Sodium fluoride
SDS-PAGE running buffer	25 mM Tris, 192 mM glycine, 0.1% SDS
SEM buffer for mito-swelling	250 mM sucrose, 1 mM EDTA, 10 mM MOPS/KOH, final pH 7.2
SILAC medium	RPMI 1640 media for SILAC
SILAC lysis buffer	LYSE buffer (preOmics)
Stacking gel (SDS-PAGE)	4% arylamide, 0.1% SDS, 0.1% APS, 0.05% TEMED, 80 mM Tris/HCl at pH 6.8
Solubilization buffer (used for mt-immunoprecipitation)	150 mM NaCl, 10% glycerol, 20 mM MgCl <sub>2</sub> , 1 mM PMSF, 50 mM Tris/HCl, 1% digitonin (final pH 7.4)
Soerengen buffer (cytospin)	133 mM Na <sub>2</sub> HPO <sub>4</sub> , 133 mM KH <sub>2</sub> PO <sub>4</sub>
TBE buffer	89 mM Tris, 89 mM boric acid, 2 mM EDTA (final pH 8.2)
TBS (Tris-Buffered Saline)	150 mM NaCl, 50 mM Tris/HCl (final pH 7.4)
TBST (TBS and Tween-20)	150 mM NaCl, 0.05% Tween-20, 50 mM Tris/HCl (final pH 7.4)
TCA dilution	72% TCA in dH <sub>2</sub> O

TH buffer for mito-isolation	300 mM Trehalose, 10 mM KCl, 10 mM HEPES (final pH 7.4)
Triton lysis buffer	10% Triton in dH <sub>2</sub> O
Washing buffer (Mito immunoprecipitation)	150 mM NaCl, 10% glycerol, 20 mM MgCl <sub>2</sub> , 1 mM PMSF, 50 mM Tris/HCl, 0.1% digitonin (final pH 7.4)
Washing buffer (Slides preparation)	0.02% Triton in TBS buffer

#### 1.4 Antibodies

Table 4. List of antibodies in immunofluorescence analysis and Western blotting

Antibody	Source
Alexa Fluor 488 goat anti mouse	Invitrogen (#A-11001)
Alexa Fluor 633 goat anti mouse	Invitrogen (#A-21052)
Alexa Fluor 633 goat anti rabbit	Invitrogen (#A-21070)
Alexa Fluor 680 goat anti rabbit	Invitrogen (#A-21109)
Alpha Tubulin monoclonal antibody	ThermoFisher (#A11126)
CLPB polyclonal antibody	Proteintech (#15743-1-AP)
Flag monoclonal antibody	Sigma (#F7425-0.2MG)
Foxo3a polyclonal antibody	Cell signaling (#2497)
GAPDH polyclonal antibody	Santacruz (#sc32233)
HAX1 monoclonal antibody	BD biosciences (#610824)
HAX1 polyclonal antibody	Proteintech (#11266-1-AP)
HRP conjugated GAPDH antibody	Proteintech (#HRP-60004)



HRP conjugated alpha Tubulin antibody	Proteintech (#HRP-66031)
HSP27 monoclonal antibody	Proteintech (#66767-1-Ig)
HSP27 polyclonal antibody	Proteintech (#18284-1-AP)
LC3B antibody	Cell signaling (#2775S)
MITARC 12 polyclonal antibody	Gift from Dr. Sven Dennerlein in Göttingen
OPA1 monoclonal antibody	BD biosciences (#612607)
Phospho-HSP27(Ser82) Antibody	Cell signaling (#2406S)
Phospho-HSP27(Ser78) Antibody	Cell signaling (#2405S)
Phospho-HSP27(Ser15) Antibody	Bioworld Technology (#AP0245)
PRKD2 polyclonal antibody	Millipore (-488)
PRKD2 Ser876 phosphorylation antibody	Abnova (# PAB31649)
SMIM12 polyclonal antibody	Gift from Dr. Sven Dennerlein in Göttingen
SLP2 monoclonal antibody	Proteintech (#60052-1-Ig)
Tim23 polyclonal antibody	Gift from Dr. Sven Dennerlein in Göttingen
Tim44 polyclonal antibody	Proteintech (# 13859-1-AP)
Tom20 monoclonal antibody	Proteintech (#66777-1-Ig)
Tom70 polyclonal antibody	Gift from Dr. Sven Dennerlein in Göttingen

## 1.5 Plasmids and Oligonucleotides

Table 5. The summary of plasmids included in this work

Plasmid	Vector	Insertion	Source
PRRL	-	-	Addgene
TRMPVIR	-	-	Addgene

PRRL-HAX1	PRRL	HAX1	This study
PRRL-HAX1- $\Delta$ 1	PRRL	HAX1 deleted exon 1	This study
PRRL-HAX1- $\Delta$ 2	PRRL	HAX1 deleted exon 2	This study
PRRL-HAX1- $\Delta$ 3	PRRL	HAX1 deleted exon 3	This study
PRRL-HAX1- $\Delta$ 4+5	PRRL	HAX1 deleted exon 4 and 5	This study
PRRL-HAX1- $\Delta$ 6+7	PRRL	HAX1 deleted exon 6 and 7	This study
PRRL-HAX1- $\Delta$ 123	PRRL	HAX1 deleted 367bp-504bp	This study
PRRL-HAX1- $\Delta$ 126	PRRL	HAX1 deleted 367bp-504bp	This study
PRRL-HAX1- $\Delta$ 137	PRRL	HAX1 deleted 376bp-504bp	This study
PRRL-HAX1- $\Delta$ 144	PRRL	HAX1 deleted 430bp-504bp	This study
PRRL-HAX1- $\Delta$ 155	PRRL	HAX1 deleted 463bp-504bp	This study
PRRL-HAX1- $\Delta$ 163	PRRL	HAX1 deleted 487bp-504bp	This study
PRRL-CLPB	PRRL	CLPB	This study
PRRL-CLPB- $\Delta$ NTD	PRRL	CLPB deleted NTD domain	This study
PRRL-CLPB- $\Delta$ ANK	PRRL	CLPB deleted ANK domain	This study

PRRL-CLPB- $\Delta$ ATP	PRRL	CLPB deleted ATPase domain	This study
PRRL-CLPB- $\Delta$ CTD2	PRRL	CLPB deleted CTD domain	This study
PRRL-HSP27	PRRL	HSP27	This study
TRbMPVIR	-	-	Addgene
TRMPVIR-scramble	TRMPVIR	shown below	This study
TRMPVIR-PKD2sh1	TRMPVIR	shown below	This study
TRMPVIR-PKD2sh2	TRMPVIR	shown below	This study

Table 6. The summary of oligonucleotides of this work

Oligonucleotides	Sequence
HAX1-PRRL-F	GAACCGGTGCCACCATGAGCCTCTTTG ATCTCTTCCGGGG
HAX1-cflag-PRRL-R	GGACTAGTCTACTTGTGTCGTCATCGTCTT TGTAGTCCCGGGACCGGAACCAACGTC
HAX1-PRRL-R	GGACTAGTCTACCGGGACCGGAACCAA CGTC
HAX1 $\Delta$ 1-cflag-PRRL-F	GAACCGGTGCCACCATGCACAGAGATC CCTTTTTTGGAGGG
HAX1 $\Delta$ 2'-OL-cFlag-R1	CCCGTAGTCTGCTCCGAGGTCCAGGAA AGCCGAAA
HAX1 $\Delta$ 2'-OL-cFlag-F2	ACCTCGGAGCAGACTACGGGAGGGAC AGACACTTC
HAX1 $\Delta$ 3-OL-cF-R1(full exon 3 deletion)	CATCATCAAAGGAGGATGGGAAGGCA AGGTCCAG
HAX1 $\Delta$ 3-OL-cF-F2(full exon 3 deletion)	CCATCCTCCTTTTGATGATGTATGGCCT ATGGACC
HAX1 $\Delta$ 3'-OL-cFlag-R1	CATCATCAAACCTCACCAGGTGTCTCTG ACTCAGGA
HAX1 $\Delta$ 3'-OL-cFlag-F2	ACCTGGTGAGTTTGATGATGTATGGCC TATGGACC
HAX1 $\Delta$ 5-OL-cFlag-R1	CCTCCACTATATTGTCCTCTCTGGTTCT AGGATGG

HAX1 $\Delta$ 5-OL-cFlag-F2	AGAGGACAATATAGTGGAGGAGCGCC GGACTGTGG
HAX1 $\Delta$ 6+7-cF-R	GGACTAGTCTACTTGTTCGTCATCGTCTT TG TAGTCCCATCTGGTTTAGTGATCTT GGTC
HAX1 $\Delta$ 123-168-OL-R1	CATCATCAAATCCCTCCCGTAGTCTCTC ACCAGGT
HAX1 $\Delta$ 123-168-OL-F1	ACGGGAGGGATTTGATGATGTATGGCC TATGGACC
HAX1 $\Delta$ 126-168-OL-R1	CATCATCAAAAAGTGTCTGTCCCTCCC GTAGTCTC
HAX1 $\Delta$ 126-168-OL-F1	ACAGACACTTTTTGATGATGTATGGCCT ATGGACC
HAX1 $\Delta$ 137-168-OL-R1	CATCATCAAAGTGACTATCTGGATACTT AAGCATT
HAX1 $\Delta$ 137-168-OL-F1	AGATAGTCACTTTGATGATGTATGGCCT ATGGACC
HAX1 $\Delta$ 144-168-OL-R1	CATCATCAAACCCCCCAAAGATCCTGG GCTGGTGA
HAX1 $\Delta$ 144-168-OL-F1	CTTTGGGGGGTTTGTATGATGTATGGCC TATGGACC
HAX1 $\Delta$ 155-168-OL-R1	CATCATCAAAGGGGGATTCACTTCTTG CATCACTC
HAX1 $\Delta$ 155-168-OL-F1	TGAATCCCCCTTTGATGATGTATGGCCT ATGGACC
HAX1 $\Delta$ 163-168-OL-R1	CATCATCAAAGGAGCCCCAGTCTGGTG CTGGTTGG
HAX1 $\Delta$ 163-168-OL-F1	CTGGGGCTCCTTTGATGATGTATGGCC TATGGACC
HAX-130LR-64F	AAGTATCCAGATAGTCACCAGCCCA
HAX-130LR-64R	ACGCATTGAGTCCCGAAGTGTCTGT
CLPB-PRRL-F	ATGCTGGGGTCCCTGGTGTGAGGAG
CLPB-cflag-PRRL-R	GGACTAGTCTACTTGTTCGTCATCGTCTT TG TAGTTCGATGGTGTGACACCTTC
CLPB-PRRL-R	GGACTAGTCTAGATGGTGTGACACACC TTC
CLPB $\Delta$ 79-cFlag-F	GAACCGGTGCCACCATGACCAAATGCC TCGCGGCTGCCACTT
CLPB $\Delta$ ANK1-4-OL-F	GAGTCCGTCCAAGCGTGAGGCTGAGG AGCGGCGCC

CLPB $\Delta$ ANK1-4-OL-R	CCTCACGCTTGGACGGACTCTTGCTGT AGCAATGA
CLPB $\Delta$ TATP-OL-F	CTGGTACGATGTCTACTTCCTCCCCTTC TGCCACT
CLPB $\Delta$ TATP-OL-R	GGAAGTAGACATCGTACCAGCCATTCT CCTTCCTC
CLPB $\Delta$ CTD2-OL-F	CTACTTCCTCACGGTGGAGGACTCAGA CAAGCAGC
CLPB $\Delta$ CTD2-OL-R	CCTCCACCGTGAGGAAGTAGACGATCT CATTGATC
CLPB-T268M-F	AAGGGCTGCATGGCCTTGAC
CLPB-T268M-R	GAAACTGGCGCGGTTGTTC
CLPB-Y272C-F	GCCTTGCACTgTGCTGTTCTTG
CLPB-Y272C-R	CGTGCAGCCCTTGAAACT
CLPB-R408G-F	GGGCTTCATCGGGCTGGACAT
CLPB-R408G-R	TTTTTAGCATCTTTGTGCATATATTTGG C
CLPB-R561Q-F	TTTCTGGGACaGATCAATGAGATCG
CLPB-R561Q-R	CTCATCCCTCCGGAAGTG
scrambled shRNA	TGCTGTTGACAGTGAGCGCGTAGCGAC TAAACACATCAAATAGTGAAGCCACAG ATGTATTTGATGTGTTTAGTCGCTACTT GCCTACTGCCTCGGA
PKD2-shRNA1	TGCTGTTGACAGTGAGCGCCACGACCA ACAGATACTATAATAGTGAAGCCACAG ATGTATTATAGTATCTGTTGGTCGTGTT GCCTACTGCCTCGGA
PKD2-shRNA2	TGCTGTTGACAGTGAGCGCTCCCAGCA ATGAACTGTTCTATAGTGAAGCCACAG ATGTATAGAACAGTTCATTGCTGGGATT GCCTACTGCCTCGGA
HSP27-cflag-PRRL-F	GAACCGGTGCCACCATGACCGAGCGC CGCGTCCCCTTC
HSP27-cflag-PRRL-R	GGAAGTACTTTACTTGTGTCATCGTCTT TGAGTCCTTGGCGGCAGTCTCATCGG

HSP27-PBBAC-F	ACGCGTCGACGCCACCATGACCGAGC GCCGCGTCCC
HSP27-PBBAC-R	CCGGAATTCGTTACTTGGCGGCAGTCT CATCGG
HSP27-PBBAC-F	ACGCGTCGACGCCACCATGACCGAGC GCCGCGTCCC
HSP27-PBBAC-R	CCGGAATTCGTTACTTGGCGGCAGTCT CATCGG

## 1.6 Cell lines

Table 7. The summary of cell lines applied for this work

Cellline	Source
HEK293T cells	DSMZ
HEK293-Flp-In <sup>TM</sup> T-REx <sup>TM</sup> (HEK239T) -HAX1-FLAG	This study
HeLa	DSMZ
HeLa-HAX1 <sup>-/-</sup>	This study
HeLa-HAX1 <sup>-/-</sup> +HAX1	This study
HeLa-CLPB <sup>-/-</sup>	This study
HeLa-CLPB <sup>-/-</sup> +CLPB	This study
PLB985	DSMZ
PLB985-HAX1 <sup>-/-</sup>	This study
PLB985-HAX <sup>-/-</sup> +HAX1	This study
PLB985-CLPB <sup>-/-</sup>	This study
PLB985-CLPB <sup>-/-</sup> +CLPB	This study
PLB985-HAX <sup>-/-</sup> +HSP27	This study

## 1.7 Animals

C57BL/6 (B6), CD45.1 (Ly5.1)-congenic, Rag1<sup>-/-</sup>, HAX1<sup>-/-</sup>, HAX1<sup>flox/flox</sup>, and HAX1<sup>LysMcre</sup> (all on a B6 background) were purchased from the Jackson Laboratory. Experiments were performed in accordance with the German Federal Veterinarian Office and Cantonal Veterinary Office guidelines.

## 1.8 Equipment and software

Table 8. The summary of equipment applied for this work

Instrument	Manufacturer
BD FACSAria Cell Sorter III	BD biosciences
BD LSRFortessa	BD biosciences
BioChem-VaccuCenter-BVC 21	VACUUBRAND
ChemiDoc XRS molecular Imager	Bio-rad
Cellspin I centrifuge	THARMAC
Centrifuge	Eppendorf
Confocal microscopy	Zeiss
Heraeus Hera cell 240 (incubator)	Thermo Scientific
Herafreeze HFU 686 Basic (freezer)	Thermo Scientific
HulaMixer Sample Mixer	Invitrogen
KS 4000 ic Control (bacterial shaker)	IKA-Werke
Light microscope	Zeiss
NanoDrop 2000	PEQLAB
Optima L-80 XP Ultracentrifuge	Beckman
Optima TLX CE Ultracentrifuge	Beckman
Schuettel water bath	Thermolab
StepOnePlus Real-Time PCR Systems	Applied Biosystems

SW 41 Ti Rotor	Beckman Coulter
SynergyH1 Hybrid Reader	BioTek
PCR machine	Peqlab
PEQSTAR Thermocycler	PEQLAB
Potter-Elvehjem with PTFE Pestle	OMNILAB
RET basic IKAMAG safety control (magnetic mixer)	IKA-Werke
Thermomixer comfort	Eppendorf
Thermo Scientific Safe 2020 (sterile hood)	Thermo scientific
Universal 320 (centrifuge)	Hettich
VortexGenie2	Scientific Industries
Wet/Tank Blotting Systems	Biorad

Table 9. The summary of softwares applied in this work

<b>Software</b>	<b>Producer</b>
Adobe Illustrator CS4	Adobe
Excel	Microsoft
FlowJo software	Tree Star Software
( <a href="http://crispr.mit.edu/">http://crispr.mit.edu/</a> )	Feng Zhang's Lab
Molecular Imager Chemi Doc	Biorad
Prism	Graphpad
Zen 2.3	Zeiss

## 2 Methods

### 2.1 Mice analysis



### 2.1.1 Bone marrow chimeras

Bone marrow cells of wild-type CD45.1-congenic and HAX1<sup>-/-</sup> CD45.2-congenic mice were harvested prior to RBC lysis for 2 min at room temperature. Same number of cells from both sources of bone marrow were mixed in the ratio of 1:1. Rag<sup>-/-</sup> mice were irradiated at 9 Gy before injected with prepared bone marrow mixture via intravenous injection (i.v.). Bone marrow chimeric mice were subsequently nurtured for 14 days with drinking water supplemented with 1 mg/ml Sulfamethoxazol and 0.2 mg/ml Trimethoprim (Bactrim®; Roche) for a reconstitution of immune cells in mice before further experiment.

### 2.1.2 Organ isolation

Bones were collected from euthanized mice via CO<sub>2</sub> inhalation and incubated in PBS buffer before further preparation. Bone marrow was flushed with a 29 G syringe filled with cold PBS prior to centrifugation and red blood cell lysis. After washing with cold PBS, cell numbers were determined with a cell counting chamber.

Spleens were isolated from euthanized mice via CO<sub>2</sub> inhalation and incubated in PBS buffer before further preparation. Spleens were smashed through 40 µm filters to acquire single cell suspension prior to centrifugation and red blood cell lysis. Followed by PBS washing, cell counts were determined by the cell counting chamber.

Thymi were isolated from euthanized mice via CO<sub>2</sub> inhalation and incubated in PBS buffer before further preparation. They were smashed through 40 µm filters in order to obtain single cell suspension prior to centrifugation, followed by PBS washing and cell counting using a cell counting chamber.

### 2.1.3 Flow cytometry

Flow cytometry and cell sorting were performed with LSRII and FACSAriaIII (Abdollahpour et al.) cytometers, respectively. Samples were stained by the following fluorochrome-labeled mAbs. Monoclonal antibodies specific for IgD (clone 11-26c), IgM (II/41), CD117 (ACK2), CD25 (PC61), CD19 (1D3), CD11b (M1/70), CD11c (N418), Gr-1 (RB6-8C5), erythroid cell marker (Ter-119), CD71 (CY1G4), CD3 (17A2), sca-1 (D7), CD135 (A2F10), CD4 (GK1.5), CD8 (53-6.7), TCRβ (H57-597), CD24 (ML5), B220 (RA3-6B2), CD45.1 (A20), CD45.2 (104) were used

purified or as various fluorescent or biotin conjugates. Antibodies were purchased from BD Biosciences and BioLegend. Data collected from Flow cytometry data were analyzed by FlowJo (9 or 10, TreeStar).

## **2.2 Cultivation of human cells**

Standard cell lines (HeLa, HEK293T, PLB-985) were purchased from the DSMZ (German Collection of Microorganisms and Cell Cultures). Human HeLa and HEK293T cells were cultured in DMEM and PLB-985 cells were cultured in Roswell Park Memorial Institute (RPMI) 1640, supplemented with 10% (v/v) FBS, 50 U/ml penicillin and streptomycin, 2 mM L-Glu and 10mM HEPES. Cells were grown in the incubator with 5% CO<sub>2</sub> at 37°C. Cells were weekly tested for mycoplasma contamination.

## **2.3 iPSCs associated cell culture and experiments**

### **2.3.1 Differentiation of iPS cells**

Undifferentiated iPS cell colonies were cultured with mTeSR medium in 6-well plates, which coated with growth factor-reduced matrigel in advance. On day 0 of iPSCs differentiation, mTeSR was supplemented with 80 ng/ml BMP4, 4 μM CHIR99021 and 80 ng/ml VEGF. On day 2, essential 6 medium supplemented with 80 ng/ml VEGF, 25 ng/ml basic FGF, 50 ng/ml SCF and 2 μM SB431542 was adopted for cell culture. On day 6, culture medium was switched to StemPro-34 supplemented with 50 ng/ml SCF, 50 ng/ml IL-3, 50 ng/ml Flt-3, 5 ng/ml TPO and 50 ng/ml VEGF. At this stage, six iPS colonies with similar size and differentiation status were kept for further steps. On day 8, StemPro medium supplemented with 50 ng/ml SCF, IL-3 Flt-3 and 5 ng/ml TPO was applied for the cell culture. From day 9 on, medium was halfly changed every 3-4 days till day 17. On day 17, medium was changed into the one with 50 ng/ml G-CSF, SCF and IL-3. From day 20 on, mature neutrophil-like cells were generated and could be analysed by flow cytometry. Healthy control fibroblast derived iPS cells were kindly provided from Dr. Drukker from Helmholtz Center, Munich.

### **2.3.2 Establishment of stable inducible expression of HSP27 or HAX1 in HAX1 knockout iPS cells**

Inducible expression transposon system PiggyBac was employed for the reconstitution of HAX1 or HSP27 in HAX1<sup>-/-</sup> iPS cells. HAX1 and HSP27 were cloned into piggyBac transposon destination vector (addgene, cat# 80478), whose expression was induced by doxycycline treatment. Indicated destination vectors together with PiggyBac transposase expression vector (System Biosciences, cat# PB210PA-1) were transfected into HAX1<sup>-/-</sup> iPS cells by electroporation. Cells contained vectors were selected by puromycin (0.5 µg/ml). Cells transfected with an empty piggybac vector served as a control. iPSC cells were stimulated with doxycycline (0.05 µg/ml) for 24 hours and subsequently tested for protein overexpression by SDS-PAGE and Western blotting.

### **2.3.3 FACS analysis and sorting**

Floating neutrophil-like cells were harvested and shortly washed with PBS buffer (PBS with 2%FBS) before surface staining with indicated antibodies. Samples were examined by flow cytometry, with which mature neutrophil population was gated by (Live/mcheery+/CD33low/CD11b+). Acquired data were subsequently analyzed by FlowJo v9 and v10.

### **2.3.4 Cytospin and light-microscopy**

Differentiated iPS cells were harvested and resuspended in PBS with 2% FBS. The cell suspension was subsequently loaded into the funnel, which was clamped with a filter paper and a slide by the cytopspin holder. Samples were centrifuged at 500 rpm for 5 min at RT utilizing a Tharmac Cellspin I Cyto centrifuge (THARMAC). After cyto centrifugation, cells were deposited onto the slide. All slides were stained with May-Grünwald Giemsa for 2 minutes prior to Giemsa (Giemsa's azur eosin methylene blue solution, diluted with sörengen buffer at 1:20) staining for 17 min. A Zeiss Axioplan 2 imaging microscope (Carl Zeiss) was applied for the examination of cell morphology and stages of cell differentiation.

## **2.4 Generation of gene knockout cell lines using the CRISPR-Cas9 system**

### **2.4.1 sgRNA design and cloning**

For generating HAX1<sup>-/-</sup> and CLPB<sup>-/-</sup> cell lines, sgRNAs targeting genes were chosen from CRISPR Design tool (<http://crispr.mit.edu/>) with lower predicted off target sites.

The sequence of sgRNAs were ordered from Eurofins genomics and cloned into PX458 vector (SgRNA-Cas9) according to Feng Zhang's protocol (Cong et al., 2013).

#### **2.4.2 Cell transfection and sorting**

Cells were seeded one day before the transfection. SgRNA-Cas9-GFP/RFP plasmid (4 µg in total) and polyethylenimine (PEI) were respectively incubated with 100 µl Opti-MEM for 5 min at RT. PEI solution was further mixed with solution containing plasmids and the whole mixture was incubated for 20 min at RT. The transfection system was subsequently added onto seeded cells. For cell transfection with suspension cells (PLB-985 cells), electroporation by Lonza® Nucleofector® II electroporation system was employed.  $3-5 \times 10^6$  cells were resuspended with 100 µl buffer (82 µl solution and 18 µl supplement) provided in the kit before mixed with 4 µg of SgRNA-Cas9-GFP/RFP plasmids. The whole mixture was further transferred into a sterile 0.2-cm cuvette (Lonza, cat# VVCA-1003), which was set into the Nucleofector® II electroporation machine and run with T-019 program. Electroporated cells were gently seeded into pre-warmed RPMI complete medium. GFP/RFP positive cells were sorted 48 hours after electroporation. Single colonies were picked up for genotyping and Western blotting for KO validation.

#### **2.5 Generation of stable cell lines with overexpressed genes**

Lentiviral vector pRRL was applied for gene (HAX1, CLPB and HSP27) delivery. Indicated genes were firstly cloned into pRRL vector prior to a lentivirus production by transiently transfecting 293T cells with lenti-gene-vector, gag-pol vector and VSVG vector. Culture medium was changed the day after transfection. Supernants were collected from 24-72h after changing medium. Supernants containing viral particles were further concentrated by ultracentrifugation at 25,000g for 2.5 hours. Transduced cells were sorted and expanded prior to analysis by SDS-PAGE and Western blotting.

#### **2.6 Inhibitor studies**

PLB-985 cells were treated with CRT0066101 at indicated concentrations shown in the data for 3 h at 37°C. Treated cells were harvested prior to the analysis by SDS-PAGE and Western blotting.

## **2.7 Mitochondrial isolation**

Freshly harvested cells were homogenized twice in TH buffer (as shown in the buffers and solutions) by a Potter S homogenizer (Sartorius). Homogenized cells were subjected to a centrifugation at 400 g, 4°C for 10 min. Harvested supernatants were purified by a centrifugation at 800 g, 4°C for 5 min. Purified supernatants were subsequently subjected to centrifugation at 10,000 × g for 10 min at 4°C. Pellets (isolated mitochondria) were washed once with TH buffer before concentration determination using BSA as a standard.

## **2.8 Mitochondrial swelling experiment**

Mitochondrial swelling was performed according to the protocol shown by Mick et al. (Mick et al., 2012). Freshly isolated mitochondria were either stabilized by SEM buffer (as shown in the buffers and solutions) or by EM buffer (as shown in the buffers and solutions) or fully ruptured by sonification prior to protease K digestion at 4°C for 10min. After neutralization by adding 1 mM PMSF to all samples at 4°C for 10min. Samples were subsequently subjected to ultracentrifugation and cooked at 95°C for 5min prior to SDS-PAGE and Western blotting.

## **2.9 Mitochondrial carbonate extraction**

Freshly isolated mitochondria were solubilized with 0.1M Na<sub>2</sub>CO<sub>3</sub> at pH 10.8 or pH 11.5 or solubilized with 1% Triton buffer. All samples were incubated on ice for 20 min prior to ultracentrifugation at 45,000 rpm, 4°C for 45 min. Supernatants and pellets were precipitated with TCA (trichloroacetic acid) before washed with acetone on ice. All samples were subjected to SDS-PAGE and Western blotting for analysis.

## **2.10 Immunoprecipitation of proteins**

### **2.10.1 Immunoprecipitation with endogenous antibodies**

Protein-A/G Sepharose beads were activated with RIPA buffer prior to incubation with specific primary antibody for 2 h, at 4°C. Afterwards, beads were pelleted and washed with RIPA buffer twice by centrifugation at 2000 rpm, 2 min. 3 mg of protein lysates obtained from HEK293T cells were incubated with activated beads overnight at 4°C. Beads were subsequently pelleted and washed 5 times with RIPA buffer for

2 min at 2000 rpm. After the last time of washing, the supernatant was removed and beads were cooked with 1 × loading dye for 5 min, at 95°C.

### **2.10.2 Immunoprecipitation with Anti-FLAG M2 agarose beads**

PRRL, HAX1<sup>FLAG</sup> and CLPB<sup>FLAG</sup> were overexpressed in HEK293T cells respectively by transient transfection. Transfected cells were lysed with RIPA buffer supplemented with protease inhibitor (as shown in the buffers and solutions). The insoluble fraction was pelleted by centrifugation (14,000 rpm at 4°C for 15 min) and the supernatant were collected and incubated with activated anti-FLAG M2 agarose beads 2 hours at 4°C. Beads with enriched proteins were further washed with RIPA buffer (as shown in the reagent list) prior to direct cook at 95°C for 10 min. The supernatants after cooking were analyzed by SDS-PAGE and Western blotting.

### **2.11 Immunofluorescent studies**

Cells were seeded onto coverslips one day before fixation with 3.7% paraformaldehyde at RT for 15 min. Fixed cells were washed with PBS once and quenched with 50 mM NH<sub>4</sub>Cl for 20-30 min. Cells were shortly washed with PBS again before permeabilized with Triton (0.2%) for 2 min at RT. Cells were further blocked with 0.02% Triton and 1% BSA in TBS (w/v). Cells were incubated with primary antibodies at 4°C overnight or 1h at RT. 4'6-diamidino-2-phenylindole (DAPI) was applied for nuclear staining. Aqueous mounting medium (Dako Cytomation) was used for coverslips to be mounted on glass slides. Permeabilization with 0.5% Triton X-100 (with 5 mM MgCl<sub>2</sub>) was adopted for the process of pre-extraction. Images were taken by a Zeiss LSM-800 microscopy with a 63 × 1.4 NA Oil Dic Plan-Apochromat immersion lens.

### **2.12 In-gel-mass spectrometry**

Mass spectrometry was performed as previously described (Schulz et al., 2011). Eluates from the immunoprecipitation of HAX1<sup>FLAG</sup> were subjected to SDS-PAGE. The SDS-PAGE gel was subsequently stained with coomassie blue and visible bands were extracted for in-gel digestion as described in Schulz et al.. First proteins were digested with trypsin overnight at 37°C. Peptides were extracted with 0.1% trifluoroacetic acid (TFA) by reverse-phase chromatography. A gradient from 9.5–90.5% acetonitrile in 0.1% TFA for 80 min were applied for peptides elution, which

was further mixed with *o*-cyano-4-hydroxycinnamic acid (HCCA). Samples were loaded and subsequently analyzed by a MALDI-TOF/TOF mass spectrometer as previously described (Bruker Daltonics) (Schulz et al., 2011).

## **2.13 SILAC analysis**

### **2.13.1 SILAC labelling**

PLB-985 cells were cultured in RPMI 1640 media for SILAC supplemented with either light (Arg0, Lys0) or medium (Arg6, Lys4) for at least 10 passages for protein incorporation, which was confirmed by mass spectrometry. Cells cultured in medium media were further incubated/pulsed with media supplemented with heavy (Arg10, Lys8) for 6 or 24 hours (Boisvert et al., 2012).  $2 \times 10^6$  pulsed cells were mixed with  $2 \times 10^6$  light cells before mitochondrial isolation or snap-frozen. Data were collected from two independent experiments and each genotype contains three independent clones.

### **2.13.2 Lysis and protein digestion**

Samples of cells or mitochondria were lysed in 40  $\mu$ l of LYSE buffer (preOmics). The lysates were cooked (95°C for 5 min) and sonicated (50% duty cycle for 8 min) before protein content measurement. Lysate contents were determined by a spectrophotometric method at emission wavelength 350 nm. Protein were further digested in LYSE buffer with endoproteinase LysC and trypsin at 37°C overnight. Peptides were acidified with 0.1% trifluoro-acetic acid (TFA) before loading and purification. The amount of recovered peptide was determined by Nanodrop.

### **2.13.3 Data Acquisition and Computational proteomics**

A reverse phase 50-cm column with 75- $\mu$ m inner diameter were used for the separation of eluted peptides. The system was kept at 60°C and detected by the SprayQC software (Scheltema and Mann, 2012). An EASY-nLC 1200 ultra-high-pressure system coupled through a nanoelectrospray source to a Q Exactive HF-X mass spectrometer was applied for the liquid chromatography. Peptides were loaded in 0.1% formic acid and a 100 minutes 5%-98% buffer containing 0.1% formic acid and 80% acetonitrile were applied at a rate of 350 nL/min. Data were acquired between a full scan and 15 data-dependent MS/MS scans. Multiple sequencing of peptides was minimized by excluding the selected peptide candidates

for 40 seconds. The MaxQuant software (version 1.6.1.13) was applied in the data analysis (Cox and Mann, 2008). Peak lists were searched against the human UniProt FASTA database version of 2018. False discovery rate (FDR) was set to 1% for peptides and proteins' determinations. Two missed cleavages at maximum were allowed during the search. An initial precursor mass deviation up to 7 ppm and a fragment mass deviation of 10 ppm were applied to the peptide identification.

## **2.14 Interactome analysis of HSP27**

pRRL or HSP27<sup>FLAG</sup> was overexpressed in HEK293T cells by transient transfection. Transfected cells were lysed with RIPA buffer supplemented with protease inhibitor (as shown in reagent list). The insoluble fraction was pelleted by centrifugation (14,000 rpm at 4°C for 15 min) and the supernatant were collected and incubated with activated anti-FLAG M2 agarose beads 2 hours at 4°C. Beads with enriched proteins were further washed with mitochondrial IP washing buffer (as shown in the buffers and solutions) prior to elution with 0.1 M glycine (pH 3.0). Protein eluates were lysed in LYSE buffer before analysis.

## **2.15 Quantification and statistical analysis**

### **2.15.1 Statistical analysis of mass-spectrometry data**

The Perseus software (version 1.5.4.2) was employed for the data analysis of SILAC assay (Tyanova et al 2016). SILAC data was collected from three independent clones and two independent experiments. HSP27 interactome data were collected from two independent experiments and each experiment contain three independent pulldowns. Proteins quantified in both experiments were used for the analysis. UniProt Keywords, KEGG and Gene Ontology were used for categorical annotations. Fischer's exact test was applied for the annotation enrichments. Benjamini-Hochberg FDR for truncation and a threshold value of 0.02 were adopted in the SILAC analysis. Student's T-tests using 0.05 FDR for truncation and 250 randomizations were applied to the interactome analysis of HSP27.

### **2.15.2 Quantification of mitochondrial complex activities, MitoSOX staining and iPS cell data**



Data of graphs are indicated as means  $\pm$  SEM. Significant differences between samples were statistically calculated with the assist of Prism (GraphPad Software) by Student's t test or two-way ANOVA as indicated in figure legends.

## **2.16 Molecular biology techniques**

### **2.16.1 PCR**

PCR was conducted with Q5 High-Fidelity DNA Polymerase. Parameters of DNA amplification were based on polymerases, DNA template and respective primers. After PCR running, DNA products were analyzed by agarose gels. Mutagenesis PCR was composed of two sub-PCR processes with primers introduced with mutation according to the mutated DNA sequence.

### **2.16.2 DNA gel extraction and sequencing**

A certain amount of PCR product was loaded into agarose gels and visible band under UV light was cut prior to gel extraction, which was conducted according to the specifications of the manufacturer (Zymoclean Gel DNA Recovery Kit, Zymo).

### **2.16.3 Transformation of E. coli**

Competent E. Coli (DH5-alpha) cells were thawed on ice for 7 min prior to incubation with desired plasmids for 20 min, at 4°C. Afterwards, mixture underwent heat shock for 1min, at 42°C prior to another 2 min incubation on ice. Bacteria were recovered in 37°C for 40 min before expansion in LB medium with specific antibiotics.

### **2.16.4 Plasmid extraction**

Plasmids were isolated from E. coli (DH5-alpha) cultured overnight using either Zyppy Plasmid Miniprep Kit (Zymo) or QIAGEN Plasmid Plus Maxi Kit (Qiagen) according to the specifications of the manufacturer.

### **2.16.5 Agarose gel electrophoresis and DNA sequencing**

DNA product from PCR were detected via agarose gel electrophoresis. Agarose powder was cooked with TBE buffer prior to addition of EtBr after cooling down to less than 60°C. DNA samples were mixed with DNA loading dye (Thermo Scientific) and run in TBE buffer at 100V in Bio-Rad electrophoresis systems. The DNA ladder from JenaBioscience applied as the control of molecular weight. DNA concentration

were analysed with the Nanodrop spectrometer. The purity of DNA was assessed by Nanodrop by the ratio of A260/280. DNA-sequencing was conducted by Eurofins Genomics and data were analysed by Ape software.

### **2.17 Protein extraction and protein concentration**

Harvested cells were directly cooked with the 2 × laemmli buffer for 5 min at 95°C, named whole cell lysates. Cell pellets were resuspended with the hypotonic lysis buffer (cell signaling) and lysed for 20 min on ice. After centrifugation of 14,000 rpm for 15 min, remaining cell pellets named as insoluble fractions and the supernatants named as soluble fractions. All samples were cooked with protein loading dye prior to analysis via SDS-PAGE and Western blotting. If necessary, protein concentration was measured by Bradford assay at 595 nm. BSA (sigma) was used as a standard for calibration.

### **2.18 Measurement of mitochondrial complex I and IV activity**

To measure the activities of respiratory chain complex I and respiratory chain complex IV, assay kits (complex I enzyme activity assay kit and complex IV assay kit) from abcam were employed. Mitochondria are isolated and complexes' activities were assessed according to the protocol provided by the manufacture.

### **2.19 Measurement of mitochondrial ROS**

To measure the mitochondrial reactive oxygen species (ROS), specific indicator (Mitosox red) was employed. In brief, cells were harvested prior to the incubator with indicator at 5 µM, 37°C for 15 min. Then the mixture was washed with prewarmed plain cell culture medium before FACS analysis at emission 580 nm.

### III RESULTS

#### 1 The functional study of Hax1 in a mouse model

##### 1.1 Hax1<sup>-/-</sup> mice

To study the effect of Hax1 deficiency in the mouse immune system, we have generated a Hax1 knockout mouse model. In accordance with previously published data by Jim Ihle's group (Chao et al., 2008), Hax1-deficient mice did not show congenital neutropenia but rather developed rapid neurological decline followed by early death. In addition, our own macroscopic observation of the bone marrow and spleen of Hax1<sup>-/-</sup> mice suggested an accumulation of erythrocytes in these organs. This finding prompted us to analyze erythropoiesis in more detail. By FACS analysis, we observed that in the absence of Hax1, the frequencies of erythropoietic progenitors in the bone marrow were twofold reduced as compared to the wild-type situation (Figure 11). On the other hand, mature erythrocytes were accumulated.

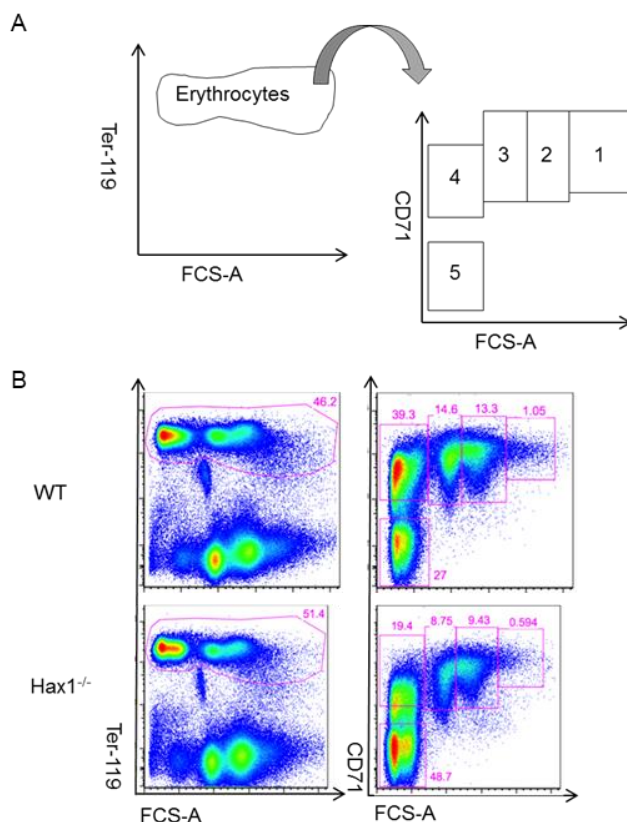


**Figure 11. Altered erythropoiesis in Hax1-deficient mice.** (A) Scheme for the analysis of erythropoiesis in WT and Hax1<sup>-/-</sup> bone marrow. The gating strategy allows distinguishing different

stages of erythrocyte differentiation and progression of maturation (from 1 to 5). (B) In the absence of Hax1, frequencies of early erythroid precursors (gate 1) are reduced and mature erythrocytes massively accumulated (gate 5). Plots are representative of one out of three experiments with 2-3 mice per group.

## 1.2 Competitive bone marrow chimeras

To define whether these effects (and potentially other effects) were intrinsic to the hematopoietic system or rather consequences of dysfunction of non-hematopoietic cells, we performed competitive repopulation experiments. As shown in Figure 12, bone marrow from WT (CD45.1) and Hax1-HET/KO (CD45.2) were harvested from donor animals and mixed in the ratio of 1:1. After red blood cells lysis, these bone marrow mixtures ( $2-5 \times 10^6$  cells) were intravenously injected into irradiated recipient Rag-knockout recipient mice. Six to eight weeks later, animals were euthanized to determine the degree of chimerism in the BM, spleen and thymus via flow cytometry (FACS) analysis.

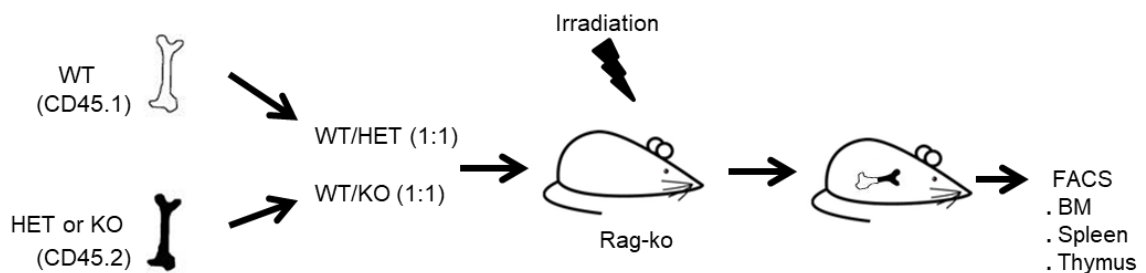


**Figure 12. Generation of bone marrow chimeras using X-ray irradiation.** Mixtures of bone marrow from mice in two genotypes were lysed with the RBC lysis buffer prior to injection to irradiated recipient mice. After 6-8 weeks, bone marrow chimeras were analyzed via flow cytometry analysis.

First, we assessed the degree of chimerism on B cells, granulocytes and hematopoietic stem cells in the bone marrow. For B cells, differentiated stages were defined as following populations: pre-B1 stage (B220+CD19+CD117+CD25-), pre-B2 stage (B220+CD19+CD25+CD117-), immature B stage (CD19+IgM<sup>lo</sup>IgD-), transitional stage (CD19+IgM<sup>hi</sup>IgD+/-) and mature stage (CD19+IgM<sup>int/-</sup>IgD+). The granulocytes were subdivided into CD11b+Gr1++ and CD11b+Gr1+ for a detailed

evaluation of granulocyte development. Hematopoietic stem cells were characterized by the marker profile Lin<sup>-</sup>Sca-1+c-kit<sup>+</sup>.

As shown in Figure 13, Hax1-KO (CD45.2) cells and WT (CD45.1) cells showed similar capacity to differentiate into B cells. In addition, the developmental potential of WT/HET or WT/KO in granulocytes (CD11b+Gr1<sup>+</sup>), dendritic cells (CD11b+CD11c<sup>+</sup>) and mature B cells in spleen and thymus was indistinguishable. Splenic B cell stages were defined as Follicular B cells (CD19+CD23+CD21/35<sup>-</sup>) and Marginal zone B cells (CD19+CD23<sup>-</sup>CD21/35<sup>+</sup>).

As indicated in Figure 13 and Figure 14, Hax1-KO (CD45.2) cells show comparable potential of development as WT (CD45.1) or Hax1-HET (CD45.2).

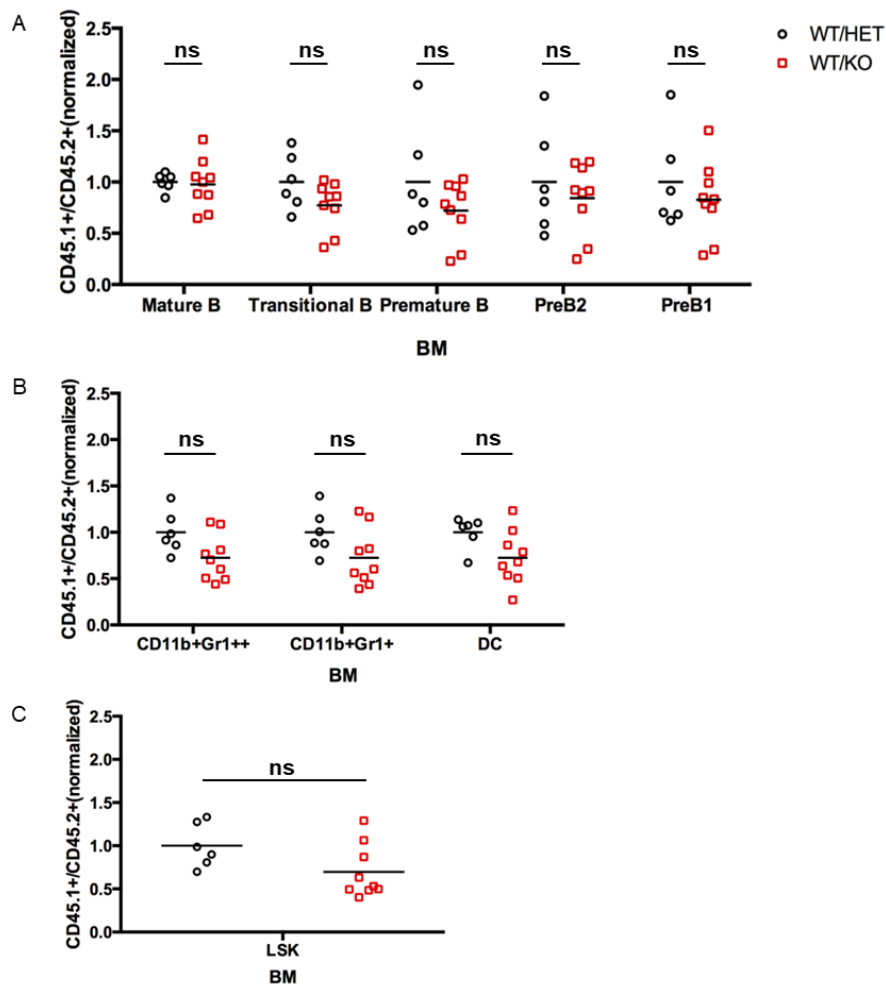


**Figure 13. FACS analysis of developmental potential of WT and Hax1-KO cells in bone marrow.**

(A, B, C) Population analysis on ratio of CD45.1+ to CD45.2+ cells in indicated cell types of bone marrow from either WT/HET or WT/KO chimeras. Quantifications are pooled from 2 independent experiments with a total of 6-9 mice per group. \*P<0.05; \*\*P<0.01; \*\*\*P<0.001; ns = not significant.

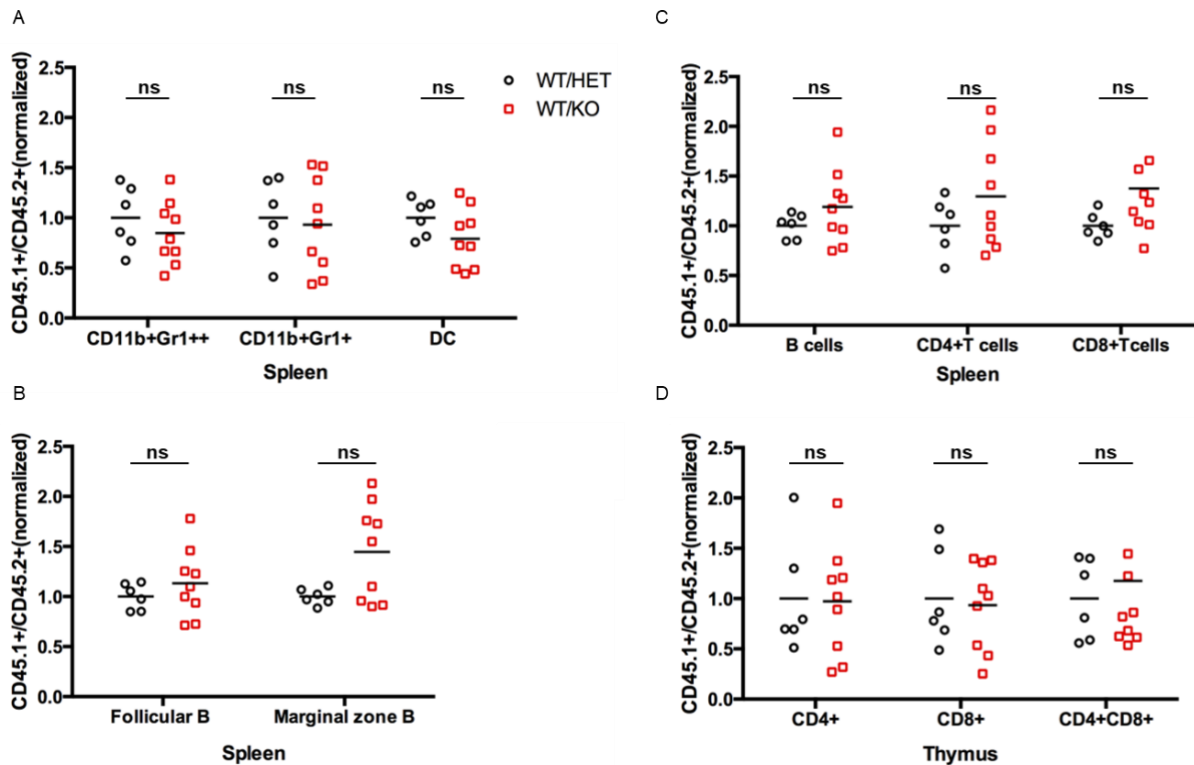


**Figure 14. FACS analysis of developmental potential of WT and Hax1-KO cells in spleen and thymus.** (A, B, C) Population analysis on ratio of CD45.1+ to CD45.2+ cells in indicated cell types of spleen from either WT/HET or WT/KO chimeras. (D) Population analysis on ratio of CD45.1+ to CD45.2+ cells in indicated cell types of thymus from either WT/HET or WT/KO chimeras. Quantifications are pooled from 2 independent experiments with a total of 6-9 mice per group. \* $P < 0.05$ ; \*\* $P < 0.01$ ; \*\*\* $P < 0.001$ ; ns = not significant.

Taken together, we were unable to discriminate any defect of Hax1-deleted hematopoietic lineage in competitive repopulation experiments.

### 1.3 Hax1<sup>ff</sup>LysM<sup>cre/+</sup> mice

In parallel, we have analyzed conditional Hax1 knockout mice to study the specific function of Hax1 in myeloid cells (LysM-Cre). We first bred homozygous Hax1<sup>fllox/fllox</sup> mice with transgenic mice with LysM-Cre to delete Hax1 in myeloid cells. After ensuring the correct genotype of LysM<sup>cre/+</sup>Hax1<sup>ff</sup> mice, we assessed the degree of Hax1 deletion in conditional mice by Western blotting. As shown in Figure 15, Hax1 was not expressed in neutrophils of LysM<sup>cre/+</sup>Hax1<sup>ff</sup> mice.

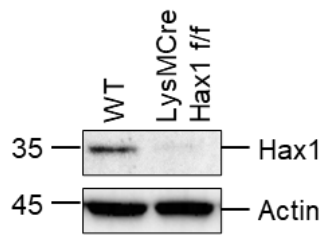


**Figure 15. The detection of Hax1 expression in neutrophils from WT and  $LysM^{cre/+}Hax1^{f/f}$  mice.** Neutrophils sorted from bone marrow of two genotypes were subjected to SDS-PAGE and Western blotting.

Next, we evaluated the percentage of neutrophils in bone marrow of  $Hax1^{f/f}$ ,  $LysM^{cre/+}Hax1^{f/null}$  and  $LysM^{cre/+}Hax1^{f/f}$  mice.  $LysM^{cre/+}Hax1^{f/f}$  mice had similar numbers of neutrophils when compared to the other two strains (Figure 16A).

Concomitantly, we also observed comparable proportions of LSK cells in bone marrow in  $Hax1^{f/f}$ ,  $LysM^{cre/+}Hax1^{f/null}$  and  $LysM^{cre/+}Hax1^{f/f}$  mice, respectively (Figure 16B). As a control, percentages of Gr-1 high and dendritic cells in spleen of three genotypes mice were analyzed (Figure 16C). Taken together,  $LysM^{cre/+}Hax1^{f/f}$  mice presented similar numbers of neutrophils and BM progenitors as WT mice.

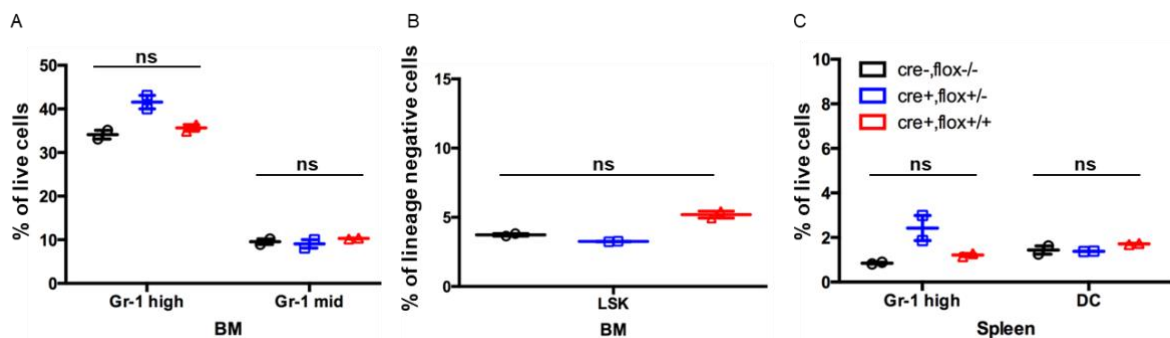


**Figure 16. Analysis of neutrophils and bone marrow progenitors in WT and  $LysM^{cre/+}Hax1^{f/f}$  mice.** (A, B) Bone marrow was flushed and harvested from  $Hax1^{f/f}$ ,  $LysM^{cre/+}Hax1^{f/null}$  and  $LysM^{cre/+}Hax1^{f/f}$  mice prior to antibody staining for indicated populations. (C) Splenocytes were flushed and harvested from  $Hax1^{f/f}$ ,  $LysM^{cre/+}Hax1^{f/null}$  and  $LysM^{cre/+}Hax1^{f/f}$  mice prior to antibody staining for indicated populations. Quantifications are pooled from 2 independent experiments with a total of 3 mice per group. \* $P < 0.05$ ; \*\* $P < 0.01$ ; \*\*\* $P < 0.001$ ; ns = not significant.

In conclusion, Hax1 deficient bone marrow cells did not have striking aberrations with respect to number of hematopoietic stem cells or neutrophil granulocytes. Therefore, to further study Hax1, we decided to make use of human myeloid cells lines to further study the effects of HAX1 deficiency.

## 2 HAX1 functional study in human cells

### 2.1 HAX1 localizes to the mitochondrial intermembrane space.

Even though HAX1 is primarily found in mitochondria (Suzuki et al., 1997), the exact distribution of HAX1 within the organelle in human cells has remained elusive. To define the exact localization of HAX1 in mitochondria, we tested the accessibility of HAX1 to externally added proteinase K under iso- or hypo-osmotic buffer conditions (SEM or EM buffer). Under iso-osmotic conditions (SEM buffer), only mitochondrial outer membrane proteins (i.e., Tom70) can be degraded by Proteinase K (Couvillion et al.). In EM buffer, not only OM proteins but also IMS proteins (i.e., Tim23) can be degraded by PK as a result of osmotic OM rupture. While in EM condition, mitochondrial matrix proteins (i.e., Tim44) remain intact as a protection of IM from PK digestion. As shown in the scheme in Figure 17, this experimental approach allows us to define whether a protein is located at the OM (outer membrane), IMS (intermembrane space) or matrix.

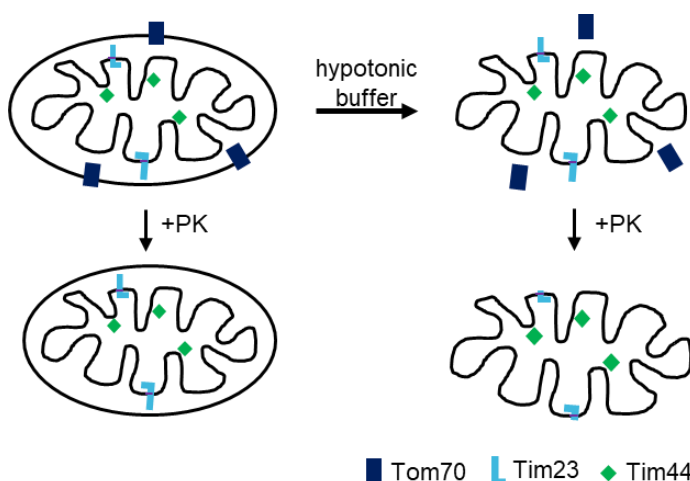


**Figure 17. The scheme of mitochondrial swelling experiment.** Intact mitochondria are double-membrane organelle. Without hypotonic treatment, proteinase K (Couvillion et al.) degrades mitochondrial OM (mitochondrial outer membrane) protein Tom70. After mitochondrial swollen via



hypotonic buffer, the OM is ruptured and subsequently both OM protein (Tom70) and IMS protein (Tim23) can be degraded upon further PK treatment. But matrix protein (Tim44) is maintained as a protection of IM (mitochondrial innermembrane).

Mitochondrial preparations from non-hematopoietic HeLa and the promyelocytic PLB-985 cell line were separated by electrophoresis and stained by antibodies to detect the reference proteins TOM70 (OM), TIM44 (Matrix) and TIM23 (IMS). As shown in Figure 18, HAX1 was cleaved by proteinase K only when the mitochondrial outer membrane was disrupted by EM buffer, similar to TIM23. This indicated that HAX1 is located in the IMS.

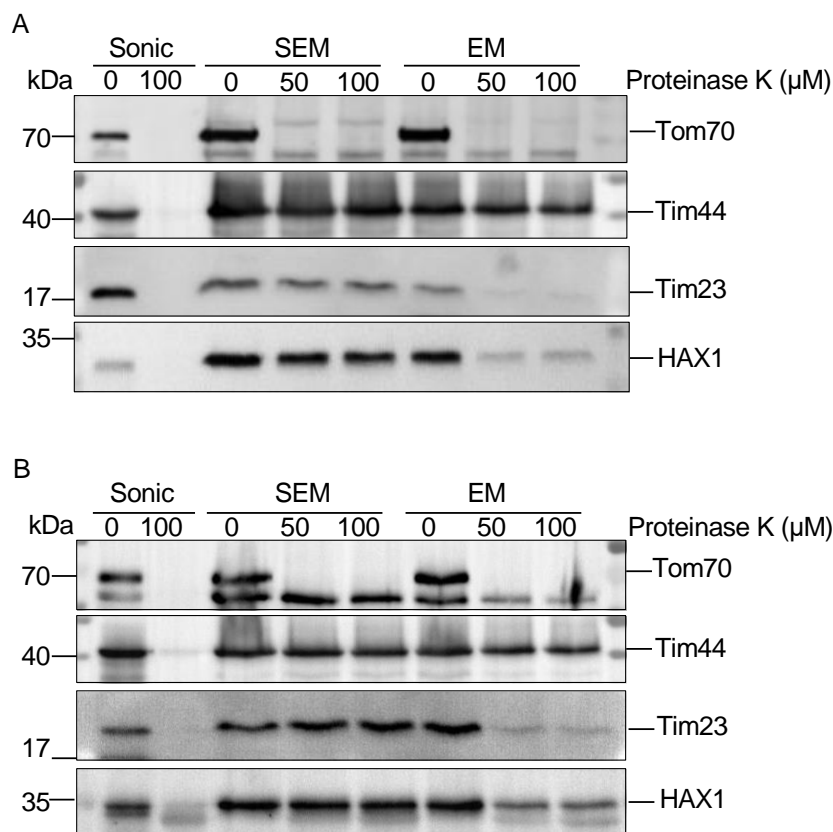


**Figure 18. Submitochondrial localization of HAX1 analyzed by protease protection.** Proteinase K (Couvillion et al.) was applied to sonicated mitochondria (sonic), intact mitochondria (SEM), or to mitoplasts (hypotonically swollen mitochondria, EM). For reference, EM buffer: EDTA, MOPS; SEM buffer: Sucrose, EDTA, MOPS.

Next, to assign the mitochondrial membrane association of HAX1, we performed carbonate extraction experiments of the isolated mitochondria. In detail, isolated

mitochondria were subjected to carbonate extraction (pH at 10.8 or 11.5) or detergent lysis and subsequently separated into supernatant (S) and pellet (P) fraction prior to Western blotting analysis. Transmembrane proteins are expected to appear in the pellet fraction independent of the pH, membrane-associated proteins appear to be in the soluble fraction upon solubilization at basic pH 11.5, whereas soluble proteins always appear in the supernatant (Figure 19). Peripheral protein Tim44 appeared to be released from the mitochondrial membrane into the supernatant (S) after carbonate extraction at pH 11.5. Similarly, HAX1 remained partially in the pellet fraction (P) upon carbonate extraction at pH 11.5. As HAX1 was partially extracted from membrane into supernatant upon carbonate extraction at pH 11.5 (Figure 20), we conclude that HAX1 is a mitochondrial protein binding to membrane.

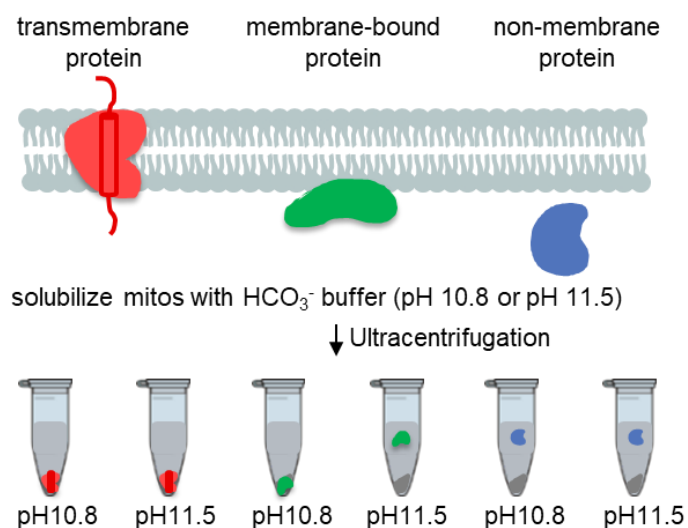


**Figure 19. The scheme of mitochondrial carbonate extraction.** To determine the relationship between proteins and mitochondrial membrane, mitochondria were isolated and solubilized with sodium carbonate buffer at pH 10.8 or 11.5, in comparison to transmembrane protein, membrane-bound protein can be extracted from membrane and shown in the supernatant after ultracentrifugation.

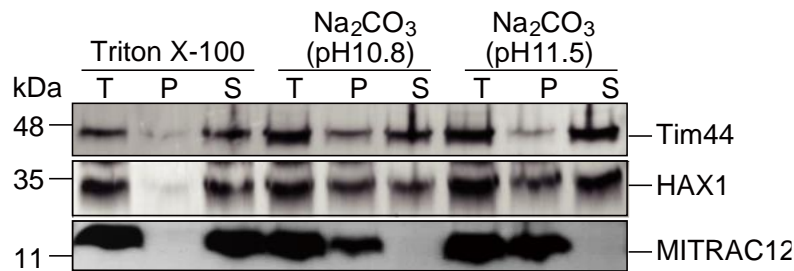


**Figure 20. HAX1 is a membrane-bound protein.** Mitochondria were subjected to carbonate extraction (at pH 10.8 or 11.5) or detergent lysis by Triton X-100, separated into supernatant (S) and pellet (P) fraction prior to analysis by Western blotting. T, total.

To validate these findings, we made use of immunofluorescence studies. To examine the localization of HAX1 in mitochondria, we stained HeLa cells with antibodies against HAX1 and the IMS marker OPA1. Consistent with the mitochondrial swelling data shown in Figure 18, HAX1 was demonstrated to be co-localized with OPA1 in HeLa (Figure 21).

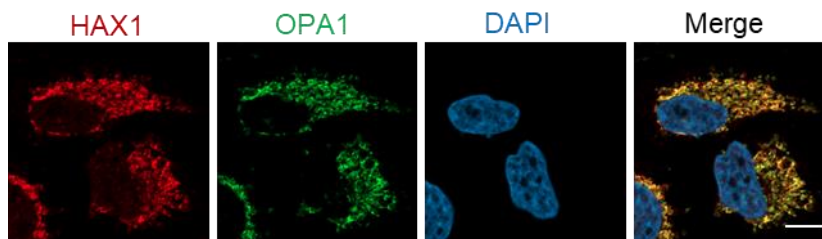


**Figure 21. Co-staining of HAX1 and OPA1 in HeLa cells.** Representative images show fixed HeLa cells costained with HAX1 (red), OPA1 (green) and DAPI (blue). Scale bar: 10  $\mu$ m.

To prove the specificity of our HAX1 staining, as a control, we applied the staining to HAX1<sup>-/-</sup> cells to ensure a much less significant signal upon loss of HAX1 (Figure 22).

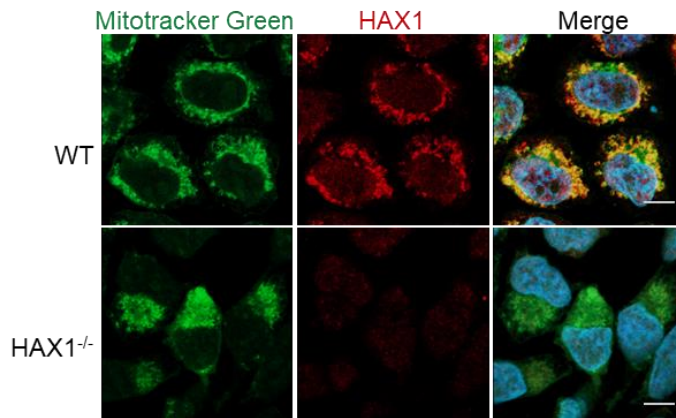


**Figure 22. The specificity of HAX1 staining.** Representative images show fixed HeLa cells costained with HAX1 (red), Mitotracker Green and DAPI (blue). Scale bar: 10  $\mu$ m.

## 2.2 CLPB controls HAX1 disaggregation

### 2.2.1 HAX1 interacts with CLPB in mitochondria

To gain insights into how HAX1 exerts its function in the IMS, we next aimed at identifying the binding partners that could be involved in the regulation of the mitochondrial function of HAX1. We performed immunoprecipitation (IP) experiments of FLAG-tagged HAX1 from HEK293T cell lysates and analyzed the IP elution by mass spectrometry (MS). As shown in Figure 23, 11 visible bands were excised upon electrophoretic separation and analyzed by mass spectrometry. MaxQuant (version 1.2.0.18) was used for data analysis and peaks listed were searched against the IPI human database (version 3.68). Given scores, based on the intensity of the peptide for each candidate, is correlated with a FDR of <1% adopting the following search criteria: first search 20 ppm precursor tolerance, 5 ppm peptide and 0.4 Da MS/MS tolerance (Mick et al., 2012).

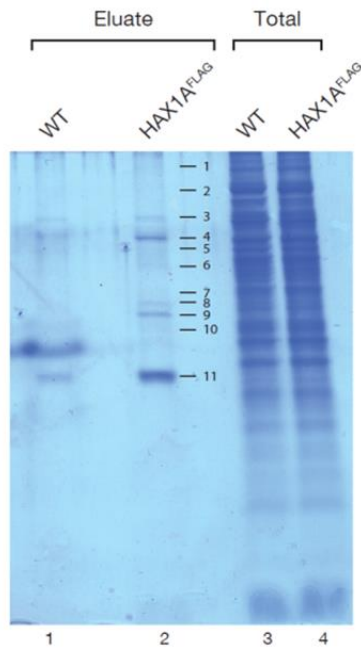


**Figure 23. Analysis of the HAX1FLAG immunoprecipitation experiment by Coomassie-blue staining.** Mitochondria were isolated from HEK293T cells overexpressing Flag-tagged HAX1. The mitochondrial lysates were subsequently subjected to immunoprecipitation with anti-flag beads. Eluates were separated by SDS-PAGE and eleven visible bands were analyzed by mass spectrometry.

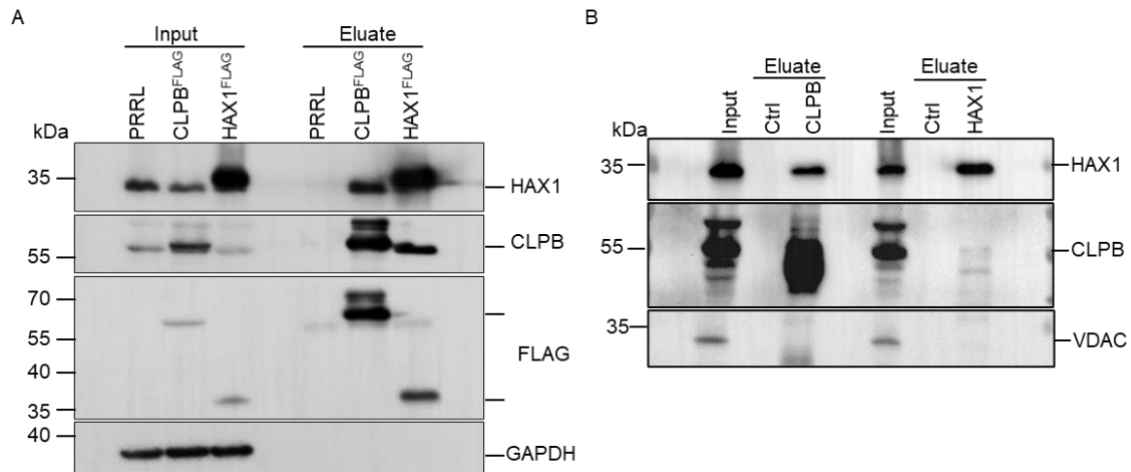
The most prominent interactor of HAX1, i.e. the protein with the highest prediction score, was Caseinolytic peptidase B protein homolog (CLPB) (Table 10). CLPB is a highly conserved member of the AAA+ superfamily, characterized by ATP-dependent catalyzation of protein unfolding, disassembly and disaggregation. In bacteria, Clpb functions as an chaperone assisting cells against heat-shock (Squires et al., 1991) and regulates thermal stress responses (Thomas and Baneyx, 1998) by threading unfolded polypeptides through the central channel of a hexamer ring (Weibezahn et al., 2004). In humans, biallelic mutations in CLPB have been identified in children suffering from a rare syndrome associating cataracts, neurodevelopmental defects, and occasionally congenital neutropenia (Saunders et al., 2015; Wortmann et al., 2015).

Table 10. List of identified HAX1-binding proteins upon immunoprecipitation

Gene symbol	Name	No. of peptides matched	%sequence coverage	Mass	Score
ASAP2_HUMAN	Arf-GAP with SH3 domain, ANK repeat and PH domain-containing protein 2	1	1	111581	33
DCD_HUMAN	Dermcidin	1	1	11277	46
HSP7C_HUMAN	Heat shock cognate 71 kDa protein	2	2	70854	97
HSP76_HUMAN	Heat shock 70 kDa protein 6	1	1	70984	50
ZN616_HUMAN	Zinc finger protein 616	1	1	90215	38
CLPB_HUMAN	Caseinolytic peptidase B protein homolog	21	17	78680	1080
STXB4_HUMAN	Syntaxin-binding protein 4	1	1	61623	41
ANR11_HUMAN	Ankyrin repeat domain-containing protein 11	3	3	297731	36
SHRM3_HUMAN	Protein Shroom3	1	1	216714	34
QRIC2_HUMAN	Glutamine-rich protein 2	1	1	180715	33
STML2_HUMAN	Stomatin-like protein 2, mitochondrial	5	5	38510	344
HERC2_HUMAN	E3 ubiquitin-protein ligase HERC2	2	2	526895	43
HORN_HUMAN	Hornerin	5	5	282228	357
HAX1_HUMAN	HCLS1-associated protein X-1	3	3	31601	282
PLAK_HUMAN	Junction plakoglobin	2	2	81693	146
PLIN5_HUMAN	Perilipin-5	3	3	50760	46
SHRM2_HUMAN	Protein Shroom2	3	3	176303	39
CILP1_HUMAN	Cartilage intermediate layer protein 1	2	2	132480	34
HYDIN_HUMAN	Hydrocephalus-inducing protein homolog	3	3	575528	32
C2D2A_HUMAN	Coiled-coil and C2 domain-containing protein 2A	2	2	186070	32
PGAM5_HUMAN	Serine/threonine-protein phosphatase PGAM5	2	2	31985	144
FRAS1_HUMAN	Extracellular matrix protein FRAS1	1	1	442928	25

Mass spectrometry for detecting potential binding partners of HAX1. The columns are based on gene symbol, name, number of unique peptides matched, percent sequence coverage, estimated MW and scores for binding by LC-MS/MS analysis (Table 10).

To validate the putative protein-protein interaction between HAX1 and CLPB, we performed bidirectional coimmunoprecipitation studies. When cellular lysates from HEK293T cells expressing flag-tagged HAX1 are precipitated and electrophoretically separated, CLPB can be detected in the eluate. Conversely, anti-HAX1 antibodies recognize a specific band in immunoprecipitations of flag-tagged CLPB lysates (Figure 24A). Interactions between HAX1 and CLPB were further confirmed by endogenous immunoprecipitation (Figure 24B). As a control for unspecific protein binding, we also probed for mitochondrial outer membrane protein VDAC. As expected, VDAC could not be detected in the elution of HAX1 immunoprecipitation. Thus, both immunoprecipitation studies revealed that HAX1 indeed interacts with CLPB.



**Figure 24. HAX1 interacts with CLPB.** (A) HEK293T cells were transfected with empty vector PRRL, plasmids expressing Flag-tagged HAX1 or CLPB as indicated. Cells were lysed 48 h after transfection; the lysates were immunoprecipitated with anti-Flag beads. The cell lysates and immunoprecipitates were analyzed by SDS-PAGE and Western blotting with antibodies as indicated. (B) Lysates of HEK293T were split and incubated with either HAX1 or CLPB antibody. Antibodies with bound material were precipitated with proteinG/A-agarose beads and analyzed by SDS-PAGE and Western blotting.

We next examined the submitochondrial localization of CLPB by swelling experiment. Similar to HAX1, CLPB was resistant to PK treatment when mitochondria were intact and could be degraded by PK upon opening the OM under hypo-osmotic buffer condition (Figure 25), indicating that HAX1 and CLPB form a complex in the mitochondria IMS.

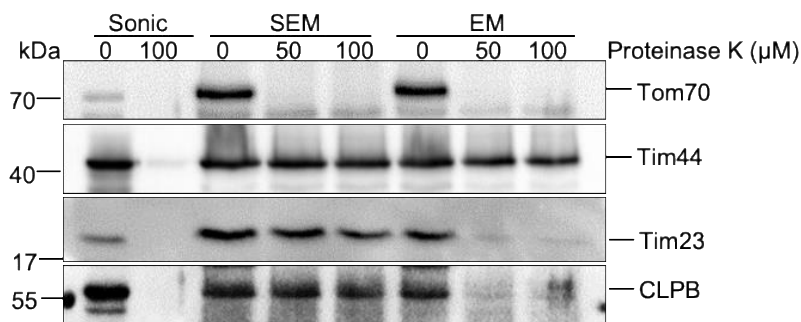


**Figure 25. CLPB is located in mitochondrial intermembrane space.** Isolated mitochondria from either PLB-985 cells (A) or HeLa cells (B) were swollen or sonicated and/or treated with proteinase K prior to analysis by Western blotting. For reference, EM buffer: EDTA, MOPS; SEM buffer: Sucrose, EDTA, MOPS.

To confirm our finding in swelling experiments, we next studied the cellular localization of HAX1 and CLPB by confocal microscopy. Interestingly, both HAX1 and CLPB were partially co-localized with the IMS protein OPA1 (Figure 26). Taken together, our studies identify a CLPB-HAX1 complex localized to the mitochondrial IMS.

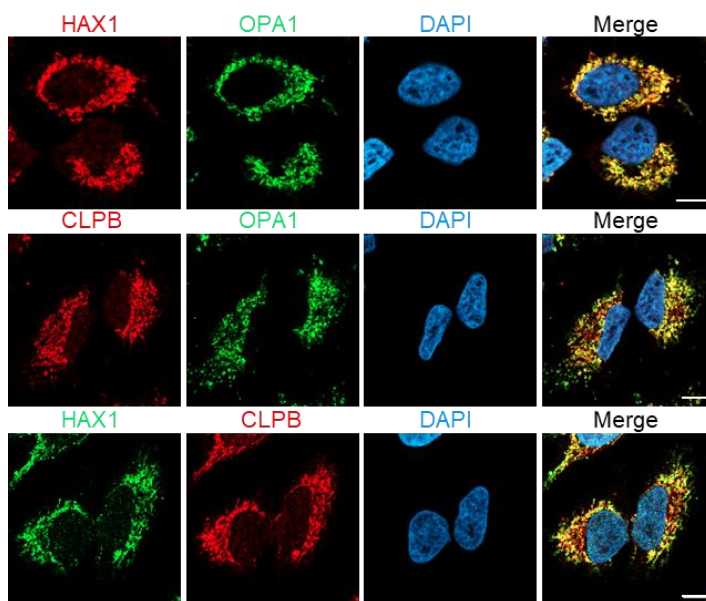


**Figure 26. Costaining of HAX1, CLPB and OPA1 in HeLa cells.** Representative images show fixed HeLa cells costained with HAX1 (red), OPA1 (green) and DAPI (blue) (the upper line); CLPB (red), OPA1 (green) and DAPI (blue) (the middle line); HAX1 (green), CLPB (red) and DAPI (blue) (the bottom line). Scale bar: 10  $\mu$ m.

### 2.2.2 CLPB ensures the solubility of HAX1 in mitochondria

Intrigued by the partial overlap in the clinical manifestation in HAX1- and CLPB-deficiency, we hypothesized that HAX1 is functionally downstream of CLPB and that the phenotype of congenital neutropenia in CLPB deficiency is mediated by defective function of HAX1. As HAX1 is a highly-disordered protein (Cupo and Shorter, 2020) we next studied whether its interaction to CLPB preserves the function of HAX1 by maintaining the solubility of HAX1. To address the question whether CLPB plays any role in controlling protein stability of HAX1, we generated CLPB- and HAX1-deficient cell lines (HeLa and myeloid PLB-985 cells) by CRISPR-Cas9-mediated gene editing. We first observed that HAX1 protein was markedly reduced in the soluble fraction of cells lacking CLPB, whereas the level of CLPB



expression in HAX1-deficient cells was comparable to wildtype cells (Figure 27A). This effect was strictly dependent on CLPB, since the defect was reconstituted upon retroviral gene transfer and expression of CLPB (Figure 27B).

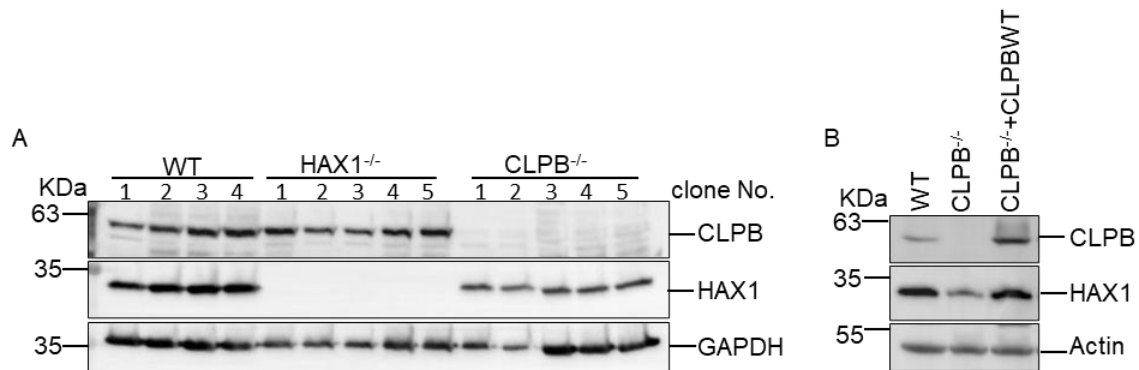


**Figure 27. The expression of HAX1 is reduced in the soluble fraction of cells lacking CLPB.**

(A) PLB-985 cells of three genotypes (WT, HAX1<sup>-/-</sup> and CLPB<sup>-/-</sup>) were subjected to solubilization in a hypotonic lysis buffer. The supernatants of lysates after centrifugation at 14,000 rpm for 15min were directly cooked with a laemmli buffer prior to SDS-PAGE and Western blotting. (B) PLB-985 cells of three genotypes (WT, CLPB<sup>-/-</sup> and CLPB<sup>-/-</sup>+CLPB) were subjected to solubilization in hypotonic lysis buffer. The supernatants of lysates were directly cooked with a laemmli buffer prior to SDS-PAGE and Western blotting.

Since Ecoli ClpB serves as a disaggregase for protein unfolding and disaggregation, we assumed that human CLPB might act at the upstream of HAX1 for ensuring the solubility of HAX1. We examined the cellular distribution of HAX1 in CLPB-deficient cells by immunofluorescent studies. In wild type HeLa cells, HAX1 showed a uniform distribution and co-localized with mitochondrial marker SLP2 (Figure 28A). However, the subcellular distribution pattern of HAX1 altered markedly in cells lacking CLPB, punctiform agglomerates of HAX1 positive granules appeared in CLPB<sup>-/-</sup> mitochondria (Figure 28A). In order to further visualize the insoluble proteins in cells by confocal microscopy, we additionally employed a pre-extraction procedure for mainly removing cytosolic soluble components during slides preparation. Indeed, after pre-extraction treatment, HAX1 was largely removed in control cells, yet HAX1 remained associated with the mitochondrial inner membrane protein SLP2 (Wai et al., 2016) (Figure 28B).

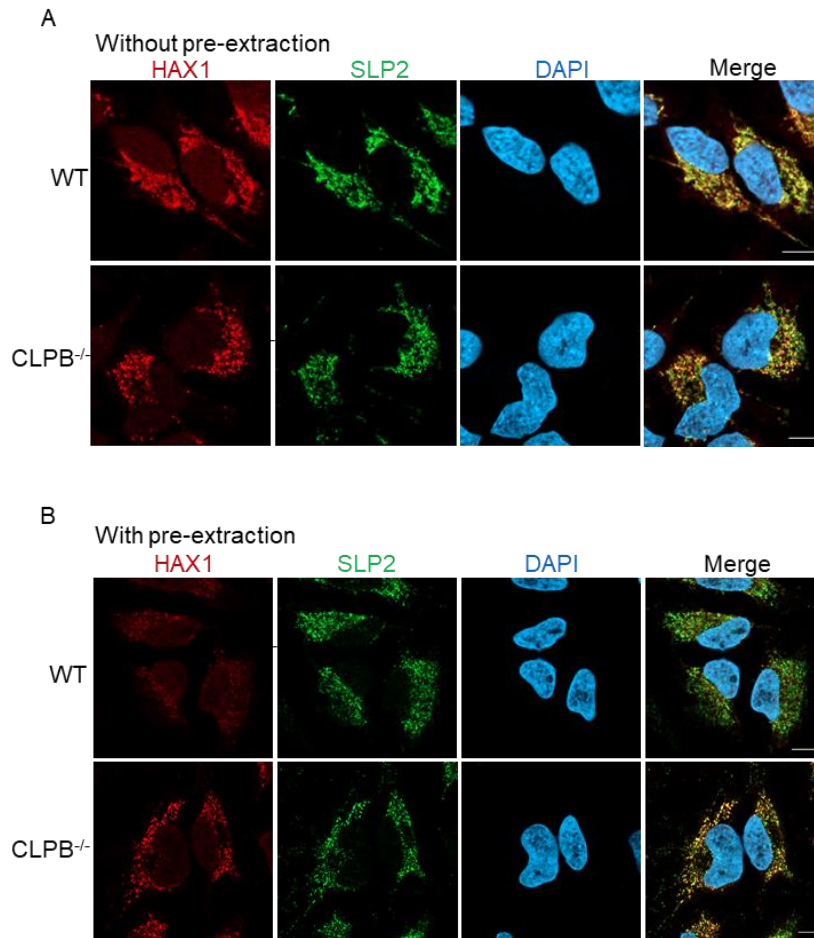


**Figure 28. In the absence of CLPB, HAX1 was characterized in punctiform.** After pre-extraction, the punctiform of HAX1 remained with mitochondrial SLP2. Representative images show fixed HeLa wildtype or CLPB<sup>-/-</sup> cells costained with HAX1 (red), SLP2 (green) and DAPI (blue) with or without pre-extraction treatment as indicated in (A) and (B). Scale bar: 10  $\mu$ m.

Furthermore, we solubilized mitochondria isolated from either WT or CLPB<sup>-/-</sup> PLB-985 cells. Consistent to immunofluorescence studies, HAX1 isolated from CLPB<sup>-/-</sup> mitochondria was not solubilized by carbonate extraction (at 10.5 or 11.5) and nonionic detergent lysis (Triton X-100), in comparison to in WT (Figure 29). This suggested that HAX1 formed aggregates in CLPB<sup>-/-</sup> mitochondria. As a control, the solubility of Tim44 behaved comparable between WT and CLPB<sup>-/-</sup> mitochondria. Taken together, these data demonstrated that CLPB ensured a proper solubility and distribution of HAX1 in mitochondria.

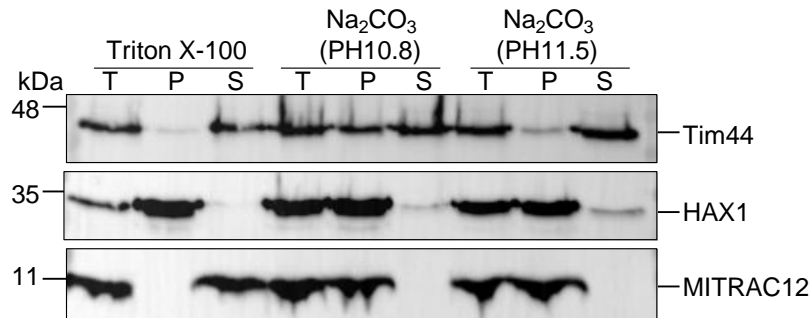


**Figure 29. HAX1 became insoluble in the absence of CLPB.** Mitochondria were subjected to carbonate extraction (at pH 10.8 or 11.5) or detergent lysis by Triton X-100, separated into supernatant (S) and pellet (P) fraction prior to analysis by Western blotting. T, total.

### 2.2.3 The detailed study on interactions between HAX1 and CLPB

To examine the functional relevance of the CLPB-HAX1 interaction, we next aimed at mapping the binding regions that could be involved in mediating interaction between HAX1 and CLPB. HAX1 is containing two putative Bcl-2 homology domains (Pandey et al.) followed by a PEST sequence and a C-terminal trans-membrane domain (Chao et al., 2008) (Figure 30A). We generated HAX1 deletion mutants lacking Exon 1, 2, 3, 5, and 6 and 7 (Figure 30A). FLAG-tagged wild-type HAX1 and a series of exon-deletion mutants were subjected to immunoprecipitation with anti-flag beads and analyzed by SDS-PAGE and Western blotting (Figure 30B). HAX1 truncation mutants lacking specifically exon3 lost the interaction with CLPB (Figure 30B). This suggested that HAX1's Exon 3 is responsible for binding with CLPB.

Furthermore, basing on the localization of known patient mutations in exon 3, a more refined series of mutations in exon 3 of HAX1 were generated and immunoprecipitation with those truncations were analyzed as shown in Figure 30C. In particular, a construct truncated in residues 126 to 168 did not associate with CLPB (Figure 30C), while a deletion construct bearing the aa 137 to 168 could confer interaction. This indicated that residues from 126 to 136 of HAX1 are critical for mediating the interaction of HAX1 with CLPB. Interestingly, this region (residues 126-136) of HAX1 also harbors a known L130R missense mutation causing SCN. We introduced L130R mutation into wildtype HAX1 via overlap-extension mutagenesis and performed immunoprecipitation with either WT or L130R mutant. Surprisingly, L130R mutation fully abolished the interaction of HAX1 with CLPB

(Figure 30D). This further indicated that L130R of HAX1 is a critical residue enabling the interaction to CLPB.

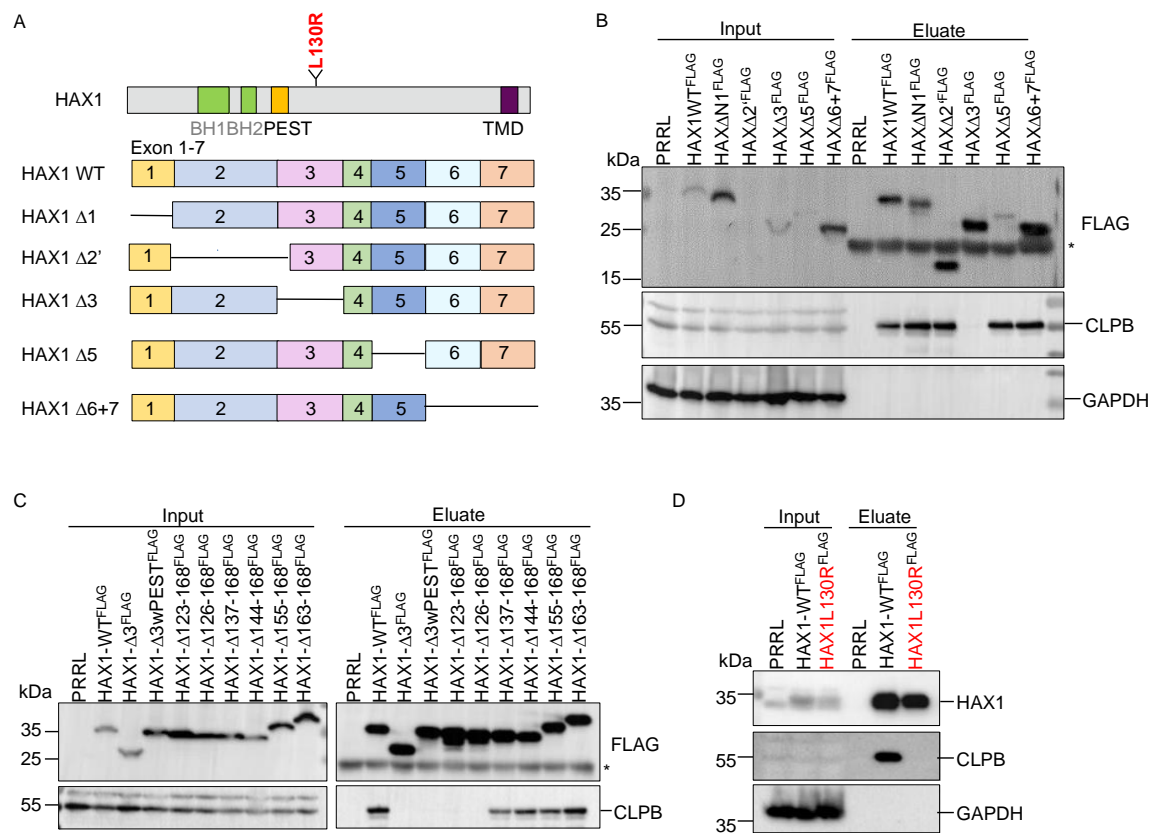


**Figure 30. Mapping of the CLPB-binding domain on HAX1.** (A) Schematic representation of HAX1 wildtype and deletion mutants in this study. (B and C) CLPB interacts with Exon 3 of HAX1; HEK293T cells expressing flag-tagged wildtype or mutants HAX1 were lysed and subjected to IP prior to SDS-PAGE and Western blotting using indicated antibodies. (D) Patient L130R mutation shown in red abolished the interaction with CLPB; HEK293T cells expression flag-tagged wildtype or patient HAX1 were lysed and subjected to IP prior to SDS-PAGE and western blotting using indicated antibodies. \* stands for unspecific binds during detection.

Before the interaction study of CLPB, it was necessary to identify the predominantly expressed transcript of CLPB in cells. According to common database and published studies on CLPB (Saunders et al., 2015; Wortmann et al., 2015), isoform 1 (amino acids 1-707) was known as the canonical transcript of CLPB. However, we found isoform 2 (amino acids 1-677) was the main isoform expressed in vivo (Figure 31). As we identified CLPB isoform 2 to be the predominant expressed form in HEK293T cells, we chose this isoform (amino acids 1-677) for further experiments.

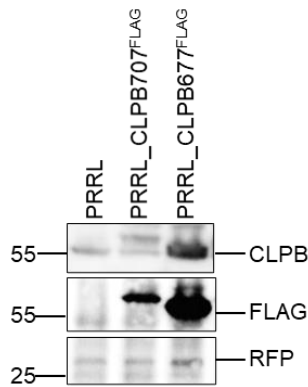


**Figure 31. Identification the predominant isoform of CLPB.** HEK293T cells expressing PRRL vector, flag-tagged CLPB isoform1 (707aa) or 2 (677aa) were lysed and subjected to SDS-PAGE and Western blotting using indicated antibodies.

Next, we set out to define the exact binding region mediating interaction of CLPB with HAX1. CLPB is comprised of an ankyrin-repeat domain (ANK), an ATPase domain (NBD) and a small C-terminal D2 domain (CTD2) (Wortmann et al., 2015) (see scheme in Figure 32A). We generated FLAG-tagged full-length and truncated versions of these functional domains of CLPB and overexpressed them in HEK293T cells. CLPB<sup>WT</sup>-FLAG and CLPB lacking the first 79 residues efficiently bound to HAX1 (Figure 32B) while CLPB absent of its ATPase and CTD2 domain associated less efficiently with HAX1. Of note, immunoblotting also indicated lower expression levels of these fragments. The CLPB mutant lacking the ANK domain, even though expressed at similar levels as the CLPB<sup>ATPase</sup> and CLPB<sup>CTD2</sup> deletion constructs, failed to interact with HAX1. This finding suggests that the interaction of CLPB with HAX1 is mediated by the ANK domain.

The partial overlap in clinical manifestations in HAX1- and CLPB-deficiency prompted us to test if patient mutations causing severe congenital neutropenia compromised the interaction between HAX1 and CLPB. Importantly, some variants clustered in the ANK domain of CLPB have been linked to the rare autosomal recessive mitochondrial disorder, 3-methylglutaconic aciduria, Type VII (MGCA7) that presents with increased levels of 3-methylglutaconic acid (3-MGA), neurologic impairment and neutropenia (Saunders et al., 2015; Wortmann et al., 2015).

Therefore, we introduced these mutants in ANK domain (Y272C, T268M) into CLPB and examined whether these mutations affected the binding to HAX1. As a control,

other mutations causing only neurological dysfunction in CLPB-deficient patients were introduced into the CLPB sequence. All constructs were overexpressed in HEK293T cells and immunoprecipitated. As shown in Figure 32C, CLPB<sup>WT</sup> and CLPB<sup>R561Q</sup> immunoprecipitated with HAX1 while CLPB<sup>T268M</sup> and CLPB<sup>R408G</sup>, two mutations identified in patients with moderate or severe neutropenia (Saunders et al., 2015; Wortmann et al., 2015) were less efficient in binding to HAX1.

In contrast, the Y272C mutant resulted in a mostly full impairment of interaction to HAX1 (Figure 32). Both SCN causative mutants (T268M, Y272C) led to a decrease in protein stability. In conclusion, our data indicated that Exon 3 of HAX1 and the ANK domain of CLPB are responsible for their interaction. Specially, human mutations leading to SCN in HAX1 (L130R) or in CLPB (T268M, Y272C) serve as critical residues enabling the formation of HAX1-CLPB complex.

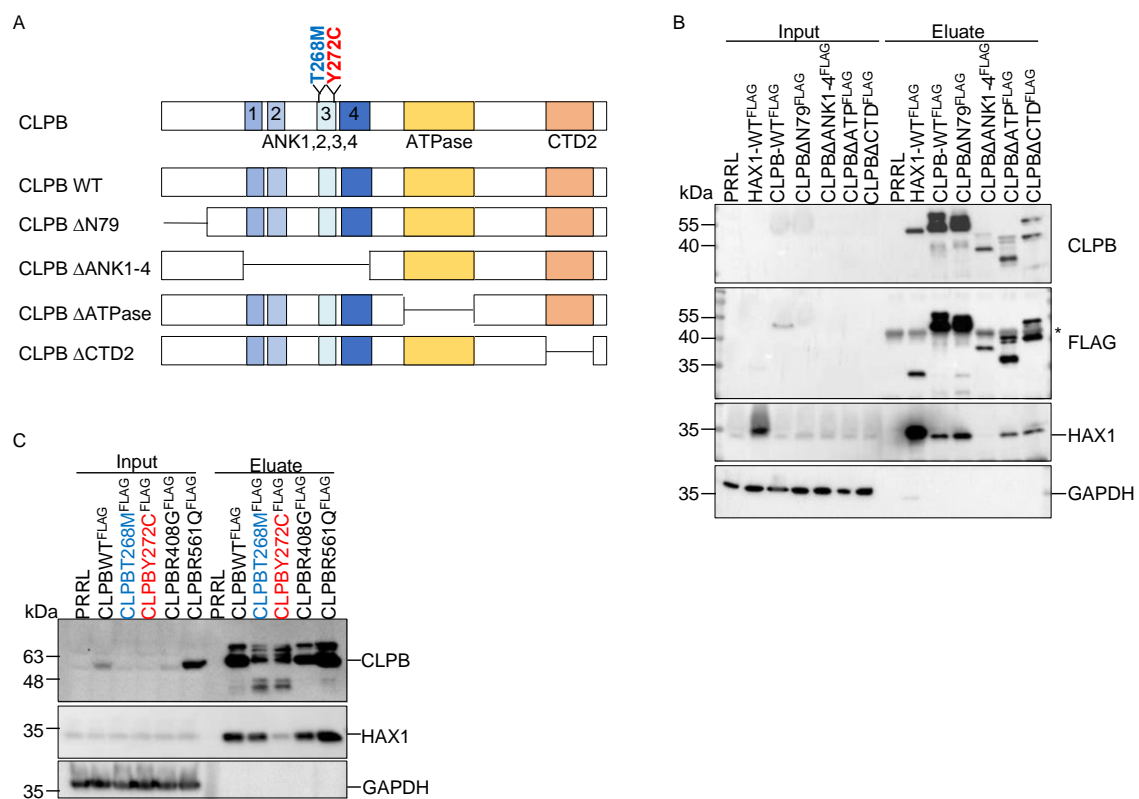


**Figure 32. Mapping of the HAX1-binding domain on CLPB.** (A) Schematic representation of CLPB wildtype and deletion mutants in this study. (B) HAX1 interacts with ANK domain of HAX1; HEK293T cells expressing flag-tagged wildtype or mutants CLPB were lysed and subjected to IP prior to SDS-PAGE and Western blotting using indicated antibodies. (D) Patient Y272C mutation shown in red largely impaired the interaction with HAX1; HEK293T cells expressing flag-tagged wildtype or patient CLPB (T268M shown in blue and Y272C shown in red) were lysed and subjected to IP prior to SDS-PAGE and western blotting using indicated antibodies.

### 2.3 Mitochondrial protein quality control in HAX1- and CLPB-deficiency

To directly address our hypothesis that the CLPB/HAX1 axis is a critical player in maintaining proteostasis in mitochondria, we designed a SILAC (stable isotope labeling with amino acids in cell culture)-based workflow to probe protein synthesis, persistence and turnover in WT, HAX1<sup>-/-</sup> and CLPB<sup>-/-</sup>. Specifically, PLB-985 cells were cultured in media containing arginine and lysine with normal light isotopes of carbon, hydrogen and nitrogen (i.e., <sup>12</sup>C<sup>14</sup>N) (light – “L”). In parallel, another portion of PLB-985 cells were cultured in media with L-arginine-<sup>13</sup>C<sub>6</sub><sup>14</sup>N<sub>4</sub> and L-lysine-<sup>2</sup>H<sub>4</sub> (medium – “M”). All samples were cultured for ten cell divisions to achieve >99% incorporation of L or M amino acids. Then, M- labelled cells were subjected to media containing L-arginine- <sup>13</sup>C<sub>6</sub>-<sup>15</sup>N<sub>4</sub> and L-lysine-<sup>13</sup>C<sub>6</sub>-<sup>15</sup>N<sub>2</sub> (heavy – “H”) to perform a pulse experiment (Boisvert et al., 2012), by which newly synthesized proteins were incorporated with H amino acids for 0, 6 and 24 hours. Thus, ratios of H/L and M/L reflected the kinetics of protein/complex synthesis, and persistence, respectively (Figure 33). These analyses were done with either whole cell extracts or purified mitochondria, so that not only cellular protein networks but also protein networks in mitochondria can be assessed.

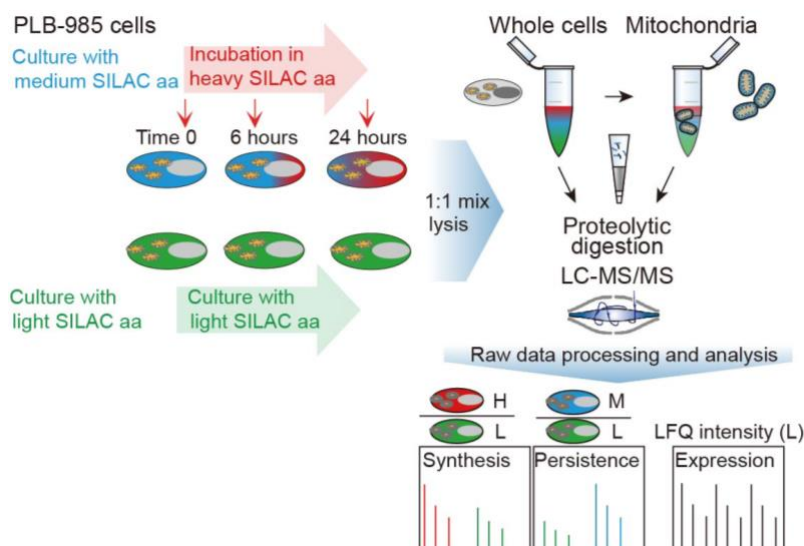


**Figure 33. Scheme of SILAC-based workflow.** SILAC-based workflow for the analysis of protein dynamics and processing of cells for peptide digestion and LC-MS/MS analysis. Ratios of H/L and M/L indicate protein synthesis and persistence. PLB-985 cells were cultured in different SILAC media containing either “light” (L), or “medium” (M) amino acids until proteins were fully incorporated. Then the cells grew with M amino acids were pulsed by culture in a “heavy” (H) medium for 0, 6, 24 hours. Cells were collected at different time points, along with the equivalent cells growing in the “light”

medium. Equal amounts of cells were mixed before proteolytic digestion or mitochondrial isolation. All samples prepared with cell or mitochondria were undergone LC-MS/MS analysis.

First, we determined the pathways whose protein kinetics were most dysregulated by HAX1 deficiency via 2D annotation enrichment analysis (Cox and Mann, 2012). In line with the localization of HAX1, protein synthesis in mitochondrial pathways such as mitochondrial translation, mitochondrial respiratory chain and TCA cycle significantly differed in HAX1<sup>-/-</sup> cells complex to WT (Figure 34A). This encouraged us to use the H/L SILAC ratio as a proxy to compare protein synthesis with WT, HAX1 KO and CLPB KO cells.

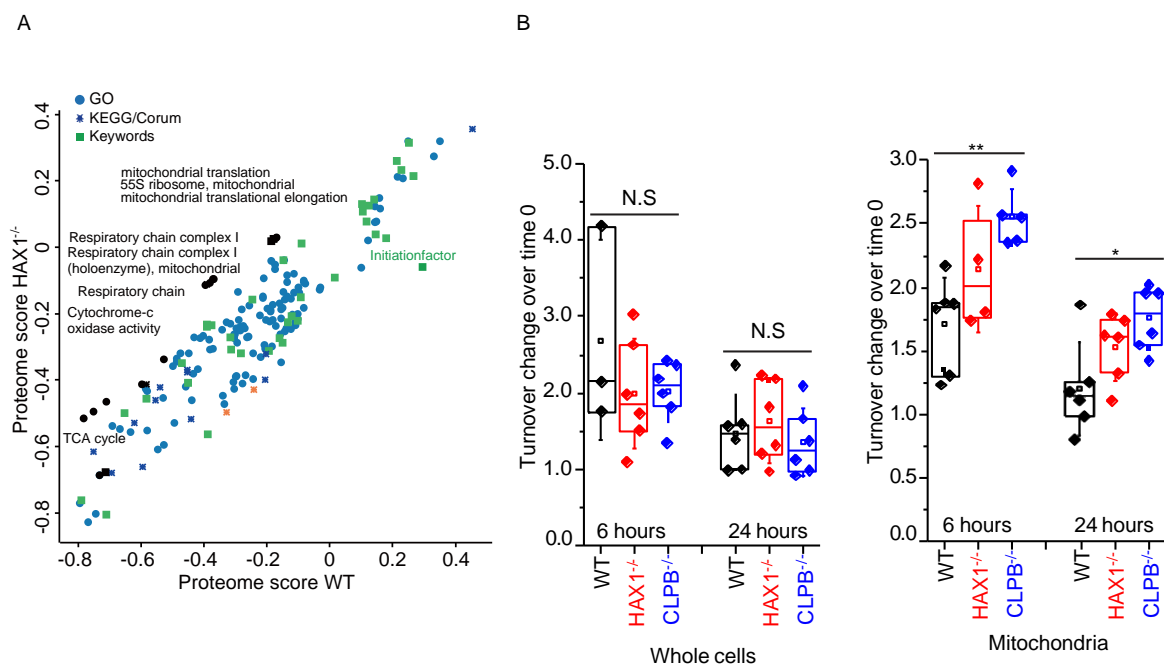


**Figure 34. Increased mitochondrial protein synthesis in HAX1<sup>-/-</sup> and CLPB<sup>-/-</sup> cells.** (A) 2D annotation enrichment in the whole cell protein synthesis (H/L) data at 24 hours. The significant annotations with largest differences are marked in black with names. Annotation type is indicated in the panel. The analysis was performed on the media of n-6. Significance was determined using Benjamini-Hochberg FDR with a threshold value of 0.02. (B) A protein synthesis rate proxy was derived by calculating the changes in median H/L SILAC ratio at 6 hours and 24 hours compared to t<sub>0</sub>. This was calculated in whole cells (left) and mitochondria (Keywords annotation, right). The difference between HAX1 and CLPB-deficient clones compared to WT was statistically significant in mitochondria (mean ± SEM, n = 6; \*P<0.05; \*\*P<0.01; ns = not significant).

Next, we determined the ratio of H/L in pathways related to mitochondrial electron transfer chain and observed that mitochondrial complex I and TCA cycle are the



most significantly upregulated pathways in mitochondria of HAX1<sup>-/-</sup> and CLPB<sup>-/-</sup> than WT. Specifically, in comparison to WT, 11 subunits (selected by GO annotation) in complex I showed significantly higher H/L ratio in HAX1<sup>-/-</sup> cells and 8 subunits showed in CLPB<sup>-/-</sup> cells. While the ratio of protein persistence (M/L) in complex I was increased in HAX1<sup>-/-</sup> and CLPB<sup>-/-</sup> deficient cells, significance was not reached (Figure 35A). In addition, a number of proteins involved in the tricarboxylic acid cycle showed significantly higher protein synthesis and slightly elevated protein persistence in both HAX1<sup>-/-</sup> cells and CLPB<sup>-/-</sup> cells (Figure 35B). There was a high overlap of differentially expressed proteins between HAX1<sup>-/-</sup> and CLPB<sup>-/-</sup> deficiency, pointing towards a strong functional link. Overall, our results indicate that mitochondrial proteostasis, mainly in pathways of complex I and TCA cycle, is perturbed in the absence of HAX1.

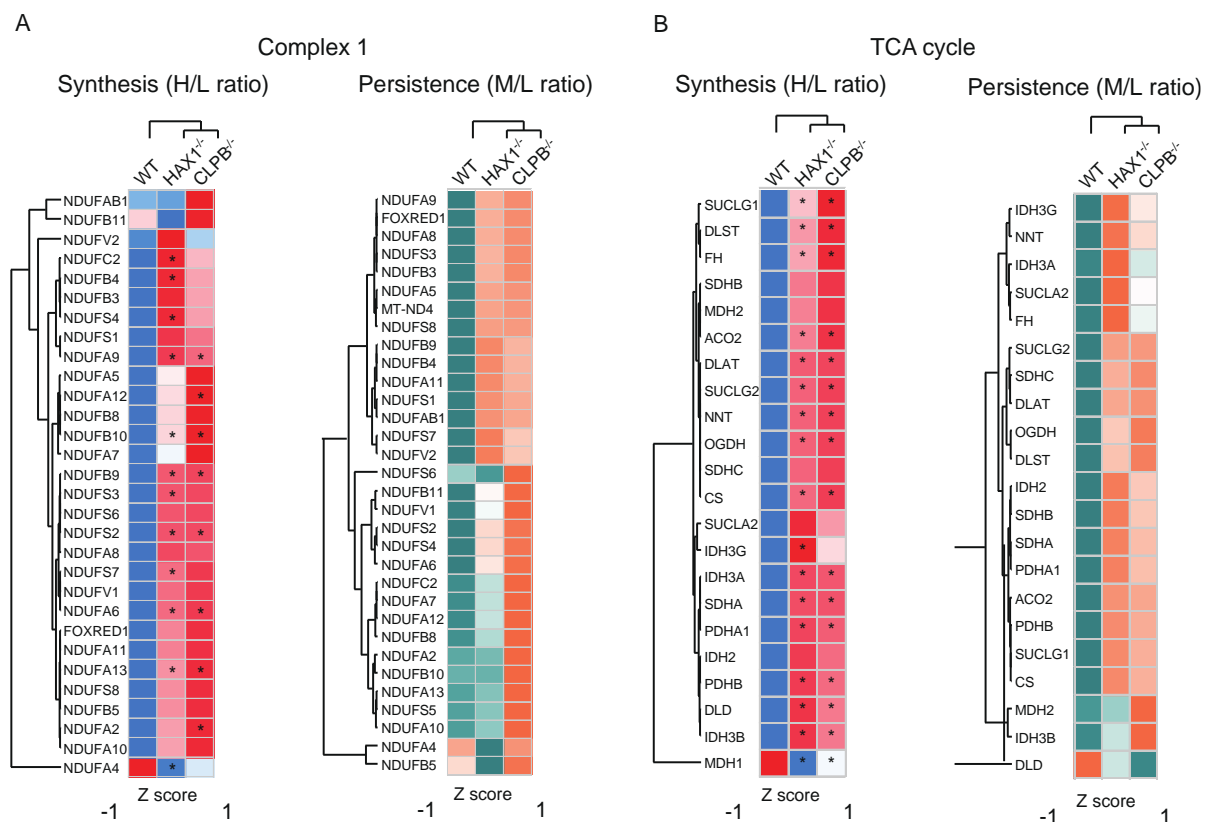


**Figure 35. Proteins with impaired protein turnover enriched in mitochondrial complex I and TCA cycle in both HAX1-KO and CLPB-KO cells.** (A) Unsupervised hierarchical clustering of protein synthesis (H/L, left) and protein persistence (M/L, right) for mitochondrial respiratory chain complex I (GO annotation), comparing WT, HAX1<sup>-/-</sup> and CLPB<sup>-/-</sup> clones after 24 hours of pulse with heavy amino acids. Clusters are based on Z scores as indicated. Significant differences ( $p < 0.05$ , t-test,  $n=6$ ) are marked with an asterisk. (B) Unsupervised hierarchical clustering of protein synthesis (H/L, left) and protein persistence (M/L, right) for the TCA cycle enzyme (represented as in (A)).

In parallel, we carried out the same analysis to non-mitochondrial pathways, such as Golgi apparatus and glycolysis. In comparison to mitochondrial complex I and TCA cycle, no consistent difference of protein synthesis/persistence was measured in Glycolysis and Golgi pathways (Figure 36).

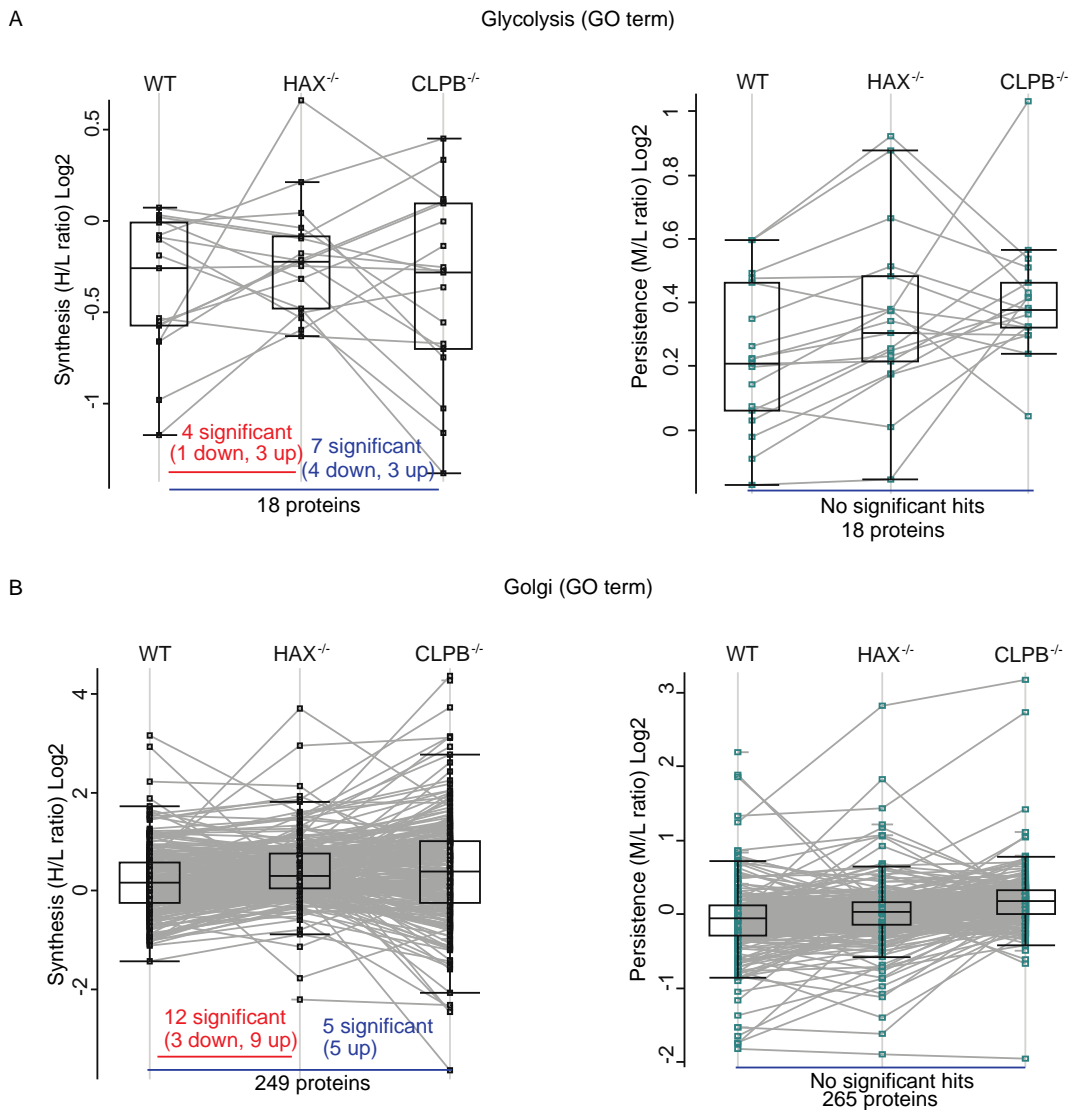


**Figure 36. The protein synthesis and persistence within glycolysis pathway and Golgi pathway.** (A) Profile plots of protein synthesis (H/L, left) and protein persistence (M/L, right) for glycolysis (GO annotation), comparing wild type (WT), HAX1<sup>-/-</sup> and CLPB<sup>-/-</sup> clones after 24 hours of pulse with heavy amino acids. Proteins related to glycolysis were selected based on Gene Ontology (GO) annotations. Significant differences ( $p < 0.05$ , t-test,  $n = 6$ ). The number of proteins with significantly different expression ( $p < 0.05$ ) between WT and each mutant is indicated at the bottom of the plot. (B) Profile plots of protein synthesis (H/L, left) and protein persistence (M/L, right) for Golgi apparatus (GO annotation), comparing wild type (WT), HAX1<sup>-/-</sup> and CLPB<sup>-/-</sup> clones after 24 hours of pulse with heavy amino acids. Proteins related to Golgi apparatus were selected based on Gene Ontology (GO) annotations. Significant differences ( $p < 0.05$ , t-test,  $n = 6$ ). The number of

proteins with significantly different expression ( $p < 0.05$ ) between WT and each mutant is indicated at the bottom of the plot.

To substantiate our MS-analyses of altered respiratory chain (RC) complex I dynamics in the absence of HAX1, we employed HAX1 knockout cells generated by CRISPR/Cas9-mediated genome editing and assessed the enzymatic activity of mitochondrial complex 1 in both WT and HAX1 KO cells. The activity of complex I (NADH dehydrogenase) was evaluated by the reduction of the provided dye during the oxidation of NADH, which led to an increased absorbance. As shown in Figure 37A, mitochondria isolated from HAX1<sup>-/-</sup> cells exhibited significantly reduced complex I activity compared to mitochondria purified from WT cells, while the activity of complex IV was not affected in HAX1 deficient cells.

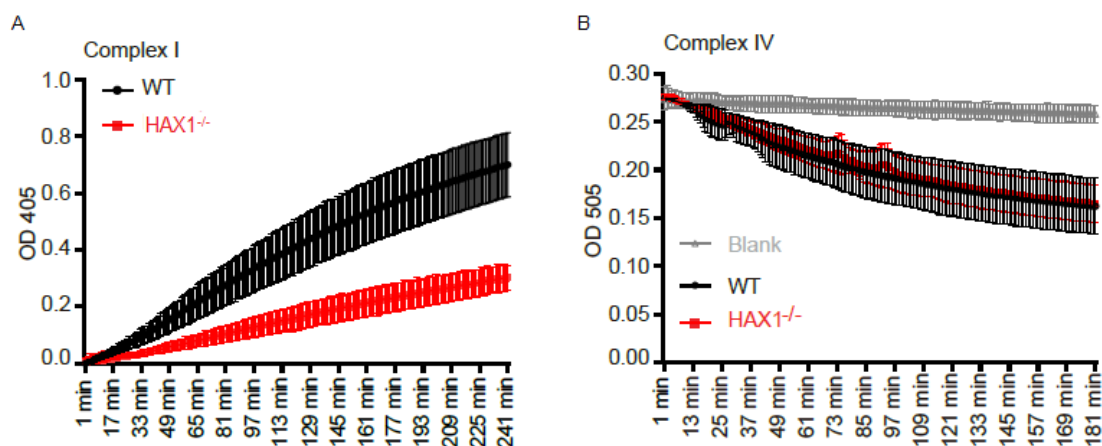


**Figure 37. Mitochondrial complex I activity was impaired in the absence of HAX1.** Mitochondria isolated from WT and HAX1-KO PLB-985 cells were used to measure (A) complex I activity and (B) complex IV activity. Data were collected from three independent experiments. Complex I activity showed significant decrease (means  $\pm$  SEM, 2way-ANOVA,  $P < 0.01$ ,  $n = 3$ ) in the absence of HAX1, whereas no significant alterations displayed in the measurement of complex IV activity.

As the mitochondrial complex I is considered to be a main source of superoxide production (Camello-Almaraz et al., 2006), we analyzed the level of mitochondrial superoxide in WT and HAX1<sup>-/-</sup> cells. Indeed, mitochondrial superoxide ( $O_2^{\cdot-}$ ) levels were significantly increased in the absence of HAX1 (Figure 38). Yet, HAX1 KO cells that were functionally complemented with HAX1 restored the upregulated  $O_2^{\cdot-}$  levels (Figure 38). Thus, our data identify HAX1 as a critical regulator of mitochondrial complex I activity.

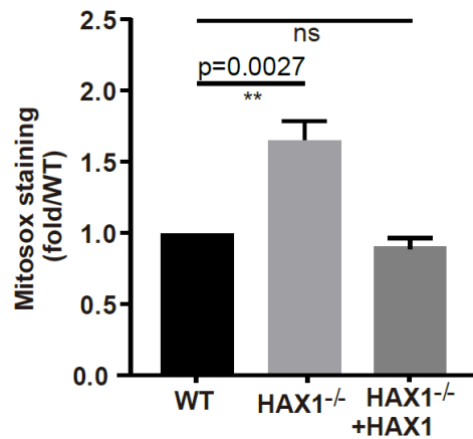


**Figure 38. HAX1 deficiency induced elevated mtROS production.** mtROS production was measured with PLB-985 cells by adopting superoxide indicator MitoSOX Red (means  $\pm$  SEM, t-test,  $n = 3$ ).

#### 2.4 HAX1 maintains solubility of HSP27 in mitochondria.

In order to further illustrate the cellular function of HAX1, we focused on proteins that were differentially expressed in HAX deficiency compared to WT. Using label-free quantification (LFQ) with mass spectrometry data, we compared the proteome of WT with HAX1 deficient PLB-985 cells for proteome-wide protein abundance changes. In the LFQ analysis, a total of 4372 proteins with  $\geq 2$  peptides used for the quantification and  $> 3$  valid values in total were applied. As shown in the volcano plot on differentially expressed proteins (Figure 39A), HSP27 stood out as highly decreased in the absence of HAX1. HSP27 belongs to a class of molecular chaperones that maintain cellular protein proteostasis by preventing the aggregation of partially unfolded proteins (Mymrikov et al., 2017), whose functions are tightly regulated by its phosphorylation. In its unphosphorylated form, HSP27 assembles into large insoluble oligomeric complexes, whereas phosphorylation results in complex dissociation into smaller soluble oligomers or dimers.

Based on our mass spectrometry data, the downregulation of HSP27 in HAX1<sup>-/-</sup> cells was validated by Western blotting analysis (Figure 39B). PLB-985 cells (WT, HAX1<sup>-/-</sup> and CLPB<sup>-/-</sup>) were solubilized with a hypertonic lysis buffer and supernatants were subjected to SDS-PAGE and Western blotting. In both HAX<sup>-/-</sup> and CLPB<sup>-/-</sup> PLB-985 cells, HSP27 was less detectable in comparison to WT and gene-reconstituted cells (Figure 39B).

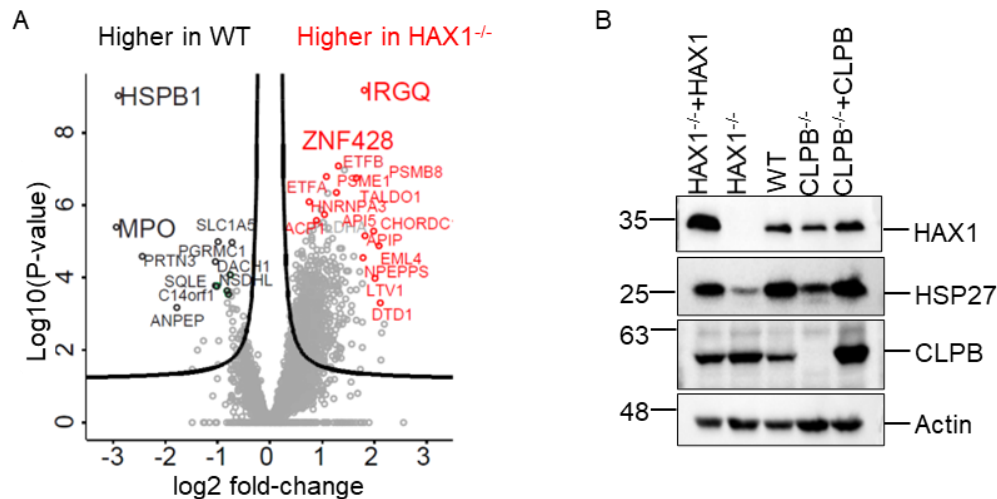


**Figure 39. The existence of HSP27 was reduced in the absence of HAX1 or CLPB.** (A) Volcano plot indicating protein expression changes between WT (n=6) and HAX<sup>-/-</sup> (n=6) PLB-985 cells. X-axis demonstrates log<sub>2</sub> fold change in comparison to WT and Y-axis indicates -log<sub>10</sub>(P-value). A total of 71 proteins were significantly elevated in WT vs HAX<sup>-/-</sup>, 159 proteins were significantly elevated in HAX<sup>-/-</sup> vs WT. Points marked in black (higher in WT) and red (higher in HAX<sup>-/-</sup>) have adjusted P-values <0.01 and absolute fold-change >2. (B) PLB-985 cells collected from indicated genotypes were subjected to hypertonic lysis prior to SDS-PAGE and Western blotting.

Interestingly, HSP27 abundance was also dependent on the type of processing. HSP27 was less detectable in cells exposed to hypotonic stress in comparison to whole cell lysate of HAX<sup>-/-</sup> PLB-985 cells, in which cells were pelleted and directly cooked in Laemmli buffer (Figure 40).

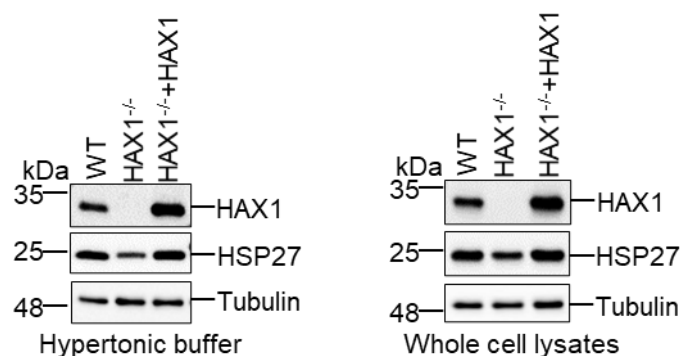


**Figure 40. HSP27 was more detectable in whole cell lysates in comparison to hypertonic lysis.** PLB-985 cells collected from indicated genotypes were subjected to either hypertonic lysis (left) or whole cell lysates preparation (Witzel et al.) prior to SDS-PAGE and Western blotting.

This prompted us to assume that there might be a portion of insoluble HSP27, remaining in the pellet of HAX1 deficiency under hypertonic lysis. Therefore, with the preparation of cell hypertonic lysis, supernatant was collected and the insoluble cell pellets were directly cooked with Laemmli buffer. All samples were subjected to SDS-PAGE and Western blotting. Intriguingly, anti-HSP27 immunoblotting showed two bands upon electrophoretic separation only in HAX1-deficient cells, and not in WT cells or in gene-reconstituted cells. Moreover, the faster migrating form failed to be detected by the specific HSP27 phosphorylation antibody (HSP27-p82) (Figure 41). This suggested that a dephosphorylated form of HSP27 appeared to be less soluble in HAX1 deficient cells.

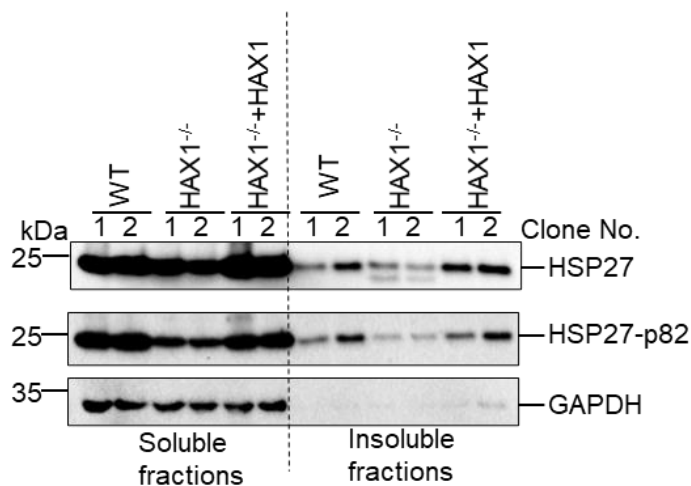


**Figure 41. A dephosphorylated form of HSP27 remained in the pellet after solubilization by hypertonic solution.** PLB-985 cells from indicated genotypes were subjected to hypertonic lysis. After centrifugation, supernatants were collected as soluble fractions, whereas remaining pellets were cooked with Laemmli buffer as insoluble fractions. All samples were loaded to SDS-PAGE prior to Western blotting.

The phosphorylation status of HSP27 has been shown to play a critical role in the regulation of its oligomerization. Upon phosphorylation, large HSP27 oligomers consisting of around 6 tetramers dissociate into single tetramers or dimers (Rogalla et al., 1999). As HSP27 was highly phosphorylated in wildtype PLB-985 cells, we hypothesized that impaired phosphorylation of HSP27 would lead to larger oligomers, which appeared to be insoluble in the absence of HAX1.

In order to visualize the insoluble HSP27 in cells lacking HAX1 through immunofluorescence studies, we employed pre-extraction treatment to WT and

HAX<sup>-/-</sup> PLB-985 cells. This method allowed us to remove most of soluble proteins in the cytosol by permeabilizing cells prior to fixation. In control and HAX1 KO cells, HSP27 was evenly distributed throughout the cytoplasm (Figure 42, upper panel). However, after pre-extraction treatment, HSP27 showed a punctiform pattern in HAX1<sup>-/-</sup> cells, whereas the staining of HSP27 was almost invisible in WT cells (Figure 42, lower panel). This is consistent with the notion that HSP27 became insoluble in HAX1 deficiency.

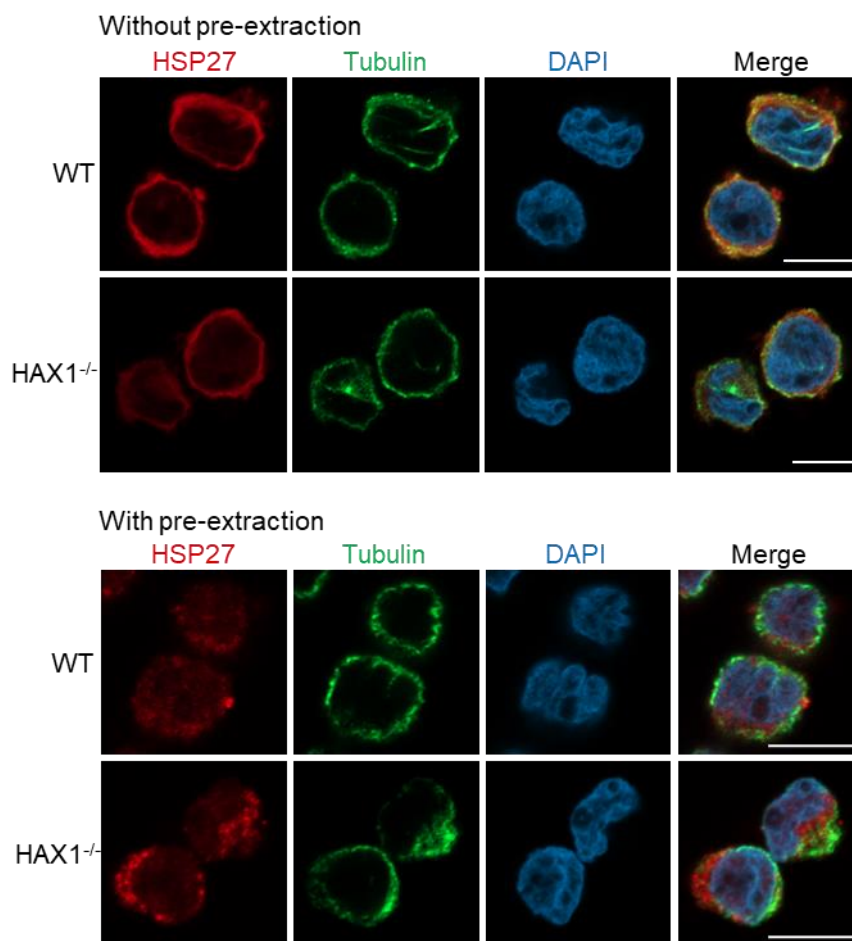


**Figure 42. HSP27 remained in punctiform in the absence of HAX1 after pre-extraction treatment.** Representative images show fixed PLB-985 cells costained with HSP27 (red), Tubulin (green) and DAPI (blue) with or without pre-extraction treatment as indicated in (A) and (B). Scale bar: 10  $\mu$ m.

Intriguingly, we were able to probe HSP27 as two differently migrating forms in HAX1<sup>-/-</sup> or CLPB<sup>-/-</sup> mitochondria (Figure 43A). Similar to HAX1 deficiency, also in CLPB-deficient mitochondria HSP27 migrated at two distinctive speeds. Furthermore, HSP27p82 was expressed at reduced abundance in HAX<sup>-/-</sup> and CLPB<sup>-/-</sup>

<sup>-/-</sup> mitochondria (Figure 43B), again suggesting that the consequences of HAX1 and CLPB deficiency are functionally linked.

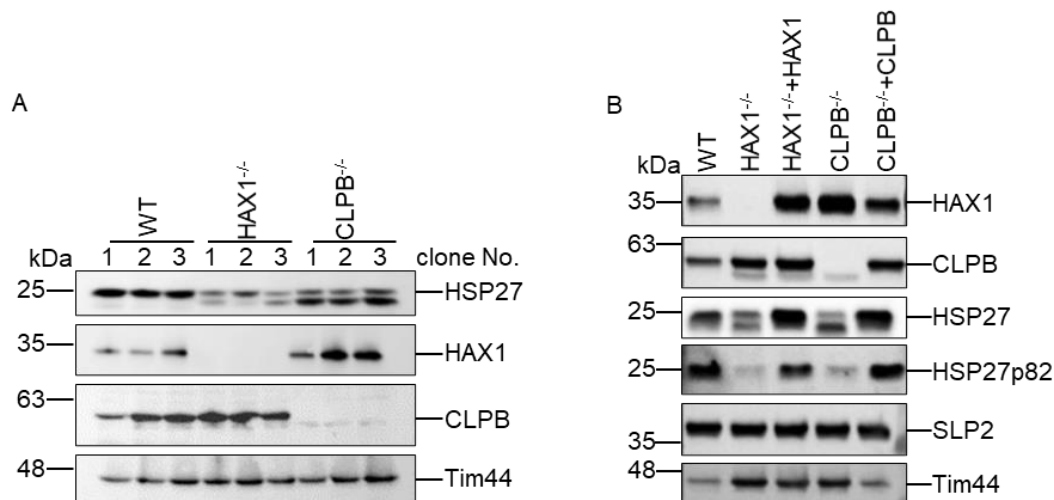


**Figure 43. Two differently migrating forms of HSP27 were detected in HAX1<sup>-/-</sup> or CLPB<sup>-/-</sup> mitochondria.** (A and B) Mitochondria were isolated from PLB-985 cells of indicated genotypes prior to SDS-PAGE and Western blotting.

We next studied whether HAX1 regulated the solubility of HSP27 in mitochondria by confocal microscopy. Without pre-extraction, WT and HAX1-deficient PLB-985 cells show evenly distributed HSP27 throughout the cytoplasm. However, after removing soluble cytosolic components by pre-extraction, punctiform HSP27 appeared to be colocalized with mitochondrial marker Tom20 in HAX1<sup>-/-</sup> PLB985 cells. Yet, HSP27 became mostly invisible after pre-extraction in WT PLB-985 cells. These results suggested that the dephosphorylation of HSP27 resulting from HAX1 deficiency led to its aggregation in mitochondria (Figure 44).



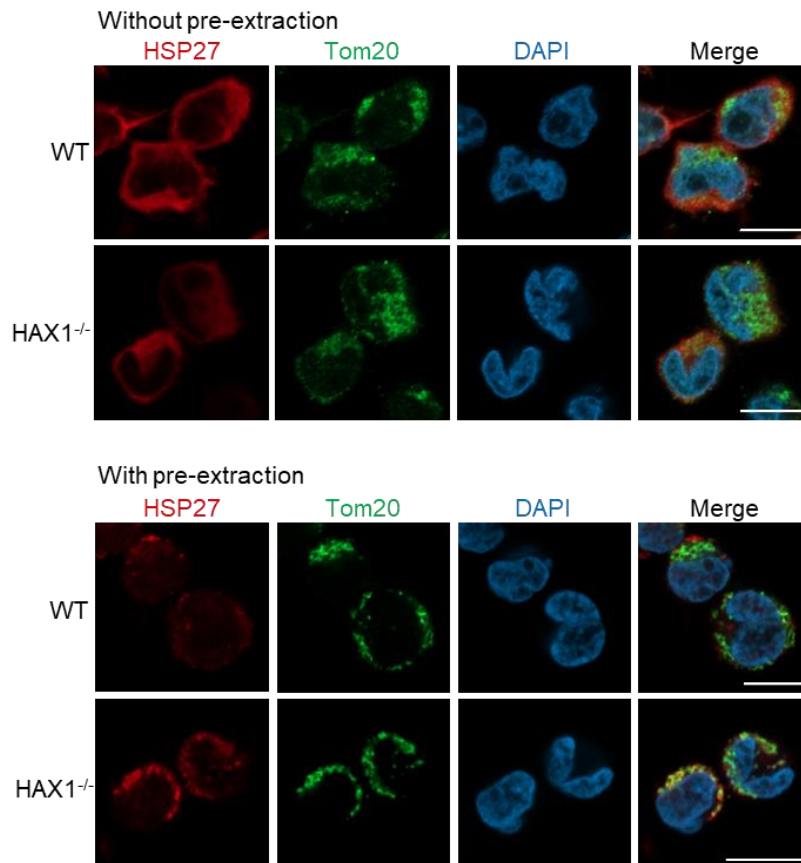


**Figure 44. HSP27 formed in punctiform in HAX1-deficient mitochondria after pre-extraction treatment.** Representative images show fixed HeLa cells costained with HSP27 (red), Tom20 (green) and DAPI (blue) with or without pre-extraction treatment as indicated in (A) and (B). Scale bar: 10  $\mu$ m.

To substantiate our findings, we performed carbonate extraction experiments of isolated mitochondria from WT, HAX1 and CLPB KO cells (Figure 45). Similar to the membrane-bound protein Tim44, HSP27 is fully solubilized into the supernatant (S) upon Triton X-100 treatment and was released from the mitochondrial membrane into the supernatant (S) at pH 11.5 in mitochondria purified from WT PLB-985 cells (Figure 45A). However, in the absence of HAX1 and CLPB, HSP27 partially remained in the pellet fraction under different lysis and extraction conditions (Figure 45B and C). In line with our previous data the unphosphorylated, insoluble/unphosphorylated form of HSP27 was enriched in the pellet fractions upon Triton X-100 and carbonate solubilization (Figure 45B and C). Taken together, these data demonstrated that CLPB and HAX1 ensure the efficient phosphorylation and solubility of HSP27 in mitochondria.

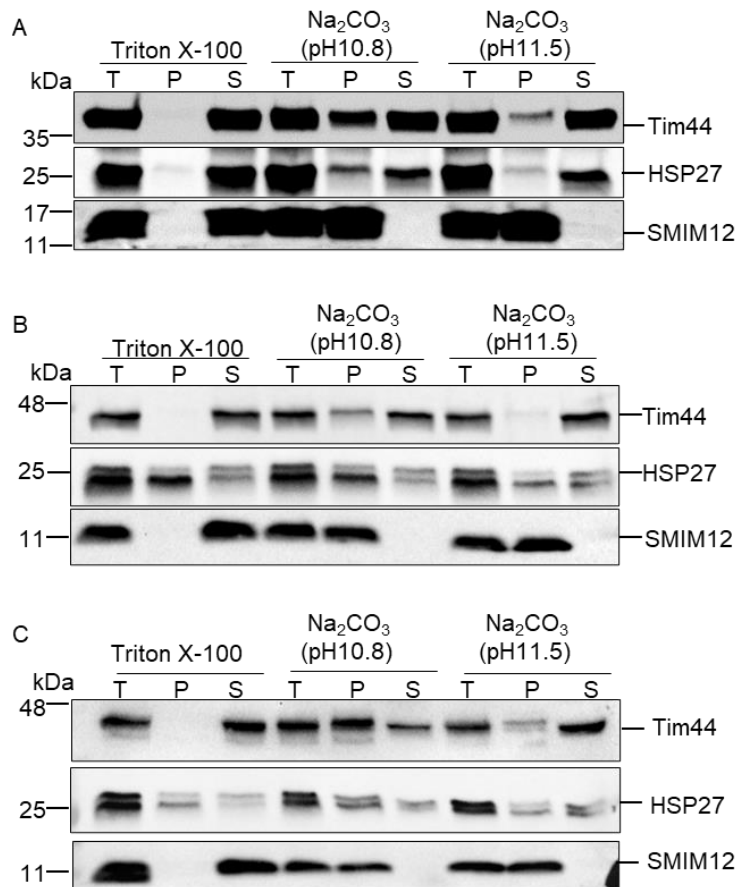


**Figure 45. The faster migrating form of HSP27 is more resistant to carbonate extraction or detergent lysis than the upper band of HSP27, in the absence of HAX1 or CLPB.** (A, B and C) WT, CLPB<sup>-/-</sup> and HAX1<sup>-/-</sup> mitochondria were subjected to carbonate extraction (at pH 10.8 or 11.5) or detergent lysis by Triton X-100, separated into supernatant (S) and pellet (P) fraction prior to analysis by Western blotting. T, total.

## 2.5 HSP27 restores perturbed mitochondrial proteostasis in HAX1 deficient cells.

Next, we were interested which kinase might be responsible for mediating HSP27 phosphorylation in mitochondria. Several protein kinase families have been shown to involve in the phosphorylation of HSP27 (Kostenko and Moens, 2009), however the potential endogenous activators of HSP27 phosphorylation are largely unknown in myeloid cells. We therefore searched for candidate kinases/phosphatases potentially effected HSP27's phosphorylation in HAX1 deficient PLB-985 cells, by comparing differentially expressed kinases and phosphatases in WT and HAX1<sup>-/-</sup> PLB-985 cells, respectively.

As shown in Figure 46, most of kinases and phosphatases were significantly upregulated in HAX1 deficient PLB-985 cells, except for PRKD2 which was significantly downregulated in HAX1 deficiency (Figure 46).

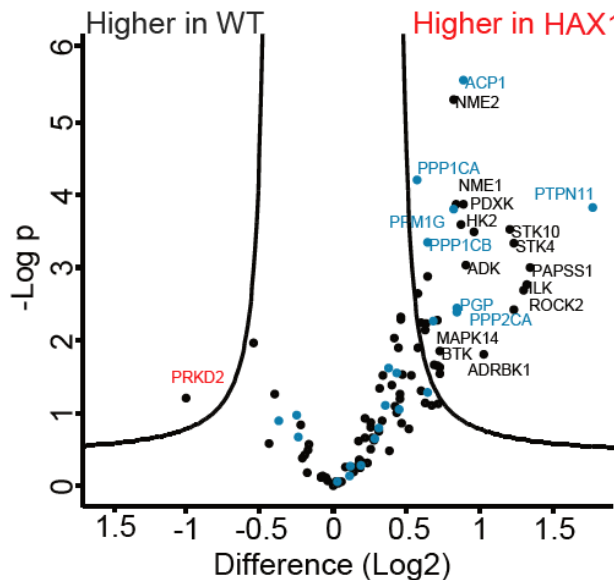


**Figure 46. PRKD2 was reduced in the absence of HAX1.** Volcano plot illustrates changes in kinases and phosphatases expression between WT (n = 6) and HAX<sup>-/-</sup> (n = 6) PLB-985 cells. X-axis showing log<sub>2</sub> fold change in comparison to WT, Y-axis showing -log<sub>10</sub>(P-value). Kinases were marked in red or black and phosphatases were marked in blue. Gate was adjusted to P-values <0.05.

Several studies identified HSP27 as a substrate of protein kinase D (PKD) serine/threonine kinase family (Doppler et al., 2005), which consists of PRKD1, PRKD2 and PRKD3. Only PRKD2 and PRKD3 are expressed in myeloid cells. We validated our LFQ-result by examining PRKD2 expression in mitochondria isolated from control, HAX1 KO or HAX1 reconstituted PLB-985 cells by immunoblotting. In comparison to WT and HAX1 reconstituted mitochondrial lysates, the expression of PRKD2 was indeed largely compromised in the cellular extracts from HAX1<sup>-/-</sup> cells (Figure 47).

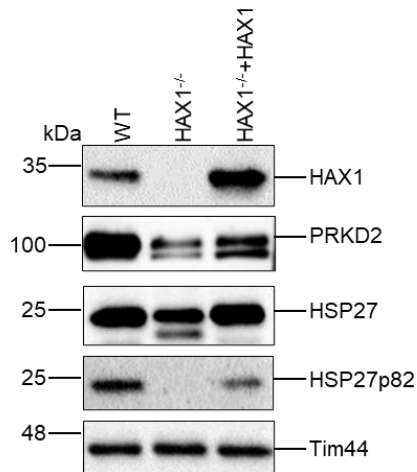


**Figure 47. PRKD2 was down-regulated in the absence of HAX1.** Mitochondria isolated from WT, HAX1<sup>-/-</sup> and HAX1<sup>-/-</sup>+HAX1 PLB-985 cells were respectively subjected to SDS-PAGE and Western blotting.

PRKD2 has not yet emerged as a kinase spatially defined in mitochondria. Thus, we next examined whether HSP27 and PRKD2 are both located inside the mitochondria by performing mitochondrial swelling assay as described in Figure 17. Only Tom70 was degraded upon PK treatment in SEM buffer (Figure 48 lane 1), whereas PRKD2, HSP27, pHSP27, Tim23, HAX1 and CLPB remained unaffected (Figure 48 lanes 3-8). Upon rupture of OM in EM buffer, similar to Tim23, HAX1 and CLPB were degraded by PK. However, a portion of PRKD2, HSP27 and pHSP27 was resistant to PK digestion in EM buffer (Figure 48 lane 6-8). This indicated that PRKD2 and pHSP27 are localized in the IMS and partially in the matrix. As a matrix control, Tim44 was resistant to PK digestion in both SEM and EM conditions.

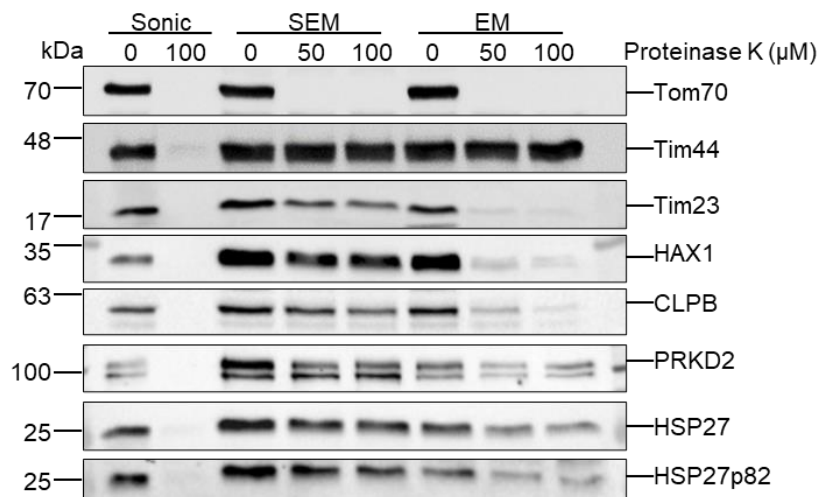


**Figure 48. PRKD2 and HSP27 were located in mitochondrial IMS and matrix.** Isolated mitochondria from PLB-985 cells were swollen or sonicated and/or treated with proteinase K prior to analysis by Western blotting. For reference, EM buffer: EDTA, MOPS; SEM buffer: Sucrose, EDTA, MOPS.

To directly test whether PRKD2 mediated phosphorylation of HSP27, we inhibited the activity of PRKD2 using CRT0066101, a pan-inhibitor of the PKD family (Harikumar et al., 2010). As shown in Figure 49A, the phosphorylation of HSP27 was impaired upon CRT0066101 treatment. To test more specifically whether PRKD2 is involved in mediating phosphorylation of HSP27, we generated retrovirus-transduced PLB-985 cell lines, containing shRNA targeting on human PRKD2 in a doxycycline-inducible expression manner. Upon doxycycline induction, the partial depletion of PRKD2 in PLB-985 cells resulted in a reduced phosphorylation of HSP27 at Ser-82 (Figure 49B). Overall, these data demonstrated that PRKD2 played a role in regulating HSP27 in PLB-985 cells.

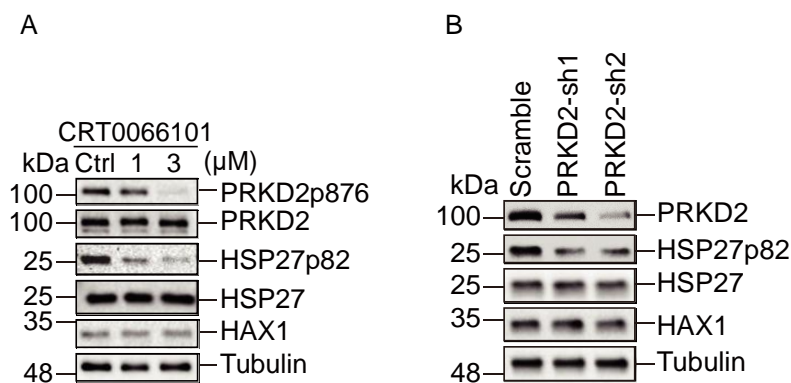


**Figure 49. Inhibition of the activity or reduced expression of PRKD2 impairs HSP27's phosphorylation.** (A) PLB-985 cells were treated with CRT0066101 at indicated concentrations for 3h before being subjected to SDS-PAGE and Western blotting. (B) PLB-985 stable cell lines, expressing constructs contained scramble shRNA or PRKD2-targeted shRNA in a doxycycline-inducible manner, were subjected to SDS-PAGE and Western blotting after 4 days of doxycycline (1μg/mL) treatment.

## 2.6 HSP27 is associated with mitochondrial complexes and translation, whose reconstitution recovers mitochondrial oxidative stress in HAX1 deficiency.

We further carried out a mitochondrial interactome assay to identify critical downstream clients/targets of HSP27 in mitochondria. Mitochondria lysates either from WT HEK293T cells overexpressing control (empty pRRL vector) or FLAG-HSP27 cells were subjected to FLAG-immunoprecipitation. The eluates collected from controls and HSP27-Ips were analyzed via mass spectrometry as described in materials and methods. The significantly increased categories in HSP27 overexpressing cells comprised respiratory electron transport chain, mitochondrial translational pathways, 'de novo' protein folding and TCA cycle (Figure 50A and B). Consistent with an involvement of HSP27 in translation (Carper et al., 1997; Cuesta et al., 2000), the group of highly up-regulated proteins included key RNA binding proteins, such as MRLP proteins, TUFM, PTCD3 and DAP3. This suggested that HSP27 involved in mitochondrial ribosomal translation.

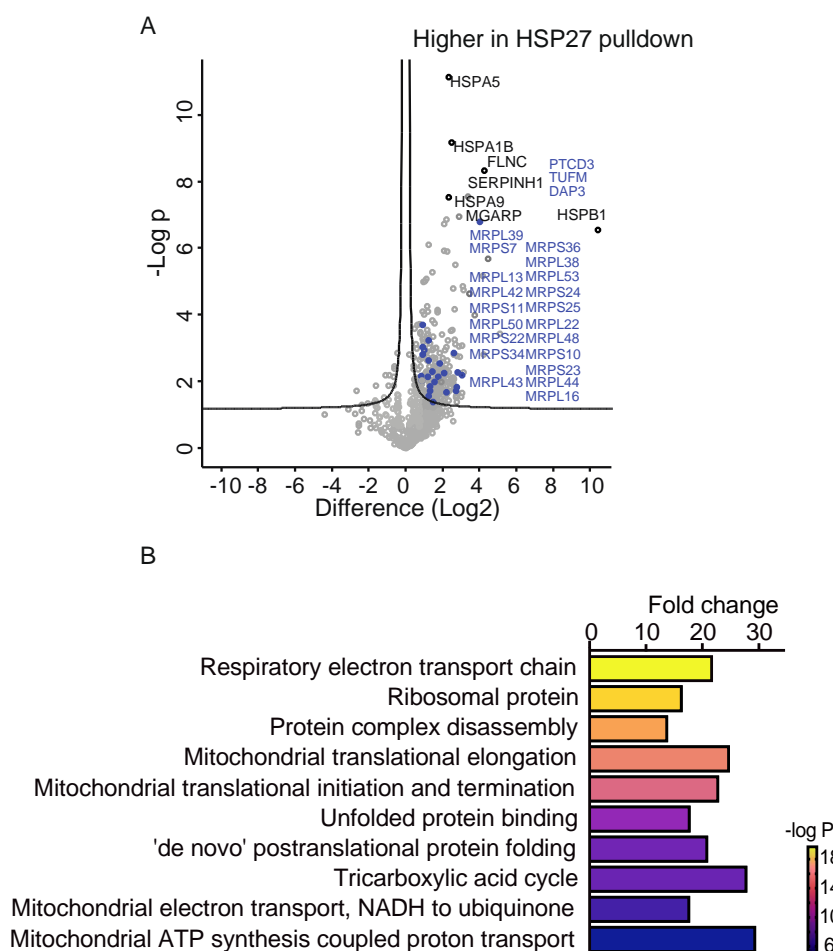


**Figure 50. The interactome of HSP27 in mitochondria.** (A) Volcano plot illustrating the mitochondrial interactome of HSP27 (n=6) versus control (non-bait) (n=6). The analysis is based on 724 proteins that were commonly identified in two biological replicates. The bait (Hsp27/HSPB1) and the interactors with highest p values are marked in black. Significant interactors annotated as

mitochondrial translation (GO) are marked in blue and listed. (B) GOBP pathway enrichment analysis of the HSP27 interactome (panel F, right side), color-coded by enrichment p value as indicated.

Like cytosolic HSP27, we assumed mitochondrial HSP27 may serve as a holdase to safeguard mitochondrial translational machinery so that unfolded or misfolded nascent peptides can be timely cleared. Insolubilization of HSP27 would then predispose nascent mitochondrial peptides to unwanted aggregation, which could further disrupt mitochondrial protein quality control and result in mitochondrial unfolded protein response in the matrix. Intriguingly, mitochondrial unfolded protein response was activated via Sirt3-FOXO3-LC3 pathway in HAX1 deficient cells (Figure 51). This suggested that perturbed mitochondrial proteostasis (shown in Figure 35) in HAX1 deficiency was probably due to a defective mitochondrial translation caused by dysfunctional/dephosphorylated HSP27.

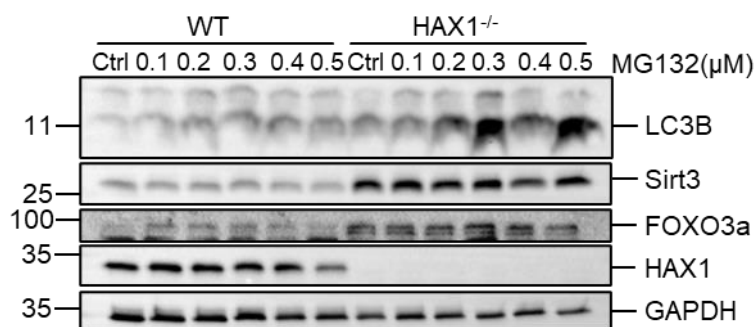


**Figure 51. HAX1 deficient cells displayed mitochondrial unfolded protein response by activating Sirt3-FOXO3a-LC3 pathway and the induction of autophagy was enhanced upon MG132 treatment in the absence of HAX1.** PLB-985 cells were treated with increasing concentrations of MG132 for 18h before being subjected to SDS-PAGE and analyzed by Western blot.

As we identified several complex I interactions in the HSP27 IP, we considered that HSP27 might be able to reverse the effects on elevated ROS production induced by the absence of HAX1. Interestingly, when HSP27 was exogenously expressed in HAX1<sup>-/-</sup> PLB-985 cells, both endogenous HSP27 and HSP27's phosphorylation was enhanced in addition to overexpression of exogenous HSP27 (Figure 52A), for some unknown reason. When we tested the mtROS production, the reconstitution of either HAX1 or HSP27 reversed the elevated mtROS production resulting from

HAX1 deficiency (Figure 52B). This demonstrated that HSP27 reconstitution can reverse mitochondrial stress induced by HAX1 deficiency.

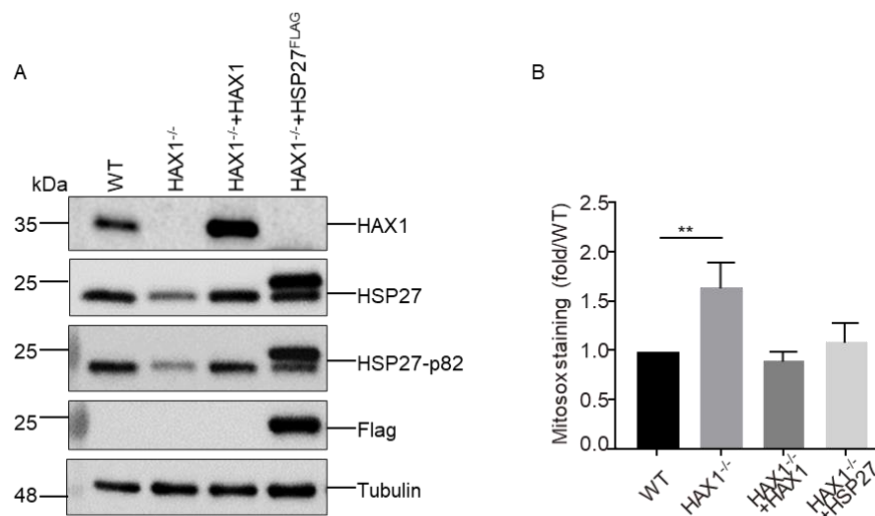


**Figure 52. The reconstitution of either HAX1 or HSP27 reversed the elevated mitochondrial ROS production in the absence of HAX1.** (A) Cells collected from indicated genotypes were subjected to SDS-PAGE and Western blotting. (B) mtROS production was measured in whole cells using MitoSOX Red Mitochondrial Superoxide Indicator (means  $\pm$  SEM, t-test,  $n = 3$ ).

## 2.7 HSP27 reconstitutes HAX1 deficiency in iPSCs model

HAX1 is a causative gene for severe congenital neutropenia, but the detailed mechanism remains debatable. Clearly, premature apoptosis of myeloid progenitor cells is a characteristic feature in many types of SCN. We therefore were interested to provide functional evidence of HSP27 in the pathophysiology of HAX1 deficiency. We established an in-vitro differentiation system allowing us to model the genetic defects in HAX1 and the rescuing effect of HSP27. We first refined a previously published protocol (Niwa et al., 2011) allowing us to differentiate bona fide neutrophils in vitro from induced pluripotent stem cells (iPSCs) and also providing a platform to genetically engineer human neutrophils by CRISPR- Cas9-mediated genome editing. Next, we differentiated primitive streak-like cells into bone fide neutrophil granulocytes in the coordinated presence of hematopoietic cytokines (details shown in materials and methods). After ensuring properties of differentiated neutrophils are indistinguishable from peripheral blood neutrophils, we focused on engineering HAX1 deficient iPSCs via CRISPR- Cas9-mediated genome editing and overexpressing HAX1, HSP27 in iPSCs via PiggyBac Transposon System. This



overexpression is based on a doxycycline-inducible system as previously described (Li et al., 2013b). As shown in Figure 53, the deletion of HAX1 and doxycycline inductive expressions of either HAX1 or HSP27 were effective in iPSCs. As a control, wildtype iPSCs were transfected with plain piggybac vector, merely expressing mcherry upon doxycycline induction.

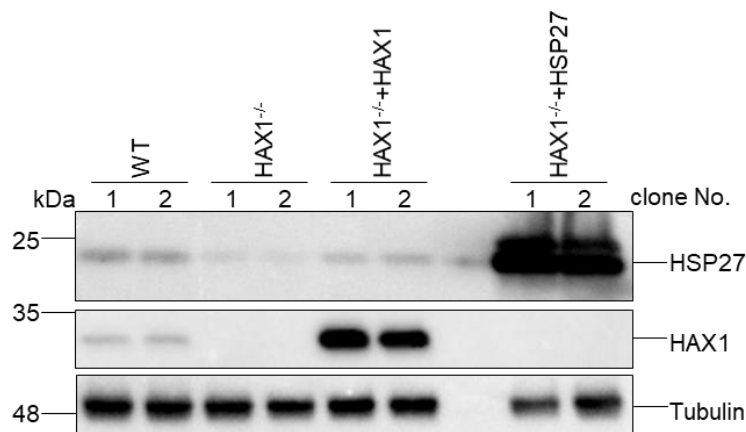


**Figure 53. The overexpression of HAX1 and HSP27 in iPSCs.** The CDS of either HAX1 or HSP27 was cloned into PiggyBac vector, which were subsequently transfected into iPSCs together with transposon-expressing vectors via electroporation. After doxycycline induction, iPSCs from indicated genotypes were collected prior to SDS-PAGE and Western blotting.

In contrast to wildtype iPSCs, HAX1 deficient iPSCs showed a significantly retarded differentiation towards flooding neutrophil granulocytes. Yet, reconstitution of either HSP27 or HAX1 via doxycycline-inducible system during differentiation in mutant iPSCs, recovered the diminished number of live floating cells to a great extent (Figure 54).

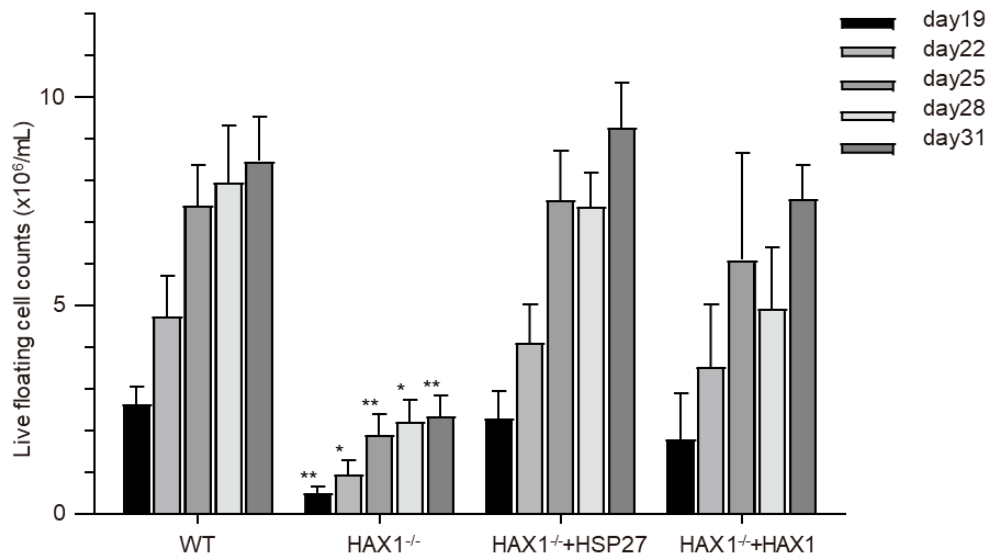


**Figure 54. The analysis of live floating cell counts.** Quantification of live floating cells per 6 iPSC colonies (per well), determined at indicated time points during differentiation (means  $\pm$  SEM, t-test, n = 3).

When we further examined maturation rates of neutrophils indicated via mcherry+CD11b/CD33<sup>low</sup> by FACS, compared to the wildtype, HAX1<sup>-/-</sup> iPSCs displayed a reduction in neutrophil maturation. This decreased maturation rate was reconstituted by either overexpression of HSP27 or HAX1 in HAX1<sup>-/-</sup> iPSCs (Figure 55).

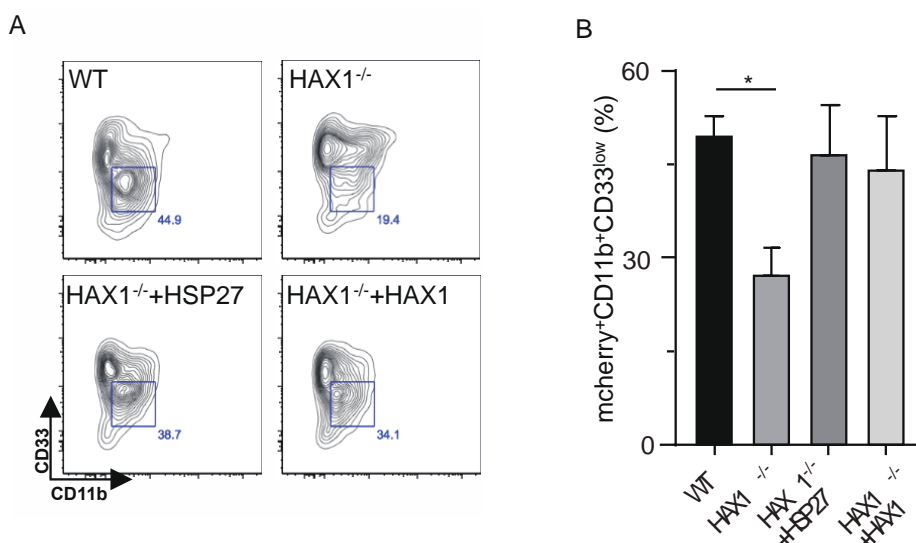


**Figure 55. FACS assay of iPSCs with mcherry+CD11b/CD33<sup>low</sup>.** (A and B) After 29 days of differentiation, floating cells were collected and stained with CD33 and CD11b antibodies prior to FACS analysis (means  $\pm$  SEM, t-test, n = 3).

We also visualized morphologic alterations and the subdistribution of myeloid progenitor cells of flooding granulocytes under the light microscope. Upon differentiation, HAX1 deficient iPSCs demonstrated an arrest of maturation at the level of promyelocytes, whereas reconstitution of HSP27 or HAX1 rescued cell differentiation to mature neutrophils (Figure 56A). Interestingly, both HSP27 and HAX1 expression reversed these effects (Figure 56B). Thus, in vitro modeling of neutrophil differentiation confirms that HSP27 overexpression is able to improve the aberrant cell viability and differentiation resulting from HAX1 dysfunction.

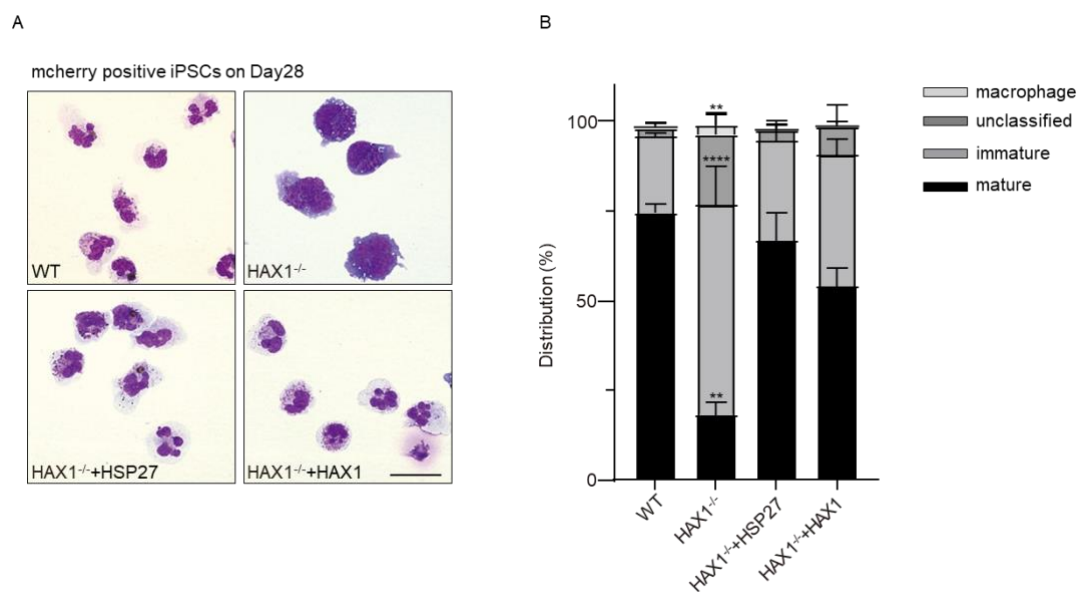


**Figure 56. Cytospin of differentiated iPSCs.** (A) Light microscopy of iPSC-derived immature and mature neutrophil granulocytes stained with May-Grünwald Giemsa ( $\times 63$ ) on day 28 after differentiation. (B) Cell distribution assay was determined by observing 200 cells from 3 independent experiments (means  $\pm$  SEM, t-test,  $n = 3$ ).

## IV DISCUSSION

### 1 HAX1 is a mitochondrial IMS protein

Since the original description of HAX1 (Suzuki et al., 1997) and the discovery of mutations in Kostmann syndrome (Klein et al., 2007), an increasing number of studies reported a wealth of data on HAX1 without convincing evidence of its function. In view of partially conflicting explanations, no unifying hypothesis has yet emerged to explain the multiple biologic functions of HAX1. Since we could document a role for HAX1 in stabilizing the mitochondrial membrane potential ( $\Delta\Psi_m$ ) in neutrophils (Klein et al., 2007), we thereby first focused on determining the subcellular localization of HAX1 in mitochondria. Using mitochondrial swelling and carbonate extraction methods, we demonstrate that HAX1 is located in mitochondrial intermembrane space (IMS) as a membrane-bound protein in human cells. In line with our data, HAX1 was identified in the IMS from a high-resolution human mitochondrial proximity interaction network, studied by Hana Antonicka et al. (Antonicka et al., 2020).

On the other hand, recent studies relate HAX1 with the cytoskeleton in mouse cells. In CHO cells, HAX1 was shown to associate with Kv3.3 potassium channel (KCNC3) and assist in mediating actin nucleation through Arp2/3 (Zhang et al., 2016). Since HAX1 is mainly displayed inside mitochondria of human cell lines as shown in Figure 18 and 21, this contradiction could be due to the existence of splicing variants of HAX1 dominantly expressed in the cytosol of mouse tissues (Grzybowska et al., 2006; Trebinska et al., 2010). Or this is by the virtue of mitochondria are associated with various organelles, such as cytoskeleton, ER, Golgi, perosome or nucleus (Boldogh and Pon, 2007; Lebieczinska et al., 2009; Monaghan and Whitmarsh, 2015; Rizzuto et al., 1998; Sargsyan and Thoms, 2020; Wieckowski et al., 2009). Those properties of mitochondria may explain why HAX1 is detected to associate with various candidate proteins from different cellular compartments in different cell types. Therefore, questions regarding the number of expressed HAX1 splicing variants and their specific functions need to be addressed in the future. Meanwhile if some protein-protein interactions of HAX1 may be attributed to non-specific effects remain to be clarified.

## The relationship between HAX1 and CLPB

### 1.1 HAX1 is the binding partner of CLPB

A putative interaction of HAX1 and CLPB was first postulated by Saskia B et al. in the paper describing that CLPB mutations in humans underlie a multi-system disease (MEGCANN syndrome) (Wortmann et al., 2015). Through mass spectrometry studies with HAX1-overexpressed mitochondrial lysates, we observed that CLPB was a predominantly binding partner of HAX1 and the mutual interaction of both proteins were further validated by endogenous immunoprecipitation with 293T cell lysates (Figure 24). In consistent with our finding, the interaction between CLPB and HAX1 was shown as well with whole THP-1 cell lysates (Chen et al., 2019). However, in addition to biochemical proof of the mutual interaction between HAX1 and CLPB, we for the first time show the co-localization of HAX1 and CLPB by immunofluorescence studies in HeLa cells.

We mapped the exquisite binding regions in both HAX1 and CLPB and discovered that Exon 3 of HAX1 and ANK domain of CLPB are responsible for mutual interactions by a series of immunoprecipitation experiments with various truncations. Additionally, HAX1 becomes aggregated resistant to Triton X-100 lysis in CLPB<sup>-/-</sup> PLB-985 cells. Thus, we can conclude that HAX1 behaves as the substrate of CLPB, in an attempt to guarantee its proper solubility. Since both HAX1 and partial CLPB variants are SCN-causative, we therefore can further assume that CLPB variants lacking interactions with HAX1 can cause SCN in patients. As expected, we specifically identified that HAX1 patient mutant HAX1\_L130R (Lanciotti et al., 2010) failed to interact with CLPB, as well as SCN-causing mutation in CLPB (CLPB\_Y272C) (Wortmann et al., 2015) significantly perturbed its association with HAX1. These findings indicate that L130 in HAX1 and Y272 in CLPB function as key residues enabling CLPB-HAX1 complex formation, importantly, they also suggest a tight genotype-phenotype correlation between HAX1 and CLPB deficiency.

Of note, our data on this correlation is sufficient but not necessary to explain all SCN-causing mutations identified in CLPB patients (Saunders et al., 2015; Wortmann et al., 2015), especially when mutations located in the C terminal domains of CLPB. It is known that N-terminal domains of Ecoli ClpB define a substrate entrance channel and position the polypeptide (substrate) above AAA+

domains (NBD1 and NBD2) in the C-terminal of ClpB for further translocation (Rizo et al., 2019; Zhang et al., 2012). Highly conservative amino acids in NBD domains have been related to substrate translocation (Biter et al., 2012). In yeast, essential Tyr residues, identified in NBD domains of HSP104, were shown to form a substrate-binding “pore loops” that mechanically couple hydrolysis to translocation (Gates and Martin, 2020). Therefore, though some CLPB patient mutants might be able to associate with HAX1, they (i.e., Y567C, Y617C and A591V located at the C terminal of CLPB) still cannot efficiently disaggregate HAX1. This probably due to an inefficient translocation of HAX1 through pore loop structure in presence of critical C-terminal mutants of CLPB. We can assume as well that SCN-causing variants of CLPB, i.e., Y272C, Y567C, A591V and Y617C, might be essential residues in CLPB for substrates binding and translocation. Those assumptions however require further studies to be illustrated. Those suppositions based on interacting domains between CLPB and HAX1 will surely provide us with clues on elucidating structures of both proteins in upcoming studies.

## 1.2 Roles of CLPB in mitochondrial biology

Through carbonate extraction assay and immunofluorescence analysis, we observed a clumped HAX1 in CLPB<sup>-/-</sup> mitochondria. This indicates that human CLPB might be highly functional conservative and share disaggregation functions with its orthologs, although for example human CLPB is only about 20% identical to its ortholog in *Escherichia coli* (Abrahamo et al., 2017).

Human CLPB has recently been shown to function as a potent “stand-alone” mitochondrial disaggregase (Cupo and Shorter, 2020). The mitochondrial inner-membrane protease, PARL – a known interaction partner of HAX1- removes an autoinhibitory peptide from CLPB to enhance its disaggregase activity (Cupo and Shorter, 2020). However, since the report focused on the isoform 1 CLPB1-707, which does not translationally exist in human cell lines according to our study, it is questionable if the dominantly existing isoform 2 CLPB1-677 can be processed by PARL and be functional in the way as shown in the report. Another study reported that CLPB served as a potential substrate of PARL and interacted with both proteolytically active and inactive PARL independent of mitochondrial membrane potential (Saita et al., 2017). Since murine Hax1 has been shown to present Omi to

Parl (Chao et al., 2008), it is conceivable that HAX1 might involve in the processing of CLPB by PARL as well.

Hsp104, the homolog of CLPB in yeast, is shown to potentially dissociate proteins from aggregates in cytosol to facilitate their entry into import complex to IMS or mitochondrial matrix for degradation by proteases and peptidases (Ruan et al., 2017). This mitochondria-mediated proteostasis mechanism MAGIC (mitochondria as guardian in cytosol) may also exist in human cells (Ruan et al., 2017). CLPB, HAX1, YME1L and SLP2 are recently detected in the interactome of PARL in FITR293T cells (Wai et al., 2016). SLP2 is moreover shown to anchor a large protease complex composed of the rhomboid protease PARL and the i-AAA protease YME1L (SLP2–PARL–YME1L complex) in the IM, to mediate protein maturation and degradation in the IMS (Wai et al., 2016). Hax1 has been shown to present Htra2 (Omi) to Parl for processing and release of Htra2 (Omi) into cytosol in mouse model (Chao et al., 2008). Based on our findings, CLPB essentially ensures the proper solubility of HAX1 in mitochondria. All the information implicates that complex PARL-YME1L-CLPB-HAX1 may functions as a critical proteolytic hub in the IMS, for mediating the processing and degradation of mitochondrial substrates or even cytosolic aggregated proteins. The detailed functional mechanisms of presumed complex PARL-YME1L-CLPB-HAX1 and its client substrates need to be further elucidated.

### **1.3 Perturbed proteostasis in HAX1 and CLPB deficiency**

Our studies on proteomes of HAX1 and CLPB deficient PLB-985 cells reveal that both deficiencies exhibit disrupted mitochondrial protein turnover. Therein, mitochondrial complex I and TCA cycle are highlighted with accumulated protein synthesis (H/L) and delayed protein degradation (M/L) in SILAC-based pulsing assay. Intriguingly, affected protein turnover members in mitochondrial complex I and TCA cycle are highly overlapped between HAX1 and CLPB deficiency, confirming a tight functional connection of CLPB-HAX1 axis. The reduced complex I activity in HAX1<sup>-/-</sup> PLB-985 cells is further validated by an Elisa assay with isolated mitochondria.

Mitochondrial complex I is a critical source of pumping protons into IMS to generate an electrochemical gradient for ATP production (Davies et al., 2011; Sazanov, 2015).

Dysfunctional mitochondrial complex I have been found as the causes for neurological diseases, as a result of a defect of energy metabolism and consequent excitotoxicity (Davies et al., 2011; Fiedorczuk and Sazanov, 2018; Sazanov, 2015; Schapira et al., 1990). When both HAX1 isoforms are affected, patients display neutropenia as well as mental defects (Boztug et al., 2010; Carlsson et al., 2008). Therefore, a dysfunctional complex I activity in HAX1<sup>-/-</sup> mitochondria sheds light on the link between HAX1 deficiency and neurological degeneration.

Of note, the overall mitochondrial protein synthesis is upregulated in HAX1 defective cells (Figure 34), indicating an imbalanced mitochondrial proteostasis in HAX1 deficiency. Aberrant proteostasis has been linked to several common and age-related human diseases (e.g., Alzheimer and Parkinson disease, type II diabetes). Yet, proteostasis in rare monogenic diseases affecting non-neurological cells has not systematically been addressed (Mannini and Chiti, 2017). Mutations in the neutrophil elastase gene ELANE, the most common variant of severe congenital neutropenia, have been shown to induce unfolded protein responses in vitro and in vivo (Grenda et al., 2007; Nanua et al., 2011; Nayak et al., 2015; Tidwell et al., 2014). We thereby speculate that disturbances of proteostasis in HAX1 defects may lead to neutropenia induced by disturbed cell survival and differentiation.

By differential protein analysis, we discovered that HSP27 is significantly reduced in both HAX1 and CLPB defects, which additionally confirms a tight functional connection of CLPB-HAX1 axis. We were able to show that HSP27 turned out to be dysfunctional due to its dephosphorylation in HAX1 deficient mitochondria and mitochondrial oxidative stress in HAX1<sup>-/-</sup> cells can be recovered upon HSP27 reconstitution. These hints imply that HSP27 acts in the downstream of HAX1, who plays a role in maintaining the protein quality control of HSP27 in mitochondria.

## **2 HSP27 and perturbed mitochondrial proteostasis**

### **2.1 The cellular localization of HSP27**

HSP27 is commonly recognized as a cytosolic protein and extensive studies on its multiple functions have been indicated in the process of disaggregation, actin polymerization, oxidative stress response in cytosol (Bakthisaran et al., 2015). Indeed, we observed a cell-wide staining of HSP27 under confocal microscopy. Yet,



a portion of HSP27 appears in mitochondrial IMS and matrix identified by mitochondrial swelling experiment (Figure 48). Especially, HSP27 became aggregated in HAX deficient mitochondria (Figure 44 and 45). Till now, no experimental proof has clearly posed that HSP27 is inside the mitochondria, though several studies link HSP27 as a mitochondrial outer membrane associated protein to mitochondrial apoptotic pathways. At the upstream of mitochondria, HSP27 is reported to interfere with apoptotic inductions mediated via Bax, Bid and Akt (Havasi et al., 2008; Paul et al., 2010; Rane et al., 2003; Wu et al., 2007). At the downstream of mitochondrial apoptosis, HSP27 binds to released cytochrome c and pro-caspase-3 for preventing the formation of apoptosome (Bruey et al., 2000; Pandey et al., 2000; Paul et al., 2002). However, through mitochondrial swelling assay and the study of HSP27 interactome in mitochondria, we are able to confirm that a portion of HSP27 is located inside mitochondria and associates with mitochondrial proteins residing in either IMS or matrix.

## **2.2 HSP27 and mitochondrial proteostasis**

In the mitochondrial interactome of HSP27, identified interactors mainly involved in respiratory electron transport chain, mitochondrial translational pathways, TCA cycle and 'de novo' protein folding (Figure 50). This is in consistent with the perturbed mitochondrial turnover (mainly in mitochondrial complex I and TCA cycle) in HAX1 deficiency demonstrated by the SILAC assay. Given that HAX1 deficiency perturbs the phosphorylation of HSP27, which is critical for its conformation and consequent distribution, we thus can presume that the impaired mitochondrial protein turnover presented in mitochondrial complex I and TCA cycle is resulting from the dysfunctional/insoluble HSP27 in HAX1 deficiency. Consistent with this presumption, Hsp25 was shown to protect mitochondrial complex I activity in submitochondrial vesicles during heat and oxidative stress in murine P12 cells (Downs et al., 1999). Intriguingly, the activity of mitochondrial complex I was shown to be impaired as well in HSP27 patients (Kalmar et al., 2017).

Respiratory electron transport chain is composed of four mitochondrial complexes (I-IV) in eukaryotes. Except for nuclear-coded complex II, subunits of the other complexes are encoded not only by mitochondrial genome but also by nuclear genome. Mitochondrial genome encodes 13 proteins and all of them involved in

mitochondrial electron transfer chain, therein more than half encoded proteins (7 out of 13) are dedicated to complex I. Mitochondrial complex I (NADH: ubiquinone oxidoreductase) is a multi-subunit (14 core and 31 accessory) around 1 megadalton, which is more than twice bigger than the other respiratory complexes. We can therefore assume that the temporal and spacial orchestrations between nuclear-coded and mitochondria-coded proteins are highly critical for maintaining the proper conformation and activity of respiratory complexes, especially for complex I. As expected, the activity of complex I is more prone to be impaired in HAX1 deficiency, where the solubility of HSP27 is evidently compromised. Since reverse electron transfer within complex I is one of the dominant sources for mtROS production, we indeed observed a evidently increased mtROS production in HAX1<sup>-/-</sup> cells than WT. Interestingly, the reconstitution of HSP27 recovers the increased mtROS production, which indicates that HSP27 acts at the downstream of HAX1.

In the aspect of protein translation, HSP27 is reported to associate with mRNAs translation initiation complex (cap-initiation complexes) eIF4F in a heat-shock dependent manner (Cuesta et al., 2000). Interestingly, in our mitochondrial interactome data of HSP27, its interactors are significantly enriched in mitochondrial translation, specifically in mitochondrial ribosomes. This implicates that HSP27 may participate in mitochondrial protein synthesis by interactions with mitochondrial ribosomal proteins. Since HSP27 additionally interacts with heat shock elements functioning in 'de novo' protein folding, we can further assume that HSP27 might play a role in mitochondrial ribosomal assembly. On the other hand, HSP27 has been reported to protect the translation machinery during recovery from heat shock (Carper et al., 1997; Li et al., 1995; Liu et al., 1992) and traps unfolding protein intermediates to prevent irreversible protein denaturation and aggregation. Thus, we can presume as well that HSP27 may act as a chaperone to secure mitochondrial native protein synthesis and folding by binding with mitochondrial ribosome. In consistency with this assumption, small heat shock protein (HSP40 system) is shown to cooperate with HSP70 and interact with exposed hydrophobic sequences of the emerging nascent chain on the ribosome, to prevent premature misfolding of the nascent chain and support co-translational folding (Preissler and Deuerling, 2012). Concomitantly, we can also assume that with chaperone-like activity, HSP27 may bind to mitochondrial translation machinery for preventing

protein premature misfolding and following denaturation. Thereby, upon dephosphorylation and subsequent oligomerization, insoluble HSP27 may fail to interact with mitochondrial translation machinery, which might further result in redundant protein misfolding and aggregation in HAX1<sup>-/-</sup> mitochondrial matrix.

Since mitochondrial complexes and mitochondrial ribosomes have dual origins, the sequestration of mitochondria-coded components can further affect the temporal synchronization of nuclear-coded proteins in aspects of protein import and assembly (Couvillion et al., 2016; Richter-Dennerlein et al., 2016), which will eventually lead to disturbed proteostasis in HAX1 deficient mitochondria. As assumed, in the absence of HAX1, the mitochondrial unfolded protein response pathway via Sirt3-Foxo3a-LC3 is activated, suggesting a perturbed proteostasis in HAX1<sup>-/-</sup> mitochondrial matrix. This imbalanced protein quality control caused by insolubilized HSP27 can due to the dysfunctional HSP27 unable to interact and guarantee a proper conformation of its client proteins in HAX1 deficiency. As a result, in HAX1 deficient proteomes, we indeed observe protein candidates with higher synthesized rate are enriched in protein degradation pathways, such as proteasome, mitochondrial proteases. This further implicates that excessively misfolded or aggregated proteins are degraded via UPS pathway or specific proteases as the result of a perturbed proteostasis in HAX1 deficient mitochondria.

### **2.3 The phosphorylation of HSP27**

In comparison to other sHSPs, functions of HSP27 highly correlate to its phosphorylation states. HSP27 is present as large oligomers at basal levels in cells (Vidyasagar et al., 2012). Upon phosphorylation at multiple serine residues (15, 78, and 82 in humans) mediated via MK2, MK3, MK5, PKC or PKD (Kostenko and Moens, 2009), large oligomers are reorganized into smaller oligomers, often dimers and tetramers (Charette and Landry, 2000; Mehlen et al., 1997; Rogalla et al., 1999). Therefore, the phosphorylation state of HSP27 is tightly linked to its functionally binding capacity with different client substrates. Here, we show that decreased PRKD2 attenuates HSP27 phosphorylation in HAX1 defect, resulting in a disturbed equilibrium of HSP27 oligomerization. This subsequently induces an insolubility of HSP27 in HAX1<sup>-/-</sup> mitochondria. Whereas previous studies have pointed out that PRKD2 is the upstream kinase in the phosphorylation of HSP27 (Doppler et al.,

2005; Harikumar et al., 2010), our data for the first time show its kinase activity on the phosphorylation of HSP27 in mitochondria of PLB-985 cells. Of note, after HAX1 reconstitution in HAX1 deficiency, the diminished expression of PRKD2 is not fully reversed. This suggests that other kinases or phosphatases additionally involve in phospho-regulation of HSP27 in HAX1 deficiency. HSP27 phosphorylation has been utilized by researchers to develop a systematic understanding of HSP27 function under multiple experimental and disease conditions. Further studies on elucidating novel mechanisms on HSP27's phosphorylation will for sure gain its prominence as a therapeutic target and biomarker of disease.

#### **2.4 The reconstitution of HSP27 in PLB-985 cells and iPS cells.**

Since we are able to show that HSP27 is a downstream player of HAX1 deficiency, we thereby overexpressed HSP27 in HAX1<sup>-/-</sup> PLB-985 cells and iPS cells to test if HAX1 deficiency can be reconstituted. Encouragingly, the overexpression of HSP27 reverses elevated mitochondrial oxidative stress in HAX1<sup>-/-</sup> PLB-985 cells. More strikingly, HSP27 reconstitution rescues the impaired cell viability and perturbed myeloid differentiation of HAX1 deficient iPS cells. Besides the exogenous HSP27, the endogenous HSP27 is also enhanced in terms of either expression or phosphorylation after HSP27 overexpression in PLB-985 cells (Figure 52). This may suggest that HSP27 is of high tendency to be phosphorylated so as to be preferably functional in human cells. Since we experimentally address defective differentiation of neutrophil granulocytes by reconstitution of HSP27 in HAX1 deficient iPS system, this provides us with promising new principles and therapeutic strategies aiming at reconstitution of proteostatic networks in severe congenital neutropenia caused by HAX1 deficiency.

## V SUMMARY

Severe congenital neutropenia (SCN) is characterized by a reduced number of mature neutrophils in human peripheral blood as a result of perturbed neutrophil differentiation. Loss-of-function mutations in HAX1 result in autosomal recessive SCN, yet the exact pathophysiological mechanisms underlying HAX1 deficiency remain largely unknown. Here, we aim to determine both the effect of Hax1 deficiency in the mouse immune system, as well as the molecular function of HAX1 during neutrophil biology. In this study, we first examine and demonstrate that Hax1 deficient murine bone marrow cells show no striking aberration in the number of murine neutrophils. To gain a deeper understanding of the molecular function of HAX1 during human neutrophil differentiation, we next employ the human promyeloid cell line and induced pluripotent stem cells (iPSCs) as cellular model systems. Using a variety of biochemical methods (e.g., mitochondrial swelling and carbonate extraction experiments), we demonstrate that HAX1 is a membrane-bound protein localized in the mitochondrial intermembrane space (IMS). Mass-spectrometry (MS) studies identify Caseinolytic peptidase B protein homolog (CLPB) as a novel interactor of HAX1. CLPB ensures the correct subcellular distribution and the solubility of HAX1 in mitochondria. Interestingly, human mutations leading to SCN in either HAX1 (L130R) or in CLPB (Y272C) serve as critical residues enabling HAX1-CLPB complex formation. SILAC proteomics shows that both HAX1 and CLPB deficiencies cause perturbed mitochondrial proteostasis in PLB-985 cells. Moreover, the endogenous expression of small chaperone HSP27 is highly reduced in HAX1 or CLPB deficiency. Meanwhile, HSP27 is dephosphorylated/insoluble in HAX1<sup>-/-</sup> and CLPB<sup>-/-</sup> mitochondria, which probably due to a reduced expression level of PRKD2. By interactome studies of HSP27, it appears to interact with components involved in mitochondrial respiratory complexes and TCA cycle, indicating that CLPB-HAX1 axis preserves the function of HSP27 for mitochondrial proteostasis. Intriguingly, HSP27 reconstitutes the skewed neutrophil differentiation in HAX1<sup>-/-</sup> iPS cells. To conclude, our data indicate that the mitochondrial complex HAX1-CLPB preserves mitochondrial proteostasis by regulating the dynamic phosphorylation status of HSP27, which is essential for efficient neutrophil differentiation.

## VI BIBLIOGRAPHY

- Abdollahpour, H., G. Appaswamy, D. Kotlarz, J. Diestelhorst, R. Beier, A.A. Schaffer, E.M. Gertz, A. Schambach, H.H. Kreipe, D. Pfeifer, K.R. Engelhardt, N. Rezaei, B. Grimbacher, S. Lohrmann, R. Sherkat, and C. Klein. 2012. The phenotype of human STK4 deficiency. *Blood*. 119:3450-3457.
- Abraham, J., D.Z. Mokry, and C.H.I. Ramos. 2017. Hsp78 (78 kDa Heat Shock Protein), a Representative AAA Family Member Found in the Mitochondrial Matrix of *Saccharomyces cerevisiae*. *Front Mol Biosci*. 4:60.
- Acin-Perez, R., P. Fernandez-Silva, M.L. Peleato, A. Perez-Martos, and J.A. Enriquez. 2008. Respiratory active mitochondrial supercomplexes. *Mol Cell*. 32:529-539.
- Al-Maghrebi, M., H. Brule, M. Padkina, C. Allen, W.M. Holmes, and Z.E. Zehner. 2002. The 3' untranslated region of human vimentin mRNA interacts with protein complexes containing eEF-1gamma and HAX-1. *Nucleic Acids Res*. 30:5017-5028.
- Aldridge, J.E., T. Horibe, and N.J. Hoogenraad. 2007. Discovery of genes activated by the mitochondrial unfolded protein response (mtUPR) and cognate promoter elements. *PLoS One*. 2:e874.
- Amm, I., T. Sommer, and D.H. Wolf. 2014. Protein quality control and elimination of protein waste: the role of the ubiquitin-proteasome system. *Biochim Biophys Acta*. 1843:182-196.
- Anckar, J., and L. Sistonen. 2011. Regulation of HSF1 function in the heat stress response: implications in aging and disease. *Annu Rev Biochem*. 80:1089-1115.
- Anderson, L. 1981. Identification of mitochondrial proteins and some of their precursors in two-dimensional electrophoretic maps of human cells. *Proc Natl Acad Sci U S A*. 78:2407-2411.
- Antonicka, H., Z.Y. Lin, A. Janer, M.J. Aaltonen, W. Weraarpachai, A.C. Gingras, and E.A. Shoubridge. 2020. A High-Density Human Mitochondrial Proximity Interaction Network. *Cell Metab*. 32:479-497 e479.
- Arlt, H., R. Tauer, H. Feldmann, W. Neupert, and T. Langer. 1996. The YTA10-12 complex, an AAA protease with chaperone-like activity in the inner membrane of mitochondria. *Cell*. 85:875-885.
- Asai, T., T. Takahashi, M. Esaki, S. Nishikawa, K. Ohtsuka, M. Nakai, and T. Endo. 2004. Reinvestigation of the requirement of cytosolic ATP for mitochondrial protein import. *J Biol Chem*. 279:19464-19470.
- Azzu, V., and M.D. Brand. 2010. Degradation of an intramitochondrial protein by the cytosolic proteasome. *J Cell Sci*. 123:578-585.
- Baker, M.J., T. Tatsuta, and T. Langer. 2011. Quality control of mitochondrial proteostasis. *Cold Spring Harb Perspect Biol*. 3.
- Bakthisaran, R., R. Tangirala, and M. Rao Ch. 2015. Small heat shock proteins: Role in cellular functions and pathology. *Biochim Biophys Acta*. 1854:291-319.
- Balchin, D., M. Hayer-Hartl, and F.U. Hartl. 2016. In vivo aspects of protein folding and quality control. *Science*. 353:aac4354.
- Bellanne-Chantelot, C., B. Schmaltz-Panneau, C. Marty, O. Fenneteau, I. Callebaut, S. Clauin, A. Docet, G.L. Damaj, T. Leblanc, I. Pellier, C. Stoven, S. Souquere, I. Antony-Debre, B. Beaupain, N. Aladjidi, V. Barlogis, F. Bauduer, P. Bensaid,

- O. Boespflug-Tanguy, C. Berger, Y. Bertrand, L. Carausu, C. Fieschi, C. Galambrun, A. Schmidt, H. Journal, F. Mazingue, B. Nelken, T.C. Quah, E. Oksenhendler, M. Ouachee, M. Pasquet, V. Saada, F. Suarez, G. Pierron, W. Vainchenker, I. Plo, and J. Donadieu. 2018. Mutations in the SRP54 gene cause severe congenital neutropenia as well as Shwachman-Diamond-like syndrome. *Blood*. 132:1318-1331.
- Bernstein, S.H., S. Venkatesh, M. Li, J. Lee, B. Lu, S.P. Hilchey, K.M. Morse, H.M. Metcalfe, J. Skalska, M. Andreeff, P.S. Brookes, and C.K. Suzuki. 2012. The mitochondrial ATP-dependent Lon protease: a novel target in lymphoma death mediated by the synthetic triterpenoid CDDO and its derivatives. *Blood*. 119:3321-3329.
- Bianchi, C., M.L. Genova, G. Parenti Castelli, and G. Lenaz. 2004. The mitochondrial respiratory chain is partially organized in a supercomplex assembly: kinetic evidence using flux control analysis. *J Biol Chem*. 279:36562-36569.
- Biter, A.B., S. Lee, N. Sung, and F.T. Tsai. 2012. Structural basis for intersubunit signaling in a protein disaggregating machine. *Proc Natl Acad Sci U S A*. 109:12515-12520.
- Boisvert, F.M., Y. Ahmad, M. Gierlinski, F. Charriere, D. Lamont, M. Scott, G. Barton, and A.I. Lamond. 2012. A quantitative spatial proteomics analysis of proteome turnover in human cells. *Mol Cell Proteomics*. 11:M111 011429.
- Boldogh, I.R., and L.A. Pon. 2007. Mitochondria on the move. *Trends Cell Biol*. 17:502-510.
- Bolliger, L., T. Junne, G. Schatz, and T. Lithgow. 1995. Acidic receptor domains on both sides of the outer membrane mediate translocation of precursor proteins into yeast mitochondria. *EMBO J*. 14:6318-6326.
- Boos, F., J. Labbadia, and J.M. Herrmann. 2020. How the Mitoprotein-Induced Stress Response Safeguards the Cytosol: A Unified View. *Trends Cell Biol*. 30:241-254.
- Borzutzky, A., M.L. Reyes, V. Figueroa, C. Garcia, and M. Cavieres. 2006. Osteoporosis in children with severe congenital neutropenia: bone mineral density and treatment with bisphosphonates. *Journal of pediatric hematology/oncology*. 28:205-209.
- Boztug, K., G. Appaswamy, A. Ashikov, A.A. Schaffer, U. Salzer, J. Diestelhorst, M. Germeshausen, G. Brandes, J. Lee-Gossler, F. Noyan, A.K. Gatzke, M. Minkov, J. Greil, C. Kratz, T. Petropoulou, I. Pellier, C. Bellanne-Chantelot, N. Rezaei, K. Monkemoller, N. Irani-Hakimeh, H. Bakker, R. Gerardy-Schahn, C. Zeidler, B. Grimbacher, K. Welte, and C. Klein. 2009. A syndrome with congenital neutropenia and mutations in G6PC3. *N Engl J Med*. 360:32-43.
- Boztug, K., X.Q. Ding, H. Hartmann, L. Ziesenitz, A.A. Schaffer, J. Diestelhorst, D. Pfeifer, G. Appaswamy, S. Kehbel, T. Simon, A. Al Jefri, H. Lanfermann, and C. Klein. 2010. HAX1 mutations causing severe congenital neutropenia and neurological disease lead to cerebral microstructural abnormalities documented by quantitative MRI. *Am J Med Genet A*. 152A:3157-3163.
- Boztug, K., P.M. Jarvinen, E. Salzer, T. Racek, S. Monch, W. Garncarz, E.M. Gertz, A.A. Schaffer, A. Antonopoulos, S.M. Haslam, L. Schieck, J. Puchalka, J. Diestelhorst, G. Appaswamy, B. Lescoeur, R. Giambruno, J.W. Bigenzahn, U. Elling, D. Pfeifer, C.D. Conde, M.H. Albert, K. Welte, G. Brandes, R. Sherkat, J. van der Werff Ten Bosch, N. Rezaei, A. Etzioni, C. Bellanne-Chantelot, G. Superti-Furga, J.M. Penninger, K.L. Bennett, J. von Blume, A. Dell, J.

- Donadieu, and C. Klein. 2014. JAGN1 deficiency causes aberrant myeloid cell homeostasis and congenital neutropenia. *Nat Genet.* 46:1021-1027.
- Brehme, M., and C. Voisine. 2016. Model systems of protein-misfolding diseases reveal chaperone modifiers of proteotoxicity. *Dis Model Mech.* 9:823-838.
- Brehme, M., C. Voisine, T. Rolland, S. Wachi, J.H. Soper, Y. Zhu, K. Orton, A. Villella, D. Garza, M. Vidal, H. Ge, and R.I. Morimoto. 2014. A chaperome subnetwork safeguards proteostasis in aging and neurodegenerative disease. *Cell Rep.* 9:1135-1150.
- Bruey, J.M., C. Ducasse, P. Bonniaud, L. Ravagnan, S.A. Susin, C. Diaz-Latoud, S. Gurbuxani, A.P. Arrigo, G. Kroemer, E. Solary, and C. Garrido. 2000. Hsp27 negatively regulates cell death by interacting with cytochrome c. *Nat Cell Biol.* 2:645-652.
- Brunet, A., L.B. Sweeney, J.F. Sturgill, K.F. Chua, P.L. Greer, Y. Lin, H. Tran, S.E. Ross, R. Mostoslavsky, H.Y. Cohen, L.S. Hu, H.L. Cheng, M.P. Jedrychowski, S.P. Gygi, D.A. Sinclair, F.W. Alt, and M.E. Greenberg. 2004. Stress-dependent regulation of FOXO transcription factors by the SIRT1 deacetylase. *Science.* 303:2011-2015.
- Burnicka-Turek, O., A. Kata, B. Buyandelger, L. Ebermann, N. Kramann, P. Burfeind, S. Hoyer-Fender, W. Engel, and I.M. Adham. 2010. Pelota interacts with HAX1, EIF3G and SRPX and the resulting protein complexes are associated with the actin cytoskeleton. *BMC Cell Biol.* 11:28.
- Camello-Almaraz, C., P.J. Gomez-Pinilla, M.J. Pozo, and P.J. Camello. 2006. Mitochondrial reactive oxygen species and Ca<sup>2+</sup> signaling. *Am J Physiol Cell Physiol.* 291:C1082-1088.
- Carlsson, G., I. van't Hooft, M. Melin, M. Entesarian, E. Laurencikas, I. Nennesmo, A. Trebinska, E. Grzybowska, J. Palmblad, N. Dahl, M. Nordenskjold, B. Fadeel, and J.I. Henter. 2008. Central nervous system involvement in severe congenital neutropenia: neurological and neuropsychological abnormalities associated with specific HAX1 mutations. *J Intern Med.* 264:388-400.
- Carper, S.W., T.A. Rocheleau, D. Cimino, and F.K. Storm. 1997. Heat shock protein 27 stimulates recovery of RNA and protein synthesis following a heat shock. *J Cell Biochem.* 66:153-164.
- Castresana, J., M. Lubben, M. Saraste, and D.G. Higgins. 1994. Evolution of cytochrome oxidase, an enzyme older than atmospheric oxygen. *EMBO J.* 13:2516-2525.
- Cavnar, P.J., E. Berthier, D.J. Beebe, and A. Huttenlocher. 2011. Hax1 regulates neutrophil adhesion and motility through RhoA. *J Cell Biol.* 193:465-473.
- Chacinska, A., C.M. Koehler, D. Milenkovic, T. Lithgow, and N. Pfanner. 2009. Importing mitochondrial proteins: machineries and mechanisms. *Cell.* 138:628-644.
- Chacinska, A., M. Lind, A.E. Frazier, J. Dudek, C. Meisinger, A. Geissler, A. Sickmann, H.E. Meyer, K.N. Truscott, B. Guiard, N. Pfanner, and P. Rehling. 2005. Mitochondrial presequence translocase: switching between TOM tethering and motor recruitment involves Tim21 and Tim17. *Cell.* 120:817-829.
- Chan, N.C., A.M. Salazar, A.H. Pham, M.J. Sweredoski, N.J. Kolawa, R.L. Graham, S. Hess, and D.C. Chan. 2011. Broad activation of the ubiquitin-proteasome system by Parkin is critical for mitophagy. *Hum Mol Genet.* 20:1726-1737.



- Chao, J.R., E. Parganas, K. Boyd, C.Y. Hong, J.T. Opferman, and J.N. Ihle. 2008. Hax1-mediated processing of HtrA2 by Parl allows survival of lymphocytes and neurons. *Nature*. 452:98-102.
- Charette, S.J., and J. Landry. 2000. The interaction of HSP27 with Daxx identifies a potential regulatory role of HSP27 in Fas-induced apoptosis. *Ann N Y Acad Sci*. 926:126-131.
- Chen, G., Z. Han, D. Feng, Y. Chen, L. Chen, H. Wu, L. Huang, C. Zhou, X. Cai, C. Fu, L. Duan, X. Wang, L. Liu, X. Liu, Y. Shen, Y. Zhu, and Q. Chen. 2014. A regulatory signaling loop comprising the PGAM5 phosphatase and CK2 controls receptor-mediated mitophagy. *Mol Cell*. 54:362-377.
- Chen, H., J.M. McCaffery, and D.C. Chan. 2007. Mitochondrial fusion protects against neurodegeneration in the cerebellum. *Cell*. 130:548-562.
- Chen, X., C. Glytsou, H. Zhou, S. Narang, D.E. Reyna, A. Lopez, T. Sakellaropoulos, Y. Gong, A. Kloetgen, Y.S. Yap, E. Wang, E. Gavathiotis, A. Tsirigos, R. Tibes, and I. Aifantis. 2019. Targeting Mitochondrial Structure Sensitizes Acute Myeloid Leukemia to Venetoclax Treatment. *Cancer Discov*. 9:890-909.
- Chiti, F., and C.M. Dobson. 2017. Protein Misfolding, Amyloid Formation, and Human Disease: A Summary of Progress Over the Last Decade. *Annu Rev Biochem*. 86:27-68.
- Cilenti, L., M.M. Soundarapandian, G.A. Kyriazis, V. Stratico, S. Singh, S. Gupta, J.V. Bonventre, E.S. Alnemri, and A.S. Zervos. 2004. Regulation of HAX-1 anti-apoptotic protein by Omi/HtrA2 protease during cell death. *J Biol Chem*. 279:50295-50301.
- Cogliati, S., J.A. Enriquez, and L. Scorrano. 2016. Mitochondrial Cristae: Where Beauty Meets Functionality. *Trends Biochem Sci*. 41:261-273.
- Cong, L., F.A. Ran, D. Cox, S. Lin, R. Barretto, N. Habib, P.D. Hsu, X. Wu, W. Jiang, L.A. Marraffini, and F. Zhang. 2013. Multiplex genome engineering using CRISPR/Cas systems. *Science*. 339:819-823.
- Couvillion, M.T., I.C. Soto, G. Shipkovenska, and L.S. Churchman. 2016. Synchronized mitochondrial and cytosolic translation programs. *Nature*. 533:499-503.
- Cox, J., and M. Mann. 2008. MaxQuant enables high peptide identification rates, individualized p.p.b.-range mass accuracies and proteome-wide protein quantification. *Nat Biotechnol*. 26:1367-1372.
- Cox, J., and M. Mann. 2012. 1D and 2D annotation enrichment: a statistical method integrating quantitative proteomics with complementary high-throughput data. *BMC Bioinformatics*. 13 Suppl 16:S12.
- Cristofani, R., V. Crippa, P. Rusmini, M.E. Cicardi, M. Meroni, N.V. Licata, G. Sala, E. Giorgetti, C. Grunseich, M. Galbiati, M. Piccolella, E. Messi, C. Ferrarese, S. Carra, and A. Poletti. 2017. Inhibition of retrograde transport modulates misfolded protein accumulation and clearance in motoneuron diseases. *Autophagy*. 13:1280-1303.
- Cuesta, R., G. Laroia, and R.J. Schneider. 2000. Chaperone hsp27 inhibits translation during heat shock by binding eIF4G and facilitating dissociation of cap-initiation complexes. *Genes Dev*. 14:1460-1470.
- Cupo, R.R., and J. Shorter. 2020. Skd3 (human ClpB) is a potent mitochondrial protein disaggregase that is inactivated by 3-methylglutaconic aciduria-linked mutations. *Elife*. 9.
- Davies, K.M., M. Strauss, B. Daum, J.H. Kief, H.D. Osiewacz, A. Rycovska, V. Zickermann, and W. Kuhlbrandt. 2011. Macromolecular organization of ATP

- synthase and complex I in whole mitochondria. *Proc Natl Acad Sci U S A*. 108:14121-14126.
- Donadieu, J., B. Beaupain, O. Fenneteau, and C. Bellanne-Chantelot. 2017. Congenital neutropenia in the era of genomics: classification, diagnosis, and natural history. *British journal of haematology*. 179:557-574.
- Donzeau, M., K. Kaldi, A. Adam, S. Paschen, G. Wanner, B. Guiard, M.F. Bauer, W. Neupert, and M. Brunner. 2000. Tim23 links the inner and outer mitochondrial membranes. *Cell*. 101:401-412.
- Doppler, H., P. Storz, J. Li, M.J. Comb, and A. Toker. 2005. A phosphorylation state-specific antibody recognizes Hsp27, a novel substrate of protein kinase D. *J Biol Chem*. 280:15013-15019.
- Downs, C.A., L.R. Jones, and S.A. Heckathorn. 1999. Evidence for a novel set of small heat-shock proteins that associates with the mitochondria of murine PC12 cells and protects NADH:ubiquinone oxidoreductase from heat and oxidative stress. *Arch Biochem Biophys*. 365:344-350.
- Doyle, S.M., and S. Wickner. 2009. Hsp104 and ClpB: protein disaggregating machines. *Trends Biochem Sci*. 34:40-48.
- Dubnikov, T., and E. Cohen. 2017. The Emerging Roles of Early Protein Folding Events in the Secretory Pathway in the Development of Neurodegenerative Maladies. *Front Neurosci*. 11:48.
- Dudkina, N.V., H. Eubel, W. Keegstra, E.J. Boekema, and H.P. Braun. 2005. Structure of a mitochondrial supercomplex formed by respiratory-chain complexes I and III. *Proc Natl Acad Sci U S A*. 102:3225-3229.
- Eaton, S., K. Bartlett, and M. Pourfarzam. 1996. Mammalian mitochondrial beta-oxidation. *Biochem J*. 320 ( Pt 2):345-357.
- Fiedorczuk, K., and L.A. Sazanov. 2018. Mammalian Mitochondrial Complex I Structure and Disease-Causing Mutations. *Trends Cell Biol*. 28:835-867.
- Fiorese, C.J., and C.M. Haynes. 2017. Integrating the UPR(mt) into the mitochondrial maintenance network. *Crit Rev Biochem Mol Biol*. 52:304-313.
- Fischer, F., A. Hamann, and H.D. Osiewacz. 2012. Mitochondrial quality control: an integrated network of pathways. *Trends Biochem Sci*. 37:284-292.
- Forster, F., P. Unverdorben, P. Sledz, and W. Baumeister. 2013. Unveiling the long-held secrets of the 26S proteasome. *Structure*. 21:1551-1562.
- Frakes, A.E., and A. Dillin. 2017. The UPR(ER): Sensor and Coordinator of Organismal Homeostasis. *Mol Cell*. 66:761-771.
- Fusakio, M.E., J.A. Willy, Y. Wang, E.T. Mirek, R.J. Al Baghdadi, C.M. Adams, T.G. Anthony, and R.C. Wek. 2016. Transcription factor ATF4 directs basal and stress-induced gene expression in the unfolded protein response and cholesterol metabolism in the liver. *Mol Biol Cell*. 27:1536-1551.
- Gallagher, A.R., A. Cedzich, N. Gretz, S. Somlo, and R. Witzgall. 2000. The polycystic kidney disease protein PKD2 interacts with Hax-1, a protein associated with the actin cytoskeleton. *Proc Natl Acad Sci U S A*. 97:4017-4022.
- Galluzzi, L., E.H. Baehrecke, A. Ballabio, P. Boya, J.M. Bravo-San Pedro, F. Cecconi, A.M. Choi, C.T. Chu, P. Codogno, M.I. Colombo, A.M. Cuervo, J. Debnath, V. Deretic, I. Dikic, E.L. Eskelinen, G.M. Fimia, S. Fulda, D.A. Gewirtz, D.R. Green, M. Hansen, J.W. Harper, M. Jaattela, T. Johansen, G. Juhasz, A.C. Kimmelman, C. Kraft, N.T. Ktistakis, S. Kumar, B. Levine, C. Lopez-Otin, F. Madeo, S. Martens, J. Martinez, A. Melendez, N. Mizushima, C. Munz, L.O. Murphy, J.M. Penninger, M. Piacentini, F. Reggiori, D.C. Rubinsztein, K.M.

- Ryan, L. Santambrogio, L. Scorrano, A.K. Simon, H.U. Simon, A. Simonsen, N. Tavernarakis, S.A. Tooze, T. Yoshimori, J. Yuan, Z. Yue, Q. Zhong, and G. Kroemer. 2017. Molecular definitions of autophagy and related processes. *EMBO J.* 36:1811-1836.
- Gates, S.N., and A. Martin. 2020. Stairway to translocation: AAA+ motor structures reveal the mechanisms of ATP-dependent substrate translocation. *Protein Sci.* 29:407-419.
- Gavrikova, E.V., and A.D. Vinogradov. 1999. Active/de-active state transition of the mitochondrial complex I as revealed by specific sulfhydryl group labeling. *FEBS Lett.* 455:36-40.
- Gray, M.W. 2014. The pre-endosymbiont hypothesis: a new perspective on the origin and evolution of mitochondria. *Cold Spring Harb Perspect Biol.* 6.
- Green, D.R. 2005. Apoptotic pathways: ten minutes to dead. *Cell.* 121:671-674.
- Grenda, D.S., M. Murakami, J. Ghatak, J. Xia, L.A. Boxer, D. Dale, M.C. Dinauer, and D.C. Link. 2007. Mutations of the ELA2 gene found in patients with severe congenital neutropenia induce the unfolded protein response and cellular apoptosis. *Blood.* 110:4179-4187.
- Grzybowska, E.A., E. Sarnowska, R. Konopinski, A. Wilczynska, T.J. Sarnowski, and J.A. Siedlecki. 2006. Identification and expression analysis of alternative splice variants of the rat Hax-1 gene. *Gene.* 371:84-92.
- Grzybowska, E.A., V. Zayat, R. Konopinski, A. Trebinska, M. Szwarc, E. Sarnowska, E. Macech, J. Korczynski, A. Knapp, and J.A. Siedlecki. 2013. HAX-1 is a nucleocytoplasmic shuttling protein with a possible role in mRNA processing. *FEBS J.* 280:256-272.
- Guzy, R.D., B. Hoyos, E. Robin, H. Chen, L. Liu, K.D. Mansfield, M.C. Simon, U. Hammerling, and P.T. Schumacker. 2005. Mitochondrial complex III is required for hypoxia-induced ROS production and cellular oxygen sensing. *Cell Metab.* 1:401-408.
- Hahn, A., K. Parey, M. Bublitz, D.J. Mills, V. Zickermann, J. Vonck, W. Kuhlbrandt, and T. Meier. 2016. Structure of a Complete ATP Synthase Dimer Reveals the Molecular Basis of Inner Mitochondrial Membrane Morphology. *Mol Cell.* 63:445-456.
- Hamdan, N., P. Kritsiligkou, and C.M. Grant. 2017. ER stress causes widespread protein aggregation and prion formation. *J Cell Biol.* 216:2295-2304.
- Han, J., L.A. Goldstein, W. Hou, C.J. Froelich, S.C. Watkins, and H. Rabinowich. 2010. Deregulation of mitochondrial membrane potential by mitochondrial insertion of granzyme B and direct Hax-1 cleavage. *J Biol Chem.* 285:22461-22472.
- Harikumar, K.B., A.B. Kunnumakkara, N. Ochi, Z. Tong, A. Deorukhkar, B. Sung, L. Kelland, S. Jamieson, R. Sutherland, T. Raynham, M. Charles, A. Bagherzadeh, C. Foxton, A. Boakes, M. Farooq, D. Maru, P. Diagaradjane, Y. Matsuo, J. Sinnott-Smith, J. Gelovani, S. Krishnan, B.B. Aggarwal, E. Rozengurt, C.R. Ireson, and S. Guha. 2010. A novel small-molecule inhibitor of protein kinase D blocks pancreatic cancer growth in vitro and in vivo. *Mol Cancer Ther.* 9:1136-1146.
- Hartl, F.U. 2011. Chaperone-assisted protein folding: the path to discovery from a personal perspective. *Nat Med.* 17:1206-1210.
- Hartl, F.U. 2017. Protein Misfolding Diseases. *Annu Rev Biochem.* 86:21-26.
- Hartl, F.U., and M. Hayer-Hartl. 2002. Molecular chaperones in the cytosol: from nascent chain to folded protein. *Science.* 295:1852-1858.

- Haslbeck, M., A. Miess, T. Stromer, S. Walter, and J. Buchner. 2005. Disassembling protein aggregates in the yeast cytosol. The cooperation of Hsp26 with Ssa1 and Hsp104. *J Biol Chem.* 280:23861-23868.
- Haslbeck, M., S. Weinkauf, and J. Buchner. 2019. Small heat shock proteins: Simplicity meets complexity. *J Biol Chem.* 294:2121-2132.
- Havasi, A., Z. Li, Z. Wang, J.L. Martin, V. Botla, K. Ruchalski, J.H. Schwartz, and S.C. Borkan. 2008. Hsp27 inhibits Bax activation and apoptosis via a phosphatidylinositol 3-kinase-dependent mechanism. *J Biol Chem.* 283:12305-12313.
- Haynes, C.M., K. Petrova, C. Benedetti, Y. Yang, and D. Ron. 2007. ClpP mediates activation of a mitochondrial unfolded protein response in *C. elegans*. *Dev Cell.* 13:467-480.
- Heo, J.M., and J. Rutter. 2011. Ubiquitin-dependent mitochondrial protein degradation. *Int J Biochem Cell Biol.* 43:1422-1426.
- Hershko, A. 2005. Early work on the ubiquitin proteasome system, an interview with Avram Hershko. Interview by CDD. *Cell Death Differ.* 12:1158-1161.
- Horwich, A.L., E.U. Weber-Ban, and D. Finley. 1999. Chaperone rings in protein folding and degradation. *Proc Natl Acad Sci U S A.* 96:11033-11040.
- Houtkooper, R.H., L. Mouchiroud, D. Ryu, N. Moullan, E. Katsyuba, G. Knott, R.W. Williams, and J. Auwerx. 2013. Mitonuclear protein imbalance as a conserved longevity mechanism. *Nature.* 497:451-457.
- Imachi, H., M.K. Nobu, N. Nakahara, Y. Morono, M. Ogawara, Y. Takaki, Y. Takano, K. Uematsu, T. Ikuta, M. Ito, Y. Matsui, M. Miyazaki, K. Murata, Y. Saito, S. Sakai, C. Song, E. Tasumi, Y. Yamanaka, T. Yamaguchi, Y. Kamagata, H. Tamaki, and K. Takai. 2020. Isolation of an archaeon at the prokaryote-eukaryote interface. *Nature.* 577:519-525.
- Jayaraj, G.G., M.S. Hipp, and F.U. Hartl. 2020. Functional Modules of the Proteostasis Network. *Cold Spring Harb Perspect Biol.* 12.
- Jin, S.M., M. Lazarou, C. Wang, L.A. Kane, D.P. Narendra, and R.J. Youle. 2010. Mitochondrial membrane potential regulates PINK1 import and proteolytic destabilization by PARL. *J Cell Biol.* 191:933-942.
- Jovaisaite, V., L. Mouchiroud, and J. Auwerx. 2014. The mitochondrial unfolded protein response, a conserved stress response pathway with implications in health and disease. *J Exp Biol.* 217:137-143.
- Kaiser, C.M., and K. Liu. 2018. Folding up and Moving on-Nascent Protein Folding on the Ribosome. *J Mol Biol.* 430:4580-4591.
- Kalmar, B., A. Innes, K. Wanisch, A.K. Kolaszynska, A. Pandraud, G. Kelly, A.Y. Abramov, M.M. Reilly, G. Schiavo, and L. Greensmith. 2017. Mitochondrial deficits and abnormal mitochondrial retrograde axonal transport play a role in the pathogenesis of mutant Hsp27-induced Charcot Marie Tooth Disease. *Hum Mol Genet.* 26:3313-3326.
- Kang, B.H., J. Plescia, T. Dohi, J. Rosa, S.J. Doxsey, and D.C. Altieri. 2007. Regulation of tumor cell mitochondrial homeostasis by an organelle-specific Hsp90 chaperone network. *Cell.* 131:257-270.
- Kang, P.J., J. Ostermann, J. Shilling, W. Neupert, E.A. Craig, and N. Pfanner. 1990. Requirement for hsp70 in the mitochondrial matrix for translocation and folding of precursor proteins. *Nature.* 348:137-143.
- Kang, Y.J., M. Jang, Y.K. Park, S. Kang, K.H. Bae, S. Cho, C.K. Lee, B.C. Park, S.W. Chi, and S.G. Park. 2010. Molecular interaction between HAX-1 and XIAP inhibits apoptosis. *Biochem Biophys Res Commun.* 393:794-799.

- Karagoz, G.E., D. Acosta-Alvear, and P. Walter. 2019. The Unfolded Protein Response: Detecting and Responding to Fluctuations in the Protein-Folding Capacity of the Endoplasmic Reticulum. *Cold Spring Harb Perspect Biol.* 11.
- Kasuske, C.A., and K.A. Hansen. 2018. Symptomatic Clitoromegaly: Case Report of a Clitoral Hemangioma. *J Pediatr Adolesc Gynecol.* 31:55-57.
- Kaushik, S., and A.M. Cuervo. 2018. The coming of age of chaperone-mediated autophagy. *Nat Rev Mol Cell Biol.* 19:365-381.
- Kenny, T.C., and D. Germain. 2017. From discovery of the CHOP axis and targeting ClpP to the identification of additional axes of the UPRmt driven by the estrogen receptor and SIRT3. *J Bioenerg Biomembr.* 49:297-305.
- Klaips, C.L., G.G. Jayaraj, and F.U. Hartl. 2018. Pathways of cellular proteostasis in aging and disease. *J Cell Biol.* 217:51-63.
- Klein, C. 2011. Genetic defects in severe congenital neutropenia: emerging insights into life and death of human neutrophil granulocytes. *Annual review of immunology.* 29:399-413.
- Klein, C. 2017. Kostmann's Disease and HCLS1-Associated Protein X-1 (HAX1). *J Clin Immunol.* 37:117-122.
- Klein, C., M. Grudzien, G. Appaswamy, M. Germeshausen, I. Sandrock, A.A. Schaffer, C. Rathinam, K. Boztug, B. Schwitzer, N. Rezaei, G. Bohn, M. Melin, G. Carlsson, B. Fadeel, N. Dahl, J. Palmblad, J.I. Henter, C. Zeidler, B. Grimbacher, and K. Welte. 2007. HAX1 deficiency causes autosomal recessive severe congenital neutropenia (Kostmann disease). *Nature genetics.* 39:86-92.
- Kollner, I., B. Sodeik, S. Schreek, H. Heyn, N. von Neuhoff, M. Germeshausen, C. Zeidler, M. Kruger, B. Schlegelberger, K. Welte, and C. Beger. 2006. Mutations in neutrophil elastase causing congenital neutropenia lead to cytoplasmic protein accumulation and induction of the unfolded protein response. *Blood.* 108:493-500.
- Komiya, T., S. Rospert, C. Koehler, R. Looser, G. Schatz, and K. Mihara. 1998. Interaction of mitochondrial targeting signals with acidic receptor domains along the protein import pathway: evidence for the 'acid chain' hypothesis. *EMBO J.* 17:3886-3898.
- Koppen, M., and T. Langer. 2007. Protein degradation within mitochondria: versatile activities of AAA proteases and other peptidases. *Crit Rev Biochem Mol Biol.* 42:221-242.
- Korbel, D., S. Wurth, M. Kaser, and T. Langer. 2004. Membrane protein turnover by the m-AAA protease in mitochondria depends on the transmembrane domains of its subunits. *EMBO Rep.* 5:698-703.
- Kostenko, S., and U. Moens. 2009. Heat shock protein 27 phosphorylation: kinases, phosphatases, functions and pathology. *Cell Mol Life Sci.* 66:3289-3307.
- Kostmann, R. 1956. Infantile genetic agranulocytosis; agranulocytosis infantilis hereditaria. *Acta Paediatr Suppl.* 45:1-78.
- Krakowiak, J., X. Zheng, N. Patel, Z.A. Feder, J. Anandhakumar, K. Valerius, D.S. Gross, A.S. Khalil, and D. Pincus. 2018. Hsf1 and Hsp70 constitute a two-component feedback loop that regulates the yeast heat shock response. *Elife.* 7.
- Kulak, N.A., P.E. Geyer, and M. Mann. 2017. Loss-less Nano-fractionator for High Sensitivity, High Coverage Proteomics. *Mol Cell Proteomics.* 16:694-705.
- Lanciotti, M., S. Indaco, S. Bonanomi, T. Coliva, E. Mastrodicasa, G. Caridi, M. Calvillo, and C. Dufour. 2010. Novel HAX1 gene mutations associated to

- neurodevelopment abnormalities in two Italian patients with severe congenital neutropenia. *Haematologica*. 95:168-169.
- Langer, T., C. Lu, H. Echols, J. Flanagan, M.K. Hayer, and F.U. Hartl. 1992. Successive action of DnaK, DnaJ and GroEL along the pathway of chaperone-mediated protein folding. *Nature*. 356:683-689.
- Lebiedzinska, M., G. Szabadkai, A.W. Jones, J. Duszynski, and M.R. Wieckowski. 2009. Interactions between the endoplasmic reticulum, mitochondria, plasma membrane and other subcellular organelles. *Int J Biochem Cell Biol*. 41:1805-1816.
- Lee, M.J., B.H. Lee, J. Hanna, R.W. King, and D. Finley. 2011. Trimming of ubiquitin chains by proteasome-associated deubiquitinating enzymes. *Mol Cell Proteomics*. 10:R110 003871.
- Leonhard, K., J.M. Herrmann, R.A. Stuart, G. Mannhaupt, W. Neupert, and T. Langer. 1996. AAA proteases with catalytic sites on opposite membrane surfaces comprise a proteolytic system for the ATP-dependent degradation of inner membrane proteins in mitochondria. *EMBO J*. 15:4218-4229.
- Letts, J.A., and L.A. Sazanov. 2017. Clarifying the supercomplex: the higher-order organization of the mitochondrial electron transport chain. *Nat Struct Mol Biol*. 24:800-808.
- Li, J., Y. Zhang, L. Cui, J. Wang, X. Pang, Y. Lai, Y. Yao, X. Liu, and Y. Li. 2013a. Mechanical stretch changes coronary artery fibroblasts function by upregulating HSF1 protein expression. *Int J Biol Macromol*. 59:105-110.
- Li, L., G. Shen, and G.C. Li. 1995. Effects of expressing human Hsp70 and its deletion derivatives on heat killing and on RNA and protein synthesis. *Exp Cell Res*. 217:460-468.
- Li, Z., I.P. Michael, D. Zhou, A. Nagy, and J.M. Rini. 2013b. Simple piggyBac transposon-based mammalian cell expression system for inducible protein production. *Proc Natl Acad Sci U S A*. 110:5004-5009.
- Lill, R. 2009. Function and biogenesis of iron-sulphur proteins. *Nature*. 460:831-838.
- Liu, R.Y., X. Li, L. Li, and G.C. Li. 1992. Expression of human hsp70 in rat fibroblasts enhances cell survival and facilitates recovery from translational and transcriptional inhibition following heat shock. *Cancer Res*. 52:3667-3673.
- Liutkute, M., E. Samatova, and M.V. Rodnina. 2020. Cotranslational Folding of Proteins on the Ribosome. *Biomolecules*. 10.
- Livnat-Levanon, N., and M.H. Glickman. 2011. Ubiquitin-proteasome system and mitochondria - reciprocity. *Biochim Biophys Acta*. 1809:80-87.
- Lobo-Jarne, T., and C. Ugalde. 2018. Respiratory chain supercomplexes: Structures, function and biogenesis. *Semin Cell Dev Biol*. 76:179-190.
- Lopez-Fabuel, I., J. Le Douce, A. Logan, A.M. James, G. Bonvento, M.P. Murphy, A. Almeida, and J.P. Bolanos. 2016. Complex I assembly into supercomplexes determines differential mitochondrial ROS production in neurons and astrocytes. *Proc Natl Acad Sci U S A*. 113:13063-13068.
- Lyszkiewicz, M., D. Kotlarz, N. Zietara, G. Brandes, J. Diestelhorst, S. Glage, E. Hobeika, M. Reth, L.A. Huber, A. Krueger, and C. Klein. 2019. LAMTOR2 (p14) Controls B Cell Differentiation by Orchestrating Endosomal BCR Trafficking. *Front Immunol*. 10:497.
- Mannini, B., and F. Chiti. 2017. Chaperones as Suppressors of Protein Misfolded Oligomer Toxicity. *Front Mol Neurosci*. 10:98.
- Margineantu, D.H., C.B. Emerson, D. Diaz, and D.M. Hockenbery. 2007. Hsp90 inhibition decreases mitochondrial protein turnover. *PLoS One*. 2:e1066.

- Martin, W.F. 2017. Physiology, anaerobes, and the origin of mitosing cells 50 years on. *J Theor Biol.* 434:2-10.
- Martin, W.F., S. Garg, and V. Zimorski. 2015. Endosymbiotic theories for eukaryote origin. *Philos Trans R Soc Lond B Biol Sci.* 370:20140330.
- Matouschek, A., N. Pfanner, and W. Voos. 2000. Protein unfolding by mitochondria. The Hsp70 import motor. *EMBO Rep.* 1:404-410.
- Mayer, A., W. Neupert, and R. Lill. 1995. Mitochondrial protein import: reversible binding of the presequence at the trans side of the outer membrane drives partial translocation and unfolding. *Cell.* 80:127-137.
- Mehlen, P., A. Mehlen, J. Godet, and A.P. Arrigo. 1997. hsp27 as a switch between differentiation and apoptosis in murine embryonic stem cells. *J Biol Chem.* 272:31657-31665.
- Meimaridou, E., S.B. Gooljar, and J.P. Chapple. 2009. From hatching to dispatching: the multiple cellular roles of the Hsp70 molecular chaperone machinery. *J Mol Endocrinol.* 42:1-9.
- Mick, D.U., S. Dennerlein, H. Wiese, R. Reinhold, D. Pacheu-Grau, I. Lorenzi, F. Sasarman, W. Weraarpachai, E.A. Shoubridge, B. Warscheid, and P. Rehling. 2012. MITRAC links mitochondrial protein translocation to respiratory-chain assembly and translational regulation. *Cell.* 151:1528-1541.
- Milenkovic, D., J.N. Blaza, N.G. Larsson, and J. Hirst. 2017. The Enigma of the Respiratory Chain Supercomplex. *Cell Metab.* 25:765-776.
- Mogk, A., C. Schlieker, K.L. Friedrich, H.J. Schonfeld, E. Vierling, and B. Bukau. 2003. Refolding of substrates bound to small Hsps relies on a disaggregation reaction mediated most efficiently by ClpB/DnaK. *J Biol Chem.* 278:31033-31042.
- Mokranjac, D., S.A. Paschen, C. Kozany, H. Prokisch, S.C. Hoppins, F.E. Nargang, W. Neupert, and K. Hell. 2003. Tim50, a novel component of the TIM23 preprotein translocase of mitochondria. *EMBO J.* 22:816-825.
- Monaghan, R.M., and A.J. Whitmarsh. 2015. Mitochondrial Proteins Moonlighting in the Nucleus. *Trends Biochem Sci.* 40:728-735.
- Morais, V.A., D. Haddad, K. Craessaerts, P.J. De Bock, J. Swerts, S. Vilain, L. Aerts, L. Overbergh, A. Grunewald, P. Seibler, C. Klein, K. Gevaert, P. Verstreken, and B. De Strooper. 2014. PINK1 loss-of-function mutations affect mitochondrial complex I activity via Ndufa10 ubiquinone uncoupling. *Science.* 344:203-207.
- Moro, F., C. Sirrenberg, H.C. Schneider, W. Neupert, and M. Brunner. 1999. The TIM17.23 preprotein translocase of mitochondria: composition and function in protein transport into the matrix. *EMBO J.* 18:3667-3675.
- Mu, T.W., D.S. Ong, Y.J. Wang, W.E. Balch, J.R. Yates, 3rd, L. Segatori, and J.W. Kelly. 2008. Chemical and biological approaches synergize to ameliorate protein-folding diseases. *Cell.* 134:769-781.
- Munch, C. 2018. The different axes of the mammalian mitochondrial unfolded protein response. *BMC Biol.* 16:81.
- Munch, C., and J.W. Harper. 2016. Mitochondrial unfolded protein response controls matrix pre-RNA processing and translation. *Nature.* 534:710-713.
- Mymrikov, E.V., M. Daake, B. Richter, M. Haslbeck, and J. Buchner. 2017. The Chaperone Activity and Substrate Spectrum of Human Small Heat Shock Proteins. *J Biol Chem.* 292:672-684.
- Nanua, S., M. Murakami, J. Xia, D.S. Grenda, J. Woloszynek, M. Strand, and D.C. Link. 2011. Activation of the unfolded protein response is associated with

- impaired granulopoiesis in transgenic mice expressing mutant Elane. *Blood*. 117:3539-3547.
- Naresh, N.U., and C.M. Haynes. 2019. Signaling and Regulation of the Mitochondrial Unfolded Protein Response. *Cold Spring Harb Perspect Biol*. 11.
- Nargund, A.M., C.J. Fiorese, M.W. Pellegrino, P. Deng, and C.M. Haynes. 2015. Mitochondrial and nuclear accumulation of the transcription factor ATFS-1 promotes OXPHOS recovery during the UPR(mt). *Mol Cell*. 58:123-133.
- Nargund, A.M., M.W. Pellegrino, C.J. Fiorese, B.M. Baker, and C.M. Haynes. 2012. Mitochondrial import efficiency of ATFS-1 regulates mitochondrial UPR activation. *Science*. 337:587-590.
- Nayak, R.C., L.R. Trump, B.J. Aronow, K. Myers, P. Mehta, T. Kalfa, A.M. Wellendorf, C.A. Valencia, P.J. Paddison, M.S. Horwitz, H.L. Grimes, C. Lutzko, and J.A. Cancelas. 2015. Pathogenesis of ELANE-mutant severe neutropenia revealed by induced pluripotent stem cells. *J Clin Invest*. 125:3103-3116.
- Neupert, W., and J.M. Herrmann. 2007. Translocation of proteins into mitochondria. *Annu Rev Biochem*. 76:723-749.
- Niwa, A., T. Heike, K. Umeda, K. Oshima, I. Kato, H. Sakai, H. Suemori, T. Nakahata, and M.K. Saito. 2011. A novel serum-free monolayer culture for orderly hematopoietic differentiation of human pluripotent cells via mesodermal progenitors. *PLoS One*. 6:e22261.
- Okada, T., H. Yoshida, R. Akazawa, M. Negishi, and K. Mori. 2002. Distinct roles of activating transcription factor 6 (ATF6) and double-stranded RNA-activated protein kinase-like endoplasmic reticulum kinase (PERK) in transcription during the mammalian unfolded protein response. *Biochem J*. 366:585-594.
- Okamoto, K., N. Kondo-Okamoto, and Y. Ohsumi. 2009. Mitochondria-anchored receptor Atg32 mediates degradation of mitochondria via selective autophagy. *Dev Cell*. 17:87-97.
- Ortiz, D.F., J. Moseley, G. Calderon, A.L. Swift, S. Li, and I.M. Arias. 2004. Identification of HAX-1 as a protein that binds bile salt export protein and regulates its abundance in the apical membrane of Madin-Darby canine kidney cells. *J Biol Chem*. 279:32761-32770.
- Pakos-Zebrucka, K., I. Koryga, K. Mnich, M. Lujic, A. Samali, and A.M. Gorman. 2016. The integrated stress response. *EMBO Rep*. 17:1374-1395.
- Palade, G.E. 1953. An electron microscope study of the mitochondrial structure. *J Histochem Cytochem*. 1:188-211.
- Pandey, P., R. Farber, A. Nakazawa, S. Kumar, A. Bharti, C. Nalin, R. Weichselbaum, D. Kufe, and S. Kharbanda. 2000. Hsp27 functions as a negative regulator of cytochrome c-dependent activation of procaspase-3. *Oncogene*. 19:1975-1981.
- Papa, L., and D. Germain. 2011. Estrogen receptor mediates a distinct mitochondrial unfolded protein response. *J Cell Sci*. 124:1396-1402.
- Papa, L., and D. Germain. 2014. SirT3 regulates the mitochondrial unfolded protein response. *Mol Cell Biol*. 34:699-710.
- Paul, C., F. Manero, S. Gonin, C. Kretz-Remy, S. Viro, and A.P. Arrigo. 2002. Hsp27 as a negative regulator of cytochrome C release. *Mol Cell Biol*. 22:816-834.
- Paul, C., S. Simon, B. Gibert, S. Viro, F. Manero, and A.P. Arrigo. 2010. Dynamic processes that reflect anti-apoptotic strategies set up by HspB1 (Hsp27). *Exp Cell Res*. 316:1535-1552.



- Pratt, W.B., J.E. Gestwicki, Y. Osawa, and A.P. Lieberman. 2015. Targeting Hsp90/Hsp70-based protein quality control for treatment of adult onset neurodegenerative diseases. *Annu Rev Pharmacol Toxicol.* 55:353-371.
- Preissler, S., and E. Deuerling. 2012. Ribosome-associated chaperones as key players in proteostasis. *Trends Biochem Sci.* 37:274-283.
- Putsep, K., G. Carlsson, H.G. Boman, and M. Andersson. 2002. Deficiency of antibacterial peptides in patients with morbus Kostmann: an observation study. *Lancet.* 360:1144-1149.
- Quinlan, C.L., A.A. Gerencser, J.R. Treberg, and M.D. Brand. 2011. The mechanism of superoxide production by the antimycin-inhibited mitochondrial Q-cycle. *J Biol Chem.* 286:31361-31372.
- Quinlan, C.L., A.L. Orr, I.V. Perevoshchikova, J.R. Treberg, B.A. Ackrell, and M.D. Brand. 2012. Mitochondrial complex II can generate reactive oxygen species at high rates in both the forward and reverse reactions. *J Biol Chem.* 287:27255-27264.
- Radke, S., H. Chander, P. Schafer, G. Meiss, R. Kruger, J.B. Schulz, and D. Germain. 2008. Mitochondrial protein quality control by the proteasome involves ubiquitination and the protease Omi. *J Biol Chem.* 283:12681-12685.
- Rampelt, H., J. Kirstein-Miles, N.B. Nillegoda, K. Chi, S.R. Scholz, R.I. Morimoto, and B. Bukau. 2012. Metazoan Hsp70 machines use Hsp110 to power protein disaggregation. *EMBO J.* 31:4221-4235.
- Ramsay, R.R., and T.P. Singer. 1992. Relation of superoxide generation and lipid peroxidation to the inhibition of NADH-Q oxidoreductase by rotenone, piericidin A, and MPP+. *Biochem Biophys Res Commun.* 189:47-52.
- Rane, M.J., Y. Pan, S. Singh, D.W. Powell, R. Wu, T. Cummins, Q. Chen, K.R. McLeish, and J.B. Klein. 2003. Heat shock protein 27 controls apoptosis by regulating Akt activation. *J Biol Chem.* 278:27828-27835.
- Richter, K., M. Haslbeck, and J. Buchner. 2010. The heat shock response: life on the verge of death. *Mol Cell.* 40:253-266.
- Richter-Dennerlein, R., S. Oeljeklaus, I. Lorenzi, C. Ronsor, B. Bareth, A.B. Schendzielorz, C. Wang, B. Warscheid, P. Rehling, and S. Dennerlein. 2016. Mitochondrial Protein Synthesis Adapts to Influx of Nuclear-Encoded Protein. *Cell.* 167:471-483 e410.
- Rizo, A.N., J. Lin, S.N. Gates, E. Tse, S.M. Bart, L.M. Castellano, F. DiMaio, J. Shorter, and D.R. Southworth. 2019. Structural basis for substrate gripping and translocation by the ClpB AAA+ disaggregase. *Nat Commun.* 10:2393.
- Rizzuto, R., P. Pinton, W. Carrington, F.S. Fay, K.E. Fogarty, L.M. Lifshitz, R.A. Tuft, and T. Pozzan. 1998. Close contacts with the endoplasmic reticulum as determinants of mitochondrial Ca<sup>2+</sup> responses. *Science.* 280:1763-1766.
- Rogalla, T., M. Ehrnsperger, X. Preville, A. Kotlyarov, G. Lutsch, C. Ducasse, C. Paul, M. Wieske, A.P. Arrigo, J. Buchner, and M. Gaestel. 1999. Regulation of Hsp27 oligomerization, chaperone function, and protective activity against oxidative stress/tumor necrosis factor alpha by phosphorylation. *J Biol Chem.* 274:18947-18956.
- Rouillard, A.D., G.W. Gundersen, N.F. Fernandez, Z. Wang, C.D. Monteiro, M.G. McDermott, and A. Ma'ayan. 2016. The harmonizome: a collection of processed datasets gathered to serve and mine knowledge about genes and proteins. *Database (Oxford).* 2016.

- Ruan, L., C. Zhou, E. Jin, A. Kucharavy, Y. Zhang, Z. Wen, L. Florens, and R. Li. 2017. Cytosolic proteostasis through importing of misfolded proteins into mitochondria. *Nature*. 543:443-446.
- Saita, S., H. Nolte, K.U. Fiedler, H. Kashkar, A.S. Venne, R.P. Zahedi, M. Kruger, and T. Langer. 2017. PARL mediates Smac proteolytic maturation in mitochondria to promote apoptosis. *Nat Cell Biol*. 19:318-328.
- Sargsyan, Y., and S. Thoms. 2020. Staying in Healthy Contact: How Peroxisomes Interact with Other Cell Organelles. *Trends Mol Med*. 26:201-214.
- Sarnowska, E., E.A. Grzybowska, K. Sobczak, R. Konopinski, A. Wilczynska, M. Szwarc, T.J. Sarnowski, W.J. Krzyzosiak, and J.A. Siedlecki. 2007. Hairpin structure within the 3'UTR of DNA polymerase beta mRNA acts as a post-transcriptional regulatory element and interacts with Hax-1. *Nucleic Acids Res*. 35:5499-5510.
- Saunders, C., L. Smith, F. Wibrand, K. Ravn, P. Bross, I. Thiffault, M. Christensen, A. Atherton, E. Farrow, N. Miller, S.F. Kingsmore, and E. Ostergaard. 2015. CLPB variants associated with autosomal-recessive mitochondrial disorder with cataract, neutropenia, epilepsy, and methylglutaconic aciduria. *Am J Hum Genet*. 96:258-265.
- Sazanov, L.A. 2015. A giant molecular proton pump: structure and mechanism of respiratory complex I. *Nat Rev Mol Cell Biol*. 16:375-388.
- Scarpulla, R.C. 2006. Nuclear control of respiratory gene expression in mammalian cells. *J Cell Biochem*. 97:673-683.
- Schagger, H. 2001. Blue-native gels to isolate protein complexes from mitochondria. *Methods Cell Biol*. 65:231-244.
- Schagger, H., and K. Pfeiffer. 2000. Supercomplexes in the respiratory chains of yeast and mammalian mitochondria. *EMBO J*. 19:1777-1783.
- Schapira, A.H., J.M. Cooper, D. Dexter, J.B. Clark, P. Jenner, and C.D. Marsden. 1990. Mitochondrial complex I deficiency in Parkinson's disease. *J Neurochem*. 54:823-827.
- Scheltema, R.A., and M. Mann. 2012. SprayQc: a real-time LC-MS/MS quality monitoring system to maximize uptime using off the shelf components. *J Proteome Res*. 11:3458-3466.
- Schon, E.A. 2000. Mitochondrial genetics and disease. *Trends Biochem Sci*. 25:555-560.
- Schulz, C., O. Lytovchenko, J. Melin, A. Chacinska, B. Guiard, P. Neumann, R. Ficner, O. Jahn, B. Schmidt, and P. Rehling. 2011. Tim50's presequence receptor domain is essential for signal driven transport across the TIM23 complex. *J Cell Biol*. 195:643-656.
- Sekine, S., Y. Kanamaru, M. Koike, A. Nishihara, M. Okada, H. Kinoshita, M. Kamiyama, J. Maruyama, Y. Uchiyama, N. Ishihara, K. Takeda, and H. Ichijo. 2012. Rhomboid protease PARL mediates the mitochondrial membrane potential loss-induced cleavage of PGAM5. *J Biol Chem*. 287:34635-34645.
- Shalgi, R., J.A. Hurt, I. Krykbaeva, M. Taipale, S. Lindquist, and C.B. Burge. 2013. Widespread regulation of translation by elongation pausing in heat shock. *Mol Cell*. 49:439-452.
- Sharma, G.T., A. Nath, S. Prasad, S. Singhal, N. Singh, N.E. Gade, P.K. Dubey, and G. Saikumar. 2012. Expression and characterization of constitutive heat shock protein 70.1 (HSPA-1A) gene in in vitro produced and in vivo-derived buffalo (*Bubalus bubalis*) embryos. *Reprod Domest Anim*. 47:975-983.

- Shorter, J. 2011. The mammalian disaggregase machinery: Hsp110 synergizes with Hsp70 and Hsp40 to catalyze protein disaggregation and reactivation in a cell-free system. *PLoS One*. 6:e26319.
- Sorrentino, V., M. Romani, L. Mouchiroud, J.S. Beck, H. Zhang, D. D'Amico, N. Moullan, F. Potenza, A.W. Schmid, S. Rietsch, S.E. Counts, and J. Auwerx. 2017. Enhancing mitochondrial proteostasis reduces amyloid-beta proteotoxicity. *Nature*. 552:187-193.
- Spoor, J., H. Farajifard, and N. Rezaei. 2019. Congenital neutropenia and primary immunodeficiency diseases. *Critical reviews in oncology/hematology*. 133:149-162.
- Squires, C.L., S. Pedersen, B.M. Ross, and C. Squires. 1991. ClpB is the *Escherichia coli* heat shock protein F84.1. *J Bacteriol*. 173:4254-4262.
- Stehling, O., and R. Lill. 2013. The role of mitochondria in cellular iron-sulfur protein biogenesis: mechanisms, connected processes, and diseases. *Cold Spring Harb Perspect Biol*. 5:a011312.
- Stoldt, S., D. Wenzel, K. Kehrein, D. Riedel, M. Ott, and S. Jakobs. 2018. Spatial orchestration of mitochondrial translation and OXPHOS complex assembly. *Nat Cell Biol*. 20:528-534.
- Stroh, A., O. Anderka, K. Pfeiffer, T. Yagi, M. Finel, B. Ludwig, and H. Schagger. 2004. Assembly of respiratory complexes I, III, and IV into NADH oxidase supercomplex stabilizes complex I in *Paracoccus denitrificans*. *J Biol Chem*. 279:5000-5007.
- Sundaresan, N.R., M. Gupta, G. Kim, S.B. Rajamohan, A. Isbatan, and M.P. Gupta. 2009. Sirt3 blocks the cardiac hypertrophic response by augmenting Foxo3a-dependent antioxidant defense mechanisms in mice. *J Clin Invest*. 119:2758-2771.
- Suzuki, Y., C. Demoliere, D. Kitamura, H. Takeshita, U. Deuschle, and T. Watanabe. 1997. HAX-1, a novel intracellular protein, localized on mitochondria, directly associates with HS1, a substrate of Src family tyrosine kinases. *J Immunol*. 158:2736-2744.
- Taipale, M., I. Krykbaeva, M. Koeva, C. Kayatekin, K.D. Westover, G.I. Karras, and S. Lindquist. 2012. Quantitative analysis of HSP90-client interactions reveals principles of substrate recognition. *Cell*. 150:987-1001.
- Tanaka, A., M.M. Cleland, S. Xu, D.P. Narendra, D.F. Suen, M. Karbowski, and R.J. Youle. 2010. Proteasome and p97 mediate mitophagy and degradation of mitofusins induced by Parkin. *J Cell Biol*. 191:1367-1380.
- Tao, R., A. Vassilopoulos, L. Parisiadou, Y. Yan, and D. Gius. 2014. Regulation of MnSOD enzymatic activity by Sirt3 connects the mitochondrial acetylome signaling networks to aging and carcinogenesis. *Antioxid Redox Signal*. 20:1646-1654.
- Tatsuta, T., and T. Langer. 2008. Quality control of mitochondria: protection against neurodegeneration and ageing. *EMBO J*. 27:306-314.
- Teske, B.F., M.E. Fusakio, D. Zhou, J. Shan, J.N. McClintick, M.S. Kilberg, and R.C. Wek. 2013. CHOP induces activating transcription factor 5 (ATF5) to trigger apoptosis in response to perturbations in protein homeostasis. *Mol Biol Cell*. 24:2477-2490.
- Tessarz, P., A. Mogk, and B. Bukau. 2008. Substrate threading through the central pore of the Hsp104 chaperone as a common mechanism for protein disaggregation and prion propagation. *Mol Microbiol*. 68:87-97.

- Thomas, J.G., and F. Baneyx. 1998. Roles of the *Escherichia coli* small heat shock proteins IbpA and IbpB in thermal stress management: comparison with ClpA, ClpB, and HtpG *In vivo*. *J Bacteriol.* 180:5165-5172.
- Tidwell, T., J. Wechsler, R.C. Nayak, L. Trump, S.J. Salipante, J.C. Cheng, J. Donadieu, T. Glaubach, S.J. Corey, H.L. Grimes, C. Lutzko, J.A. Cancelas, and M.S. Horwitz. 2014. Neutropenia-associated ELANE mutations disrupting translation initiation produce novel neutrophil elastase isoforms. *Blood.* 123:562-569.
- Trebinska, A., A. Rembiszewska, K. Ciosek, K. Ptaszynski, S. Rowinski, J. Kupryjanczyk, J.A. Siedlecki, and E.A. Grzybowska. 2010. HAX-1 overexpression, splicing and cellular localization in tumors. *BMC Cancer.* 10:76.
- Triot, A., P.M. Jarvinen, J.I. Arostegui, D. Murugan, N. Kohistani, J.L. Dapena Diaz, T. Racek, J. Puchalka, E.M. Gertz, A.A. Schaffer, D. Kotlarz, D. Pfeifer, C. Diaz de Heredia Rubio, M.A. Ozdemir, T. Patiroglu, M. Karakukcu, J. Sanchez de Toledo Codina, J. Yague, I.P. Touw, E. Unal, and C. Klein. 2014. Inherited biallelic CSF3R mutations in severe congenital neutropenia. *Blood.* 123:3811-3817.
- Tsaytler, P., H.P. Harding, D. Ron, and A. Bertolotti. 2011. Selective inhibition of a regulatory subunit of protein phosphatase 1 restores proteostasis. *Science.* 332:91-94.
- Ungermann, C., W. Neupert, and D.M. Cyr. 1994. The role of Hsp70 in conferring unidirectionality on protein translocation into mitochondria. *Science.* 266:1250-1253.
- Vabulas, R.M., S. Raychaudhuri, M. Hayer-Hartl, and F.U. Hartl. 2010. Protein folding in the cytoplasm and the heat shock response. *Cold Spring Harb Perspect Biol.* 2:a004390.
- Vafiadaki, E., D.A. Arvanitis, S.N. Pagakis, V. Papalouka, D. Sanoudou, A. Kontrogianni-Konstantopoulos, and E.G. Kranias. 2009. The anti-apoptotic protein HAX-1 interacts with SERCA2 and regulates its protein levels to promote cell survival. *Mol Biol Cell.* 20:306-318.
- Vandecasteele, G., G. Szabadkai, and R. Rizzuto. 2001. Mitochondrial calcium homeostasis: mechanisms and molecules. *IUBMB Life.* 52:213-219.
- Varshavsky, A. 2017. The Ubiquitin System, Autophagy, and Regulated Protein Degradation. *Annu Rev Biochem.* 86:123-128.
- Venditti, P., L. Di Stefano, and S. Di Meo. 2013. Mitochondrial metabolism of reactive oxygen species. *Mitochondrion.* 13:71-82.
- Vidyasagar, A., N.A. Wilson, and A. Djamali. 2012. Heat shock protein 27 (HSP27): biomarker of disease and therapeutic target. *Fibrogenesis Tissue Repair.* 5:7.
- Wai, T., S. Saita, H. Nolte, S. Muller, T. Konig, R. Richter-Dennerlein, H.G. Sprenger, J. Madrenas, M. Muhlmeister, U. Brandt, M. Kruger, and T. Langer. 2016. The membrane scaffold SLP2 anchors a proteolytic hub in mitochondria containing PARL and the i-AAA protease YME1L. *EMBO Rep.* 17:1844-1856.
- Walter, P., and D. Ron. 2011. The unfolded protein response: from stress pathway to homeostatic regulation. *Science.* 334:1081-1086.
- Wang, C., and R.J. Youle. 2009. The role of mitochondria in apoptosis\*. *Annu Rev Genet.* 43:95-118.
- Wang, Z., H. Jiang, S. Chen, F. Du, and X. Wang. 2012. The mitochondrial phosphatase PGAM5 functions at the convergence point of multiple necrotic death pathways. *Cell.* 148:228-243.

- Wegrzyn, R.D., K. Bapat, G.P. Newnam, A.D. Zink, and Y.O. Chernoff. 2001. Mechanism of prion loss after Hsp104 inactivation in yeast. *Mol Cell Biol.* 21:4656-4669.
- Weibezahn, J., P. Tessarz, C. Schlieker, R. Zahn, Z. Maglica, S. Lee, H. Zentgraf, E.U. Weber-Ban, D.A. Dougan, F.T. Tsai, A. Mogk, and B. Bukau. 2004. Thermotolerance requires refolding of aggregated proteins by substrate translocation through the central pore of ClpB. *Cell.* 119:653-665.
- Weinberg, S.E., L.A. Sena, and N.S. Chandel. 2015. Mitochondria in the regulation of innate and adaptive immunity. *Immunity.* 42:406-417.
- Wieckowski, M.R., C. Giorgi, M. Lebedzinska, J. Duszynski, and P. Pinton. 2009. Isolation of mitochondria-associated membranes and mitochondria from animal tissues and cells. *Nat Protoc.* 4:1582-1590.
- Witzel, M., D. Petersheim, Y. Fan, E. Bahrami, T. Racek, M. Rohlf, J. Puchalka, C. Mertes, J. Gagneur, C. Ziegenhain, W. Enard, A. Stray-Pedersen, P.D. Arkwright, M.R. Abboud, V. Pazhakh, G.J. Lieschke, P.M. Krawitz, M. Dahlhoff, M.R. Schneider, E. Wolf, H.P. Horny, H. Schmidt, A.A. Schaffer, and C. Klein. 2017. Chromatin-remodeling factor SMARCD2 regulates transcriptional networks controlling differentiation of neutrophil granulocytes. *Nat Genet.* 49:742-752.
- Wolff, S., J.S. Weissman, and A. Dillin. 2014. Differential scales of protein quality control. *Cell.* 157:52-64.
- Wortmann, S.B., S. Zietkiewicz, M. Kousi, R. Szklarczyk, T.B. Haack, S.W. Gersting, A.C. Muntau, A. Rakovic, G.H. Renkema, R.J. Rodenburg, T.M. Strom, T. Meitinger, M.E. Rubio-Gozalbo, E. Chrusciel, F. Distelmaier, C. Golzio, J.H. Jansen, C. van Karnebeek, Y. Lillquist, T. Lucke, K. Ounap, R. Zordania, J. Yapliito-Lee, H. van Bokhoven, J.N. Spelbrink, F.M. Vaz, M. Pras-Raves, R. Ploski, E. Pronicka, C. Klein, M.A. Willemsen, A.P. de Brouwer, H. Prokisch, N. Katsanis, and R.A. Wevers. 2015. CLPB mutations cause 3-methylglutaconic aciduria, progressive brain atrophy, intellectual disability, congenital neutropenia, cataracts, movement disorder. *Am J Hum Genet.* 96:245-257.
- Wu, R., H. Kausar, P. Johnson, D.E. Montoya-Durango, M. Merchant, and M.J. Rane. 2007. Hsp27 regulates Akt activation and polymorphonuclear leukocyte apoptosis by scaffolding MK2 to Akt signal complex. *J Biol Chem.* 282:21598-21608.
- Yakistan, E., E. Schirg, C. Zeidler, N.J. Bishop, A. Reiter, A. Hirt, H. Riehm, and K. Welte. 1997. High incidence of significant bone loss in patients with severe congenital neutropenia (Kostmann's syndrome). *The Journal of pediatrics.* 131:592-597.
- Yankovskaya, V., R. Horsefield, S. Tornroth, C. Luna-Chavez, H. Miyoshi, C. Leger, B. Byrne, G. Cecchini, and S. Iwata. 2003. Architecture of succinate dehydrogenase and reactive oxygen species generation. *Science.* 299:700-704.
- Zhang, T., E.A. Ploetz, M. Nagy, S.M. Doyle, S. Wickner, P.E. Smith, and M. Zolkiewski. 2012. Flexible connection of the N-terminal domain in ClpB modulates substrate binding and the aggregate reactivation efficiency. *Proteins.* 80:2758-2768.
- Zhang, Y., S. Sun, J. Chen, P. Ren, Y. Hu, Z. Cao, H. Sun, and Y. Ding. 2014. Oxymatrine induces mitochondria dependent apoptosis in human

- osteosarcoma MNNG/HOS cells through inhibition of PI3K/Akt pathway. *Tumour Biol.* 35:1619-1625.
- Zhang, Y., X.F. Zhang, M.R. Fleming, A. Amiri, L. El-Hassar, A.A. Surguchev, C. Hyland, D.P. Jenkins, R. Desai, M.R. Brown, V.R. Gazula, M.F. Waters, C.H. Large, T.L. Horvath, D. Navaratnam, F.M. Vaccarino, P. Forscher, and L.K. Kaczmarek. 2016. Kv3.3 Channels Bind Hax-1 and Arp2/3 to Assemble a Stable Local Actin Network that Regulates Channel Gating. *Cell.* 165:434-448.
- Zhao, Q., J. Wang, I.V. Levichkin, S. Stasinopoulos, M.T. Ryan, and N.J. Hoogenraad. 2002. A mitochondrial specific stress response in mammalian cells. *EMBO J.* 21:4411-4419.
- Zheng, N., and N. Shabek. 2017. Ubiquitin Ligases: Structure, Function, and Regulation. *Annu Rev Biochem.* 86:129-157.
- Zhu, J., K.R. Vinothkumar, and J. Hirst. 2016. Structure of mammalian respiratory complex I. *Nature.* 536:354-358.
- Zorov, D.B., M. Juhaszova, and S.J. Sollott. 2014. Mitochondrial reactive oxygen species (ROS) and ROS-induced ROS release. *Physiol Rev.* 94:909-950.
- Zwirowski, S., A. Klosowska, I. Obuchowski, N.B. Nillegoda, A. Pirog, S. Zietkiewicz, B. Bukau, A. Mogk, and K. Liberek. 2017. Hsp70 displaces small heat shock proteins from aggregates to initiate protein refolding. *EMBO J.* 36:783-796.

## VII ACKNOWLEDGEMENT

First and foremost, I would like to thank Prof. Dr. Christoph Klein for providing me the opportunity to conduct PhD study in his lab and the scientifically interesting topic to attract me into research. I would like to express my gratitude for his full support, patience and guidance throughout these past few years. I would like to thank Prof. Dr. Klaus Förstemann for kindly providing me the opportunity to study in the faculty of Chemistry and Pharmacy of LMU and his consistent support during my PhD study.

I would like to thank all members of my PhD defense committee— Prof. Klaus Förstemann, Prof. Christoph Klein, Prof. Lucas Jae, Prof. Julian Stingele, Prof. Karl-Peter Hopfner, Prof. Sebastian Theurich for reviewing my thesis and their constructive criticisms and suggestions regarding my study in the PhD thesis defense.

I am especially grateful to Dr. Natalia Zietara, Dr. Marcin Lyszkiewicz. They introduced me to the laboratory routines and various experiments with their rigorous and scientific attitudes. I am very grateful to their valuable guidance and critical discussion during the first few years of my PhD study.

Many deepest thanks go to Dr. Sven Dennerlein, Dr. Marta Murgia and Dr. Monika Linder for their helpfulness, great advice and professional experience during the study of HAX1 protein. Without their help and support, my studies would not have been as deep and fruitful. In addition, I would like to thank Dr. Monika Linder for proofreading my thesis and great help on the manuscript.

I would like to thank Dr. Megumi Tatematsu for her generous help and insightful discussions on the project. She is the most helpful person that I have ever seen. I would also like to thank Dr. Yoko Mizoguchi for introducing me to the iPS culture and her guidance for iPS differentiation. I would also like to thank Dr. Meino Rohlf and Tim Jeske for their great help on RNA sequencing.

I would like to thank the animal caretakers in the Institute for Prophylaxis and Epidemiology of Circulatory Diseases (ipek), in particular Dr. Melanie Dobler, Dr. Katharina Ebert, for their well-organized teamwork and the competent, responsible and reliable care of the mice.

I would like to thank my current and former lab members for creating a stimulating environment. I especially would like to thank all lovely members of “Chinatown” for discussions, support and joyfulness inside and outside the lab.

A special thanks to all my friends in China and Germany for joyful moments in the past and future. Precious friendship fueled me a lot in each down course. I would like to thank all the people who help me go through each step of the ups and downs before and after coming to Munich.

Of importance in the financial support, I would like to express my thanks to my scholarship sponsor, the China Scholarship Council (CSC) and Care for Rare Foundation (Germany).

Finally, I am grateful to my family who are always believing in me, supporting me and trying their best to help me grow and become the person I am today. I will forever owe my achievements to my dedicated, caring and thoughtful family.



## VIII CURRICULUM VITAE

Name Yanxin Fan  
Nationality China  
Date of birth 31.10.1989  
Place of birth Beijing, China

### Publications

**Fan, Y.**, Murgia, M., Linder M., Mizoguchi Y., Wang C., Łyszkiewicz, M., Ziętara, N., Liu Y., Frenz S., Sciuccati G., Gaytan A., Alizadeh Z., Rezaei N., Rehling P., Dennerlein S., Mann M., Klein C. HAX1-dependent control of mitochondrial proteostasis governs neutrophil granulocyte differentiation. *Journal of Clinical Investigation* (accepted).

Łyszkiewicz, M., Ziętara, N., Frey, L., Pannicke, U., Stern, M., Liu, Y., **Fan, Y.**, Puchałka, J., Hollizeck, S., Somekh, I., Rohlf, M., Yilmaz, T., Ünal, E., Karakukcu, M., Patiroğlu, T., Kellerer, C., Karasu, E., Sykora, K. W., Lev, A., Simon, A., Klein, C. (2020). Human FCHO1 deficiency reveals role for clathrin-mediated endocytosis in development and function of T cells. *Nature Communications*, 11(1), 1031.

Witzel, M., Petersheim, D., **Fan, Y.**, Bahrami, E., Racek, T., Rohlf, M., Puchałka, J., Mertes, C., Gagneur, J., Ziegenhain, C., Enard, W., Stray-Pedersen, A., Arkwright, P. D., Abboud, M. R., Pazhakh, V., Lieschke, G. J., Krawitz, P. M., Dahlhoff, M., Schneider, M. R., Wolf, E., Klein, C. (2017). Chromatin-remodeling factor SMARCD2 regulates transcriptional networks controlling differentiation of neutrophil granulocytes. *Nature Genetics*, 49(5), 742–752.

Xie, X., Le, L., **Fan, Y.**, Lv, L., & Zhang, J. (2012). Autophagy is induced through the ROS-TP53-DRAM1 pathway in response to mitochondrial protein synthesis inhibition. *Autophagy*, 8(7), 1071–1084.

## **Honors and Awards**

2018-2020	Scholarship of Care-For-Rare Foundation
Jun. 2018	Best E-Poster Award in meeting of the European Society for Immunodeficiencies (ESID)
2014-2018	Scholarship of China Scholarship Council
Nov. 2012	National Scholarship for Postgraduate
Nov. 2009	National Scholarship for Undergraduate